A STUDY OF PROTEIN DYNAMICS AND COFACTOR INTERACTIONS IN PHOTOSYSTEM I

A Dissertation
Presented to
The Academic Faculty

By

Shana L. Bender

In Partial Fulfillment
of the Requirements for the Degree
Doctorate of Philosophy in the
School of Chemistry and Biochemistry

Georgia Institute of Technology
December 2008

A STUDY OF PROTEIN DYNAMICS AND COFACTOR INTERACTIONS IN PHOTOSYSTEM I

Approved by:

Dr. Bridgette Barry, Advisor
School of Chemistry and Biochemistry
Georgia Institute of Technology

Dr. Donald Doyle
School of Chemistry and Biochemistry
Georgia Institute of Technology

Dr. Wendy Kelly
School of Chemistry and Biochemistry
Georgia Institute of Technology

Dr. Ingeborg Schmidt-Krey
School of Biology
Georgia Institute of Technology

Dr. Nael McCarty
Department of Pediatrics
Emory University

Date Approved: October 15, 2008

ACKNOWLEDGEMENTS

I would like to thank my parents, who have given my strength, moral support and practical advice throughout my educational endeavors. I would also like to thank my husband who has always put my goals and education above his own ambitions. I would like to acknowledge my entire family for their constant support in my education. I would like to thank my grandparents who have kept me in their prayers, and my sister who has never doubted my career goals. I would like to acknowledge my advisor, Dr. Bridgette Barry for her valuable support throughout the years. She has been a great advisor, always challenging me to think critically. She has helped me become a better scientist. I would like to thank the past members of the Barry group: Dr. Idelisa Ayala who trained me, Dr. Colette Sacksteder who taught me to be critical of everything, and Dr. Lori Anderson for her guidance and support. I would like to thank the current members of the Barry group: Ian Cooper, Robin Sibert, David Jensen, Jun Chen, Adam Offenbacher, Tina Dreaden, James Keough, and Brandon Polander. The members of the Barry group have been supportive of each other, and have created a great working environment.

TABLE OF CONTENTS

LIST OF TABLES

LIST OF FIGURES

Chapter 4

Chapter 5

LIST OF SYMBOLS

δ	delta
A_1	phylloquinone electron acceptor in Photosystem I
A_0	chlorophyll electron acceptor in Photosystem I
F_A	iron-sulfur cluster electron acceptor in Photosystem I
F_B	iron-sulfur cluster electron acceptor in Photosystem I
F_X	iron-sulfur cluster electron acceptor in Photosystem I
P_{700}	chlorophyll dimer electron donor in Photosystem I
Q	quinone

LIST OF ABBREVIATIONS

ALA	δ-aminolevulinic acid
Asp	aspartic acid
chl	chlorophyll
CoA	coenzyme A
CDRP	carboxyphenylamino-1-deoxyribulose
DAHP	3-deoxy-D-arabino-heptulosonate-7-phosphate
DFT	density functional theory
E. coli	*Escherichia coli*
EPR	electron paramagnetic resonance
EPSP	enolpyruvyl shikimate-3-phosphate
FT-IR	Fourier-transform infrared
Glu	glutamic acid
IGP	indole-3-glycerol phosphate
Leu	leucine
MALDI	matrix assisted laser desorption ionization
NADPH	nicotinamide adenine dinucleotide phosphate
PCC	pasteurized cell culture
PEP	enolpyruvate
PhQ	phylloquinone
PSI	Photosystem I
PSII	Photosystem II
Thr	threonine
tRNA	transfer ribonucleic acid
Trp	tryptophan

UVRR	ultraviolet resonance Raman

SUMMARY

Previous research has underscored the importance of protein dynamics during light-induced electron transfer; however, specific interactions have not been well characterized. It is of particular importance to understand the role of protein dynamics and cofactor interactions in controlling electron transfer in oxygenic photosynthesis. These factors include hydrogen bonding, π-stacking and electrostatic interactions. Reaction-induced FT-IR spectroscopy is sensitive to these interactions as well as isotopic incorporation, and is useful to probe protein dynamics associated with light-induced electron transfer in Photosystem I (PSI). Density functional theory (DFT) provides information concerning the vibrational frequencies of molecules as well as the amplitudes of the vibrations and sensitivity to isotope incorporation. Combining these approaches, protein dynamics associated with light-induced electron transfer in PSI were studied. The work presented here describes specific protein cofactor interactions and specific protein relaxation events associated with light-induced electron transfer. The results reported here are consistent with noncovalent protein cofactor interactions that modulate the redox potential of the secondary electron acceptor of PSI. Furthermore, the studies presented here describe novel protein dynamics associated with the oxidation of the terminal electron donor of PSI. These results characterize specific protein dynamics that may be associated with interactions of the soluble electron donors. These studies highlight the importance of protein dynamics in oxygenic photosynthesis.

CHAPTER 1

INTRODUCTION

Photosynthesis is a biological process, which utilizes light energy to produce a charge separated state across a membrane. This biological process occurs in plants, green algae and cyanobacteria. In plants, the organelles known as the chloroplasts house the photosynthetic machinery responsible for light-induced charge separation. Inner membranes known as thylakoid membranes are stacked within the chloroplasts. Embedded within the thylakoid membranes are the proteins involved in light-induced charge separation and electron transfer. The overall reaction consists of CO_2 being reduced to an aldehyde via the Calvin cycle, and water being oxidized to molecular oxygen and H^+.

Figure 1 shows a schematic diagram of the proteins involved in the electron transfer reactions of photosynthesis. There are two protein complexes directly responsible for light-induced charge separation and electron transfer across the thylakoid membrane, Photosystem II (PSII) and Photosystem I (PSI). PSII is responsible for the reduction of quinone to quinol via two sequential electron transfer events, and the oxidation of water to molecular oxygen and H^+ via four sequential photon absorption events. The cytochrome b_6f complex oxidizes the quinol molecule produced by PSII to quinone. The cytochrome b_6f complex transfers electrons between PSII and Photosystem I (PSI), and participates in the formation of the transmembrane electrochemical proton gradient by transferring protons from the stromal side of the thylakoid membrane to the

luminal side (Figure 1). The hydrogen gradient produced by these reactions is used by ATP synthase to produce ATP from ADP and inorganic phosphate. The cytochrome b_6f complex is also responsible for the reduction of plastocyanin, a monomeric, copper-containing protein.

PSI is responsible for the light-induced reduction of ferredoxin, an iron-sulfur protein, which reduces the enzyme $NADP^+$ reductase. $NADP^+$ reductase is an oxidoreductase, and functions to reduce $NADP^+$ to NADPH. NADPH is the reducing power for the biosynthetic reactions of the Calvin cycle in photosynthesis. Plastocyanin reduces PSI, resetting the system.

1.1 Photosystem I

Photosystem I (PSI) is responsible for the reduction of ferredoxin and the oxidation of plastocyanin or cytochrome c_6. It is a membrane-bound protein consisting of twelve subunits, three of which are responsible for binding the electron transfer cofactors. Figure 2 depicts the polypeptide composition of PSI from the 2.5 Å resolution crystal structure (Jordan et al. 2001). The crystal structure reveals that subunits PsaA and PsaB form a heterodimer spanning the membrane and bind chlorophyll (chl), phylloquinone, and an iron-sulfur cluster as shown in Figure 3A. The subunit PsaC, located on the stromal side of the thylakoid membrane, is responsible for binding the terminal electron acceptors, two iron-sulfur clusters as shown in Figure 3B (Jordan et al. 2001).

Charge separation is believed to begin on an accessory chl monomer, which reduces a second chl monomer designated A_0 (Holzwarth et al. 2006). A_0 reduces a phylloquinone known as A_1. From here, the iron sulfur cluster known as F_X accepts the

electron from A_1, and reduces F_A, a second iron-sulfur cluster. F_A reduces F_B, a third iron-sulfur cluster, and the terminal electron acceptor of PSI.

The primary donor is reduced by P_{700}, a chl heterodimer comprised of a chl a molecule and a chl a' molecule. P_{700} is the terminal electron donor of PSI and is reduced by the soluble electron carrier plastocyanin, or cytochrome c depending on copper availability. The electron transfer scheme in PSI starting with the radical species P_{700}^{+} A_0^{-} is shown in Figure 4. The arrangement of electron cofactors in PSI is depicted in Figure 5. The accessory chl along with the electron acceptors A_0 and A_1 are arranged with apparent C_2 structural symmetry around P_{700}. The arrangement of the cofactors results in two branches; the A branch representing the cofactors bound by the PsaA subunit, and the B branch representing the cofactors bound by the PsaB subunit. Recent studies have suggested both branches support light-induced electron transfer (Guergova-Kuras et al. 2001; Hastings et al. 2001b; Muhiuddin et al. 2001; Rigby et al. 2002; Fairclough et al. 2003; Ramesh et al. 2004; Santabarbara et al. 2005a; Santabarbara et al. 2005b; Li et al. 2006; Santabarbara et al. 2006).

1.2 Primary Donor

As stated previously, recent studies have revealed an accessory chl monomer may be the primary donor in PSI (Holzwarth et al. 2006). These studies utilized ultrafast transient absorption spectroscopy in the femtosecond and nanosecond time range to characterize the electron transfer reactions. These studies reported charge separation occurring in the picosecond time scale, with the first radical pair being accessory chl^{+}/A_0^{-}. P_{700} reduces the accessory chl cation during a second electron transfer event on the

picosecond time scale. The ultrafast transient absorption studies indicate that electron transfer in PSI is similar to PSII, with the initial charge separated state originating on an accessory chl and the positive charge being transferred to the chl dimer (Diner et al. 2002; Groot et al. 2005; Holzwarth et al. 2006).

1.3 Primary Electron Acceptor: A_0

The first electron acceptor in PSI is A_0, a chl monomer located between the accessory chl and the phylloquinone, A_1. From the crystal structure, A_0 is most likely the chlorophyll designated eC2 or eC3 (Figure 5) (Fromme et al. 2001; Jordan et al. 2001; Grotjohann et al. 2005). Measurements of the first electron transfer step by optical spectroscopy is difficult; due to the common time scale of excitation energy transfer from antenna chl to the primary donor and electron transfer from the primary electron donor to acceptor. Furthermore, both processes give rise to absorbance changes in the same spectral region (Brettel, K. et al. 2001). However, spectroscopic studies have suggested A_0 is reduced in 7-10 ps ((Brettel, Klaus 1997; Brettel, K. et al. 2001; Ramesh et al. 2007) and references therein). The time constant of electron transfer from A_0^- to the phylloquinone electron acceptor A_1 has been estimated from kinetic absorption spectroscopy by monitoring the reoxidation of A_0^-, and has been reported to be 30 ps (reviewed in (Brettel, K. et al. 2001)). Other spectroscopic techniques used to determine the time constant for the oxidation of A_0^- include photo-voltage measurements, and monitoring the reduction of A_1 by ultra-fast spectroscopy in the near-UV (Hecks et al. 1994; Brettel, K. et al. 1999). All the mentioned spectroscopic studies have assigned the time constant for oxidation of A_0^- to be in the range of 21-50 ps.

1.4 Secondary Electron Acceptor: A_1

The secondary electron acceptor of PSI is a phylloquinone molecule (vitamin K) designated A_1. It is reduced by A_0, a chl monomer, and is oxidized by the iron-sulfur [4Fe4S] cluster F_X. There are two A_1 molecules per PSI reaction center designated A_{1A} and A_{1B} (Figure 5). Previous studies have revealed biphasic oxidation kinetics of A_1, with a fast decaying component of 20 ns and a longer decaying component of 150 ns (Setif et al. 1993; Brettel, K. et al. 1999). These two phases have been proposed to represent electron transfer from A_{1B} and A_{1A} to F_X respectively. Both molecules have been suggested to be active during electron transfer reactions. However, quantitative treatments reveal slightly different kinetics in eukaryotes and prokaryotes (Guergova-Kuras et al. 2001; Hastings et al. 2001b; Muhiuddin et al. 2001; Purton et al. 2001; Rigby et al. 2002; Fairclough et al. 2003; Xu et al. 2003a; Xu et al. 2003b; Cohen et al. 2004; Ramesh et al. 2004; Dashdorj et al. 2005; Santabarbara et al. 2005a; Santabarbara et al. 2005b; Ali et al. 2006; Li et al. 2006; Santabarbara et al. 2006). A_1 has the lowest known redox potential of any quinone found in nature. Substitution of the A_1 phylloquinone with other quinones such as ubiquinone give a reduction in midpoint potential of up to 300 mV (Iwaki et al. 1994; Itoh et al. 2001). The redox potential measured for phylloquinone in DMF is -581 mV (Prince et al. 1983). These results suggest that protein interactions at the A_1 site lower the midpoint potential of the quinone bound. The protein binding pocket consists of a conserved tryptophan within π-π stacking distance, with the ring planes being almost parallel, and an asymmetric hydrogen bond to the C_4O carbonyl group from the amide backbone of Leu (Jordan et al. 2001; Grotjohann et al. 2005). Recent studies have also revealed an aspartate residue which may interact

electrostatically with A_1 (Feldman et al. 2007). Figure 6 depicts the noncovalent interactions of the A_1 binding site in PSI.

The protein environment of A_1 in PSI has been compared to the Q_A binding site in the bacterial reaction center. In this system, a tryptophan residue is within π-π stacking distance to the quinone. The bacterial reaction center also contains a hydrogen bond to the C_4O group of Q_A, however a second hydrogen bond is observed at the C_1O position as well. One method applied to the study of the secondary electron acceptor in PSI and the bacterial reaction center is EPR spectroscopy. This technique has determined hyperfine coupling (hfc) tensors of the protons of the two quinones. Drastically different hfc tensors have been measured for the two molecules, illustrating the difference in protein interactions during reduction, and protein dynamics during electron transfer in PSI and the bacterial reaction center (Van der Est et al. 1997).

1.5 Terminal Electron Donor: P_{700}

P_{700}, the terminal electron donor of PSI, is comprised of two chl molecules designated P_B and P_A. The difference between the chl molecules comprising P_{700} arises from the stereochemistry at the 13^2 carbon position. An examination of the protein environment of the two halves of the dimer reveals an asymmetric hydrogen bonding pattern. P_A's keto group is known to be involved in a hydrogen bonding network with a conserved threonine (Thr 743). A water molecule and tyrosine (Tyr 603) complete the network, which also involves the ester group of P_A (Fromme et al. 2001; Jordan et al. 2001; Pantelidou et al. 2004). The corresponding protein environment around P_B lacks hydrogen bond donors to the carbonyl or ester group of P_B. Comparing the midpoint

potential of P_{700} to chl in solution reveals a 400mV decrease in redox potential of the terminal electron donor (Wasielewski et al. 1981). The hydrogen bonding network of P_A has been implicated to modulate the redox properties.

EPR studies of P_{700}^+ have revealed the spin density is mainly localized on the P_B half of P_{700}, and that P_A carries little to no charge density (Kaess et al. 1995; Kaess et al. 2001). The lack of spin density delocalization of the dimer might be the result of small coupling between the two chl molecules, or because the energetic difference between the two chls is rather large. In contrast, FTIR studies have concluded the spin density is equally shared between P_B and P_A (Breton et al. 1999; Breton et al. 2002).

Reduction of P_{700}^+ to P_{700} is catalyzed by plastocyanin or cytochrome c in cyanobacteria. Unlike eukaryotes, which form a transient complex with plastocyanin, in cyanobacteria, PSI interacts with plastocyanin or cytochrome c by following a collisional reaction mechanism, with no formation of any kinetically detectable transient complex *in vitro* (Bottin et al. 1985; Drepper et al. 1996; Hervas et al. 1996; Hippler et al. 1996). However, recent *in vivo* studies of whole cells have indicated a transient complex of PSI with cytochrome c. The interaction between plastocyanin and PSI is believed to proceed through long-range electrostatic interactions and hydrophobic contacts during random collisions. In both plastocyanin and cytochrome c, there is a large flat hydrophobic surface around the redox centers. Mutations to residues residing in this hydrophobic patch have revealed this area is essential for electron transfer to PSI (Sigfridsson et al. 1997; Young et al. 1997; Sigfridsson et al. 1998; Xue et al. 1998).

The subunits PsaA and PsaB contain extra-membrane luminal loops that have been reported to be important for interactions with plastocyanin (Navarro et al. 2000; Fromme et al. 2003). In eukaryotes, the subunit PsaF has an amphipatic helix consisting of basic residues facing the binding site of plastocyanin (Hippler et al. 1998; Sommer et al. 2006). In contrast to eukaryotic organisms, the cyanobacterium *Synechocystis* sp PCC 6803 does not require the PsaF subunit for efficient electron transfer from plastocyanin or cytochrome c to PSI (Van Der Est et al. 2004). Therefore, PsaA and PsaB are solely responsible for interacting with plastocyanin and cytochrome c in cyanobacteria. Mutation studies of the luminal J loop of the PsaB protein from cyanobacteria demonstrated the importance of the loop in interacting with soluble electron donor proteins (Fromme et al. 2003).

Two conserved tryptophan residues have been reported to be important in electron transfer from plastocyanin to P_{700}^{+}. Mutation studies in *Chlamydomonas reinhardtii* show both tryptophan molecules are crucial for high affinity binding of plastocyanin and cytochrome c to PSI (Sommer et al. 2004). These two Trp residues are within π-π stacking distance and are located in the proposed binding pocket of the soluble electron carriers to PSI (Fromme et al. 2003).

1.6 Iron Sulfur Clusters: F_X, F_A and F_B

PSI contains three iron sulfur clusters: F_X, F_A and F_B. Before the crystal structure was resolved to 2.5 Å, and the arrangement of cofactors was resolved, it was difficult to distinguish spectroscopically among the three iron sulfur clusters (Brettel, K. et al. 2001; Vassiliev et al. 2001). F_X is bound by the subunits PsaA and PsaB, (Figure 3A) while F_A

and F_B are bound to the PsaC subunit located on the stromal side of the membrane (Figure 3B). F_X is reduced by the phylloquinone molecule A_1^-, and is oxidized by the iron-sulfur cluster F_A. The terminal electron acceptor of PSI F_B, which mediates electron transfer to ferredoxin, by oxidizing F_A^-.

The reduction potential for F_X measured by reductive titration of PSI by low temperature EPR spectroscopy was found to be -705 ± 15 mV ((Vassiliev et al. 2001) and references therein). Higher values of -670 mV using room temperature optical spectroscopy were reported in PSI samples that did not contain the iron-sulfur clusters F_A and F_B (Parrett et al. 1989). The protein interactions that make F_X one of the most electronegative iron-sulfur clusters is not well understood.

Electron transfer from F_X^- to F_A occurs in about 200 ns ((Brettel, K. et al. 2001; Vassiliev et al. 2001) and references therein). The midpoint potential of F_A, measured by low temperature EPR studies, was found to be -540 mV and -590 mV for F_B. However, a different technique, employing optical detection of charge recombination between the F_A, F_B and P_{700}, measured a midpoint potential of -440 mV for F_B and -465 mV for F_A ((Vassiliev et al. 2001) and references therein). The range of redox potentials comes from the different techniques used in the studies. Both techniques required the pre-reduction of F_A to measure the redox potential of F_B. Furthermore, neither study used PSI samples containing ferredoxin, which may influence the redox potential of F_B. Binding of ferredoxin may decrease the reduction potential of F_B. This mechanism may avoid reducing oxygen, which is potentially harmful to PSI (Setif 2001).

1.7 Interaction of PSI with Ferredoxin and Flavodoxin

Electrons from PSI are transferred to the iron sulfur protein ferredoxin in the microsecond time regime ((Setif 2001) and references therein). Flavodoxin may substitute for ferredoxin in cyanobacteria and some algae under iron limiting conditions. Ferredoxin reduces ferredoxin-$NADP^+$ reductase, which acts in reducing $NADP^+$ to form NADPH. The subunits PsaC, PsaD, and PsaE, located on the stromal side of the membrane, participate in the docking of ferredoxin/flavodoxin. A patch of basic residues on the PsaD, PsaA and PsaE subunits has been suggested to be the docking site for ferredoxin (Fromme et al. 2001; Grotjohann et al. 2005). Mutagenesis studies along with chemical crosslinking experiments have shown direct evidence for the interaction of ferredoxin to this docking site (Zanetti et al. 1987; Zilber et al. 1988; Wynn et al. 1989; Andersen et al. 1992; Lelong et al. 1994; Fischer et al. 1998). Upon binding to PSI, it has been postulated that ferredoxin modulates the redox potential of F_B for efficient electron transfer between the proteins.

1.8 Fourier-Transform Infrared Spectroscopy

Vibrational spectroscopy such as Fourier transform-infrared (FT-IR) spectroscopy is a highly sensitive technique used to obtain information about enzymatic reactions, dynamics, and structure. For membrane-bound proteins, such as PSI, it is one of the few techniques sensitive enough to identify changes accompanied with charge separation. An FT-IR spectrum reflects important information concerning amino acid side chains such as charge, hydrogen bonding, conformation, and the protein environment of cofactors. For a diatomic molecule, the vibrational frequency is proportional to the reduced masses of the

atoms that are involved in the chemical bond, as well as the bond strength. Assignment of the stretching frequencies of the molecule can be approximated with the application of Hooke's law in which the bond connecting the two atoms together is regarded as a spring. The system is treated as a simple harmonic oscillator (Wilson et al. 1980).

However, larger molecules consisting of more than two atoms have 3N-6 vibrations, where N is the number of atoms comprising the molecule (Wilson et al. 1980). Normal mode of vibrations of molecules consists of each atom of the molecule oscillating about its equilibrium position in space by simple harmonic motion (outlined above). When the frequency and phase of the motion of the atoms are the same, each atom will reach its maximum displacement position at the same time. Furthermore, each atom will pass through its equilibrium at the same time. The position and momentum of the atoms can be represented by vectors and theoretical calculations of the vibrational frequencies of molecule can be calculated. Density functional theory (DFT) is a quantum mechanical theory used to describe the electronic structure of a molecule. DFT calculations describe normal mode vibrations of a molecule and are able to predict frequencies, amplitudes, and isotope shifts of the molecule. In DFT calculations, the electronic state of the molecule can be described as a wavefunction, satisfying the many-electron Shrödinger equation. Gaussian basis sets are functions used as atomic orbitals for the computation of electron orbitals in molecules. The Gaussian basis DFT method breaks down the Hamiltonian described in the wavefunction into basic one-electron and two electron components, which can be solved by computational chemistry (Lewer 2003).

Vibrational transitions are narrow in line-shape; however in non-homogeneous mixtures, such as proteins, the lineshape will broaden due to the multiple vibrations

contributing to the absorption spectrum. Difference FT-IR spectroscopy is technique that simplifies a rather complex spectrum. To obtain a difference spectrum, an absorption spectrum is obtained before and after the reaction has occurred. These spectra are subtracting from one another, the resulting spectrum consists of frequencies that were perturbed due to the reaction. Those vibrational frequencies not affected will be subtracted from the difference spectrum. Light-induced difference spectroscopy is a technique able to monitor the oxidized and reduced states of PSI electron-transfer cofactors. Detection of changes in the electronic structure is possible because of the high signal to noise and internal frequency calibration of FT-IR spectrophotometers (Kim et al. 1998; Breton et al. 1999)

Although the FT-IR spectrum is characteristic to an entire molecule, certain groups of atoms give rise to characteristic frequencies regardless of the structure of the rest of the molecule. Therefore, these characteristic bands can be used as molecular probes of the system. One application that has been widely used in the study of photosynthetic proteins is isotope incorporation into amino acids or cofactors involved in electron transfer reactions. IR frequencies are dependent on the reduced masses of the atoms involved; therefore FT-IR spectroscopy is a technique that is sensitive to isotope incorporation. Previous studies have incorporated various isotopes into the electron donor and acceptor molecules of PSI (Kim et al. 2000; Hastings et al. 2001a; Hastings et al. 2001b). Isotope-edited spectra have been invaluable in the study of electron transfer in various photosystems and bacterial reaction centers (Rothschild et al. 1981; Rothschild et al. 1982; MacDonald et al. 1993; Breton et al. 1994; Breton 1997).

1.9 Thesis Outline

To gain greater knowledge about protein dynamics and electron cofactor interactions, isotope labeling of amino acid side chains, electron acceptors, and electron donors of PSI was performed to generate isotope-edited spectra. The spectra presented here will have contributions for only those groups perturbed by the isotope incorporation, and light-induced electron transfer. The results presented here have shown profound effects on protein environment of the vibration spectra of the electron cofactors of PSI, and have given novel insight into protein dynamic effects on electron transfer.

In this thesis, light-induced Fourier-transform infrared (FT-IR) spectroscopy is utilized to probe the spectroscopic properties of the secondary electron acceptor, A_1, the terminal electron donor, P_{700}, and protein dynamics during light-induced electron transfer. This work utilizes isotope incorporation into particular functional groups of the cofactors and amino acids. Chapter 2 reviews the biosynthetic pathway of chl, phylloquinone and the aromatic amino acids. The particular steps in the biosynthetic pathways that were utilized to incorporate the isotopes are also discussed. In Chapter 3, the isotope-edited vibrational spectrum of A_1^--minus-A_1 is presented. Bands arising from the reduced and oxidized forms of A_1 are assigned, and the effects of protein interactions with A_1 are discussed.

Chapter 4 described the spectroscopic studies performed on the terminal electron donor P_{700}. Assignments for the reduced and oxidized forms of P_{700} are discussed, as well as protein dynamics associated with oxidation of P_{700}. These studies are very important because they suggest novel protein dynamics that may be associated with

charge transfer from plastocyanin to PSI. An examination of the protein dynamics associated with the PsaA and PsaB subunits is given in Chapter 5. Isotope-edited spectra of amino acid side chains perturbed doing electron transfer are analyzed and a discussion of the importance of the protein dynamics is presented.

1.10 References

Ali, K., S. Santabarbara, P. Heathcote, M. C. W. Evans and S. Purton (2006). "Bidirectional electron transfer in photosystem I: replacement of the symmetry-breaking tryptophan close to the PsaB-bound phylloquinone A_{1B} with a glycine residue alters the redox properties of A_{1B} and blocks forward electron transfer at cryogenic temperatures." *Biochim Biophys Acta* **1757**: 1623-1633.

Andersen, B., B. Koch and H. V. Scheller (1992). "Structural and functional analysis of the reducing side of Photosystem I." *Plant Cell Physiology* **84**: 154-161.

Bottin, H. and P. Mathis (1985). "Interaction of plastocyanin with the photosystem I reaction center: a kinetic study by flash absorption spectroscopy " *Biochemistry* **24**: 6453-6460.

Breton, J. (1997). "Efficient exchange of the primary quinone acceptor Q_A in isolated reaction centers of *Rhodopsuedomonas viridis*." *Proc. Natl. Acad. Sci. USA* **94**: 11318-11323.

Breton, J., C. Boullais, J. R. Burie, E. Nabedryk and C. Mioskowski (1994). "Binding sites of quinones in photosynthetic bacterial reaction centers investigated by light-induced FTIR difference spectroscopy: assignment of the interactions of each carbonyl of Q_A in Rhodobacter sphaeroides using site-specific ^{13}C-labeled ubiquinone." *Biochemistry* **33**: 14378-14386.

Breton, J., E. Nabedryk and W. Leibl (1999). "FTIR study of the primary electron donor of photosystem I (P_{700}) revealing delocalization of the charge in P_{700}^+ and localization of the triplet character in $^3P_{700}$." *Biochemistry* **38**: 11585-11592.

Breton, J., W. Xu, B. A. Diner and P. R. Chitnis (2002). "The two histidine axial ligands of the primary electron donor chlorophylls (P_{700}) in photosystem I are similarly perturbed upon P_{700}^+ formation." *Biochemistry* **41**: 1200-1210.

Brettel, K. (1997). "Electron transfer and arrangement of the redox cofactors in Photosystem I." *Biochim. Biophys. Acta* **1318**: 322-373.

Brettel, K. and W. Leibl (2001). "Electron transfer in photosystem I." *Biochim. Biophys. Acta* **1507**: 100-114.

Brettel, K. and M. H. Vos (1999). "Spectroscopic resolution of the picosecond reduction kinetics of the secondary electron acceptor A_1 in photosystem I." *FEBS Letters* **447**: 315-317.

Cohen, R. O., G. Shen, J. H. Golbeck, W. Xu, P. R. Chitnis, A. I. Valieva, A. van der Est, Y. Pushkar and D. Stehlik (2004). "Evidence for asymmetric electron transfer in

cyanobacterial photosystem I: analysis of a methionine-to-luecine mutation of the ligand to the primary electron acceptor A_0." *Biochemistry* **43**: 4741-4754.

Dashdorj, N., W. Xu, R. O. Cohen, J. H. Golbeck and S. Savikhin (2005). "Asymmetric electron transfer in cyanobacterial Photosystem I: charge separation and secondary electron transfer dynamics of mutations near the primary electron acceptor A_0." *Biophys. J.* **88**: 1238-1249.

Diner, B. A. and F. Rappaport (2002). "Structure, dynamics, and energetics of the primary photochemistry of Photosystem II of oxygenic photosynthesis." *Annual Review of Plant Biology* **23**.

Drepper, F., M. Hippler, W. Nitschke and W. Haehnel (1996). "Binding dynamics and electron transfer between plastocyanin and photosystem I." *Biochemistry* **35**: 1282-1295.

Fairclough, W. V., A. Forsyth, M. C. W. Evans, M. C. Evans, S. E. J. Rigby, S. Purton and P. Heathcote (2003). "Bidirection electron transfer in photosystem I: electron transfer on the PsaA side is not essential for phototrophic growth in *Chlamydomonas*." *Biochim. Biophys. Acta* **1606**: 43-55.

Feldman, K. S., D. K. Hester 2nd and J. H. Golbeck (2007). "A relationship between amide hydrogen bond strength and quinone reduction potential: Implications for photosystem I and bacterial reaction center quinone function." *Bioorg. Med. Chem. Lett.* **17**: 4891-4894.

Fischer, N., M. Hippler, P. Setif, J.-P. Jacqout and J. D. Rochaix (1998). "The PsaC subunit of Photosystem I provides an essential lysine residue for fast electron transfer to ferredoxin." *EMBO Journal* **17**: 849-858.

Fromme, P., P. Jordan and N. Krauss (2001). "Structure of photosystem I." *Biochim Biophys Acta* **1507**: 5-31.

Fromme, P., A. Melkozernv, P. Jordan and N. Krauss (2003). "Structure and function in Photosystem I: interaction with its soluble electron carriers and external antenna systems." *FEBS Letters* **555**: 40-44.

Groot, M. L., N. P. Pawlowicz, L. J. van Wildren, J. Breton, I. H. van Stokkum and R. van Grondelle (2005). "Initial electron donor and acceptor in isolated Photosystem II reaction centers identified with femtosecond mid-IR spectroscopy." *Proc. Natl. Acad. Sci. USA* **102**: 13087-13092.

Grotjohann, I. and P. Fromme (2005). "Structure of cyanobacterial photosystem I." *Photosynth. Res.* **85**: 51-72.

Guergova-Kuras, M., B. Boudreaux, A. Joliot, P. Joliot and K. Redding (2001). "Evidence for two active branches for electron transfer in photosystem I." *Proc. Natl. Acad. Sci. USA* **98**: 4437-4442.

Hastings, G., V. M. Ramesh, R. Wang, V. Sivakumar and A. Webber (2001a). "Primary donor photo-oxidation in photosystem I: a re-evaluation of (P_{700}^+ - P_{700}) Fourier transform infrared difference spectra." *Biochemistry* **40**: 12943-12949.

Hastings, G. and V. Sivakumar (2001b). "A Fourier transform infrared absorption difference spectrum associated with the reduction of A_1 in Photosystem I: are both phylloquinones involved in electron transfer?" *Biochemistry* **40**: 3681-3689.

Hecks, B., K. Wulf, J. Breton, W. Leibl and H.-W. Trissl (1994). "Primary charge separation in Photosystem I: a two-step electrogenic charge separation connected with $P_{700}^+A_0^-$ and $P_{700}^+A_1^-$ formation." *Biochemistry* **447**: 8619-8624.

Hervas, M., J. A. Navarro, A. Diaz and M. A. De la Rosa (1996). "A comparative thermodynamic analysis by laser-flash absorption spectroscopy of Photosystem I reduction by plastocyanin and cytochrome c_6 in *Anabaena* PCC 7119, *Synechocystis* PCC 6803, and spinach." *Biochemistry* **35**: 2693-2698.

Hippler, M., F. Drepper, W. Haehnel and J. D. Rochaix (1998). "The N-terminal domain of PsaF: Precise recognition site for binding and fast electron transfer from cytochrome c(6) and plastocyanin to photosystem I of *Chlamydomonas reinhardtii*." *Proc. Natl. Acad. Sci. USA* **95**: 7339-7344.

Hippler, M., J. Reichert, M. Sutter, E. Zak, L. Altschmied, U. Schroer, R. G. Herrmann and W. Haehnel (1996). "The plastocyanin binding domain of Photosystem I." *EMBO Journal* **15**: 6374-6384.

Holzwarth, A. R., M. G. Muller, J. Niklas and W. Lubitz (2006). " Ultrafast transient absorption studies on photosystem I reaction centers from *Chlamydomonas reinhardtii*. 2: Mutations near the P_{700} reaction center chlorophylls provide new insight into the nature of the primary electron donor." *Biophys. J.* **90**: 552-565.

Itoh, S., M. Iwaki and I. Ikegami (2001). "Modification of photosystem I reaction center by the extraction and exchange of chlorophylls and quinones." *Biochim. Biophys. Acta* **1507**: 115-138.

Iwaki, M. and S. Itoh (1994). "Reaction of reconstituted acceptor quinone and dynamic equilibration of electron transfer in the Photosystem I reaction center." *Plant Cell Physiol.* **35**: 983-993.

Jordan, P., P. Fromme, H. T. Witt, O. Klukas, W. Saenger and N. Krauss (2001). "Three-dimensional structure of cyanobacterial photosystem I at 2.5A resolution." *Nature* **411**: 909-917.

Kaess, H., E. Biitersmann-Weidlich, L.-E. Andreasson, B. Boenigk and W. Lubitz (1995). "ENDOR and ESEEM of the ^{15}N labeled radical cations of chlorophyll and the primary donor P_{700} in photosystem I." *Chem. Phys.* **194**: 419-432.

Kaess, H., P. Fromme, H. T. Witt and W. Lubitz (2001). "Orientation and electronic structure of the primary donor radical cation P_{700}^{+} in photosystem I: a single crystal EPR and ENDOR study." *J. Phys. Chem. B* **105**: 1225-1239.

Kim, S. and B. A. Barry (1998). "The protein environment surrounding tyrosyl radicals D· and Z· in photosystem II: a difference Fourier-transform infrared spectroscopic study." *Biophys. J.* **74**: 2588-2600.

Kim, S. and B. A. Barry (2000). "Identification of carbonyl modes of P_{700} and P_{700}^{+} by in situ chlorophyll labeling in photosystem I." *J. Am. Chem. Soc.* **122**: 4980-4981.

Lelong, C., P. Setif, B. Lagoutte and H. Bottin (1994). "Identification of the amino acids involved in the functional interaction between photosystem I and ferredoxin from *Synechocystis* sp. PCC 6803 by chemical crosslinking." *J. Biol. Chem.* **269**: 10034-10039.

Lewer, E. (2003) *Computational Chemistry:Introduction to the Theory and Applications of Molecular and Quantum Mechanics.* Norwell, Kluwer Academic Publisher.

Li, Y., A. van der Est, M. G. Lucas, V. M. Ramesh, F. Gu, A. Petrenko, S. Lin, A. N. Webber, F. Rappaport and K. Redding (2006). "Directing electron transfer within Photosystem I by breaking H-bonds in the cofactor branches." *Proc. Natl. Acad. Sci. USA* **103**: 2144-2149.

MacDonald, G. M., K. A. Bixby and B. A. Barry (1993). "A difference Fourier-transform infrared study of two redox-active tyrosine residues in photosystem II." *Proc. Natl. Acad. Sci. USA* **90**: 11024-11028.

Muhiuddin, I. P., P. Heathcote, S. Carter, S. Purton, S. E. J. Rigby and M. C. W. Evans (2001). "Evidence from time resolved studies of the P_{700}^{+}/A_1^{-} radical pair for photosynthetic electron transfer on both the PsaA and PsaB branches of the photosystem I reaction centre." **503**: 56-60.

Navarro, J. A., M. Hervas, J. Sun, B. De la Cerda, P. R. Chitnis and M. A. De la Rosa (2000). "Negatively charged residues in the H loop of PsaB subunit in Photosystem I from *Synechocystis* sp PCC 6803 appear to be responsible for electrostatic repulsions with plastocyanin." *Photosynth. Res.* **65**: 63-68.

Pantelidou, M., P. R. Chitnis and J. Breton (2004). "FTIR spectroscopy of *Synechocystis* 6803 mutants effected on the hydrogen bonds to the carbonyl groups of the PsaA chlorophyll of P_{700} supports an extensive delocalization of the charge in P_{700}^{+}." *Biochemistry* **43**: 8380-8390.

Parrett, K. G., T. Mehari, P. G. Warren and J. H. Golbeck (1989). "Purification and properties of the intact P_{700} and F_X containing Photosystem I core protein." *Biochim Biophys Acta* **973**: 324-332.

Prince, R.C., P. Dutton, L. Bruce, J. Malcolm (1983). "Electrochemistry of ubiquinones. Menoquinones and plastoquinones in aprotic solvents." *FEBS Letters* **160: 273-276.**

Purton, S., D. R. Stevens, I. P. Muhiuddin, M. C. W. Evans, S. Carter, S. E. J. Rigby and P. Heathcote (2001). "Site-directed mutagenesis of PsaA residue W693 affects phylloquinone binding and function in the photosystem I reaction center of *Chlamydomonas reinhardtii*." *Biochemistry* **40**: 2167-2175.

Ramesh, V. M., K. Gibasiewicz, S. Lin, S. E. Bingham and A. N. Webber (2004). "Bidirectional electron transfer in photosystem I: accumulation of A_0^- in A-side or B-side mutants of the axial ligand to chlorophyll A_0." *Biochemistry* **43**: 1369-1375.

Ramesh, V. M., K. Gibasiewicz, S. Lin, S. E. Bingham and A. N. Webber (2007). "Replacement of the methionine axial ligand to the primary electron acceptor A0 slows the A_0^- reoxidation dynamics in photosystem I." *Biochim Biophys Acta* **1767**: 151-160.

Rigby, S. E. J., I. P. Muhiuddin, M. C. W. Evans, S. Purton and P. Heathcote (2002). "Photoaccumulation of the PsaB phyllosemiquinone in photosystem I of *Chlamydomonas* reinhardtii." *Biochim. Biophys. Acta* **1556**: 13-20.

Rothschild, K. J. and H. Marrero (1982). "Infrared evidence that the Schiff base of bacteriorhodopsin in protonated: bR570 and K intermediates." *Proc. Natl. Acad. Sci. USA* **79**: 4045-4049.

Rothschild, K. J., M. Zagaeski and W. A. Cantore (1981). "Conformational changes of bacteriorhodopsin detected by Fourier transform infrared difference spectroscopy." *Biochem. Biophys. Res. Commun.* **103**.

Santabarbara, S., P. Heathcote and M. C. Evans (2005a). "Modeling of the electron transfer reactions in Photosystem I by electron tunneling theory: the phylloquinones bound to the PsaA and the PsaB reaction centre subunits of PS I are almost isoenergetic to the iron-sulfur cluster F_X." *Biochim Biophys Acta* **1708**: 283-310.

Santabarbara, S., I. Kuprov, W. V. Fairclough, S. Purton, P. J. Hore, P. Heathcote and M. C. W. Evans (2005b). "Bidirectional electron transfer in photosystem I: determination of two distances between P_{700}^+ and A_1^- in spin-correlated radical pairs." *Biochemistry* **44**: 2119-2128.

Santabarbara, S., I. Kuprov, P. J. Hore, A. Casal, P. Heathcote and M. C. Evans (2006). "Analysis of the spin-polarized electron spin echo of the P_{700}^+ A_1^- radical pair of photosystem I indicates that both reaction center subunits are competent in electron transfer in cyanobacteria, green algae, and higher plants." *Biochemistry* **45**: 7389-7403.

Setif, P. (2001). "Ferredoxin and flavodoxin reduction in Photosystem I." *Biochimica Biophysica Acta* **1507**: 161-179.

Setif, P. and K. Brettel (1993). "Forward electron transfer from phylloquinone A_1 to iron-sulfur centers in spinach photosystem I." *Biochemistry* **32**.

Sigfridsson, K., S. Young and O. Hansson (1997). "Electron transfer between spinach plastocyanin mutants and photosystem 1." *Eur. J. Biochem.* **245**: 805-812.

Sigfridsson, K., S. Young and O. Hansson (1998). "Electron transfer between spinach plastocyanin mutants and photosystem 1 (vol 245, pg 805, 1998)." *Eur. J. Biochem.* **255**: 324-324.

Sommer, F., F. Drepper, W. Haehnel and M. Hippler (2004). "The hydrophobic recognition site formed by residues PsaA-Trp651 and PsaB-Trp627 of photosystem I in *Chlamydomonas reinhardtii* confers distinct selectivity for binding of plastocyanin and cytochrome c6." *J. Biol. Chem.* **279**: 20009-20017.

Sommer, F., F. Drepper, W. Haehnel and M. Hippler (2006). "Identification of precise electrostatic recognition sites between cytochrome c(6) and the photosystem I subunit PsaF using mass spectrometry." *J. Biol. Chem.* **281**: 35097-35103.

Van der Est, A., T. Prisner, R. Bittl, P. Fromme, W. Lubitz, K. Mobius and D. Stehlik (1997). "Time-resolved X-, K-, and W-Band EPR of the radical pair State $P_{700}^{+}A_1^{-}$ of Photosystem I in comparison with $P_{865}^{+}Q^{-}$ in bacterial reaction centers." *J. Phys. Chem. B* **101**: 1437-1443.

Van Der Est, A., A. I. Valieva, Y. E. Kandrashkin, G. Shen, D. A. Bryant and J. H. Golbeck (2004). "Removal of PsaF alters forward electron transfer in photosystem I: evidence for fast reoxidation of QK-A in subunit deletion mutants of *Synechococcus* sp. PCC 7002." *Biochemistry* **43**: 1264-1275.

Vassiliev, I. R., M. L. Antonkine and J. H. Golbeck (2001). "Iron-sulfur clusters in type I reaction centers." *Biochimica Biophysica Acta* **1507**: 139-160.

Wasielewski, M., J. Norris, L. Shipman, C. Lin and W. Svec (1981). "Monomeric chlorophyll a enol: evidence for its possible role as the primary electron donor in photosystem I of plant photosynthesis." *Proc. Natl. Acad. Sci. USA* **78**: 2957-2961.

Wilson, E. B., J. C. Decium and P. C. Cross (1980). *Molecular Vibrations: The theory of infrared and Raman vibrational spectra*. New York, Dover Publications Inc.

Wynn, R. M., J. Omaha and R. Malkin (1989). "Structural and functional properties of the cyanobacterial Photosystem I complex." *Biochemistry* **28**: 5554-5560.

Xu, W., P. Chitnis, A. Valieva, A. van der Est, Y. N. Pushkar, M. Krzystyniak, C. Teutloff, S. G. Zech, R. Bittl, D. Stehlik, B. Zybailov, G. Shen and J. H. Golbeck (2003a). "Electron transfer in cyanobacterial photosystem I: I. Physiological and spectroscopic characterization of site-directed mutants in a putative electron transfer pathway from A_0 through A_1 to F_x." *J. Biol. Chem.* **278**: 27864-27875.

Xu, W., P. R. Chitnis, A. Valieva, A. van der Est, K. Brettel, M. Guergova-Kuras, Y. N. Pushkar, S. G. Zech, D. Stehlik, G. Shen, B. Zybailov and J. H. Golbeck (2003b). "Electron transfer in cyanobacterial photosystem I: II. Determination of forward electron

transfer rates of site-directed mutants in a putative electron transfer pathway from A_0 through A_1 to F_x." *J. Biol. Chem.* **278**: 27876-27887.

Xue, Y. F., M. Okvist, O. Hansson and S. Young (1998). "Crystal structure of spinach plastocyanin at 1.7 angstrom resolution." *Protein Sci.* **7**: 2099-2105.

Young, S., K. Sigfridsson, K. Olesen and O. Hansson (1997). "The involvement of the two acidic patches of spinach plastocyanin in the reaction with photosystem I." *Biochim. Biophys. Acta* **1322**: 106-114.

Zanetti, G. and G. Merati (1987). "Identification by chemical crosslinking of the polypeptide which binds ferredoxin." *Eur. J. Biochem.* **169**: 143-146.

Zilber, A. L. and R. Malkin (1988). "Ferredoxin cross-links to a 22 kD subunit of Photosystem I." *Plant Physiol.* **88**: 810-814.

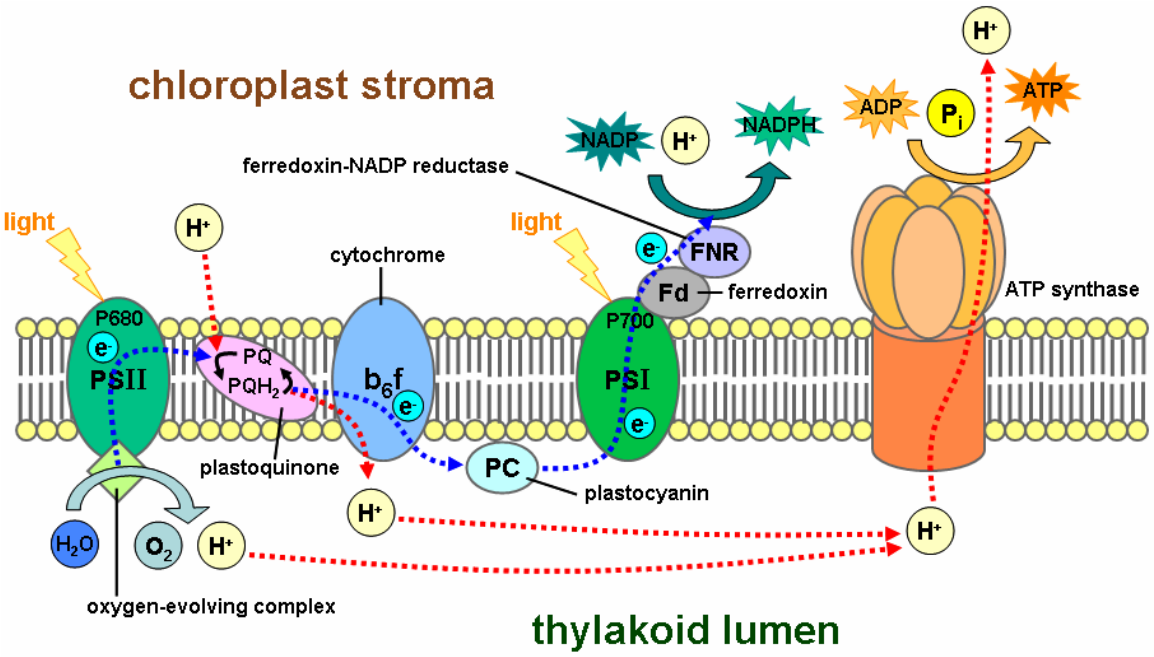

Figure 1. The protein complexes embedded in the thylakoid membrane involved in the light-induced electron transfer reactions in photosynthesis. Stoichiometry of the oxidation of water is not implied. Original figure can be found at http://en.wikipedia.org/wiki/Image:Thylakoid_membrane.png.

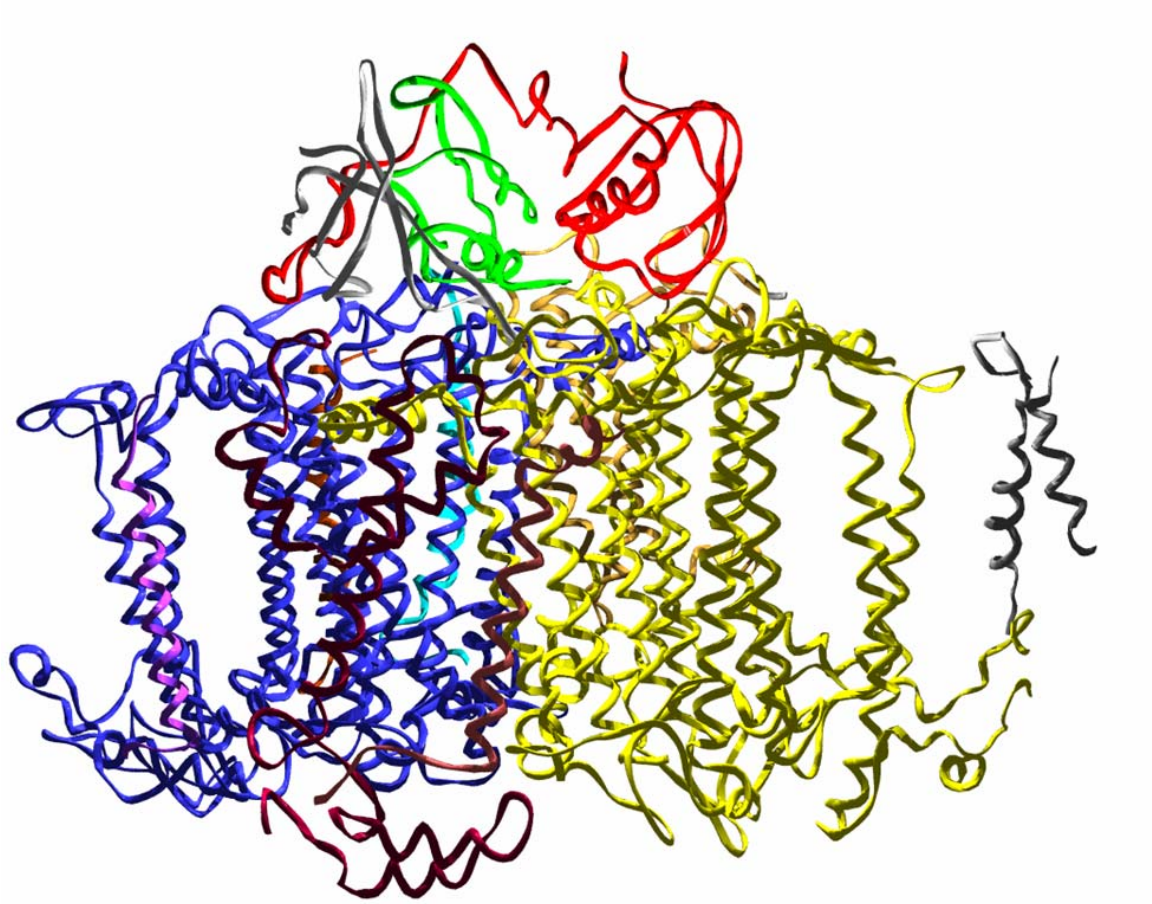

Figure 2. The arrangement of subunits in PSI: PsaA subunit, yellow; PsaB, blue; PsaC, green; PsaD, red; PsaE, grey; PsaF, purple; PsaI, cyan; PsaJ, pink; PsaK, dark grey; PsaL, light brown; and PsaM, dark brown. The figure is reproduced from the 2.5 Å resolution crystal structure of PSI from *S. elongatus* (PDB file accession number 1JB0 (Jordan et al. 2001)) using Swiss-Pdb viewer (v3.7; www.expasy.ch/spdbc) and rendered using POV-Ray (v3.5; www.povray.org).

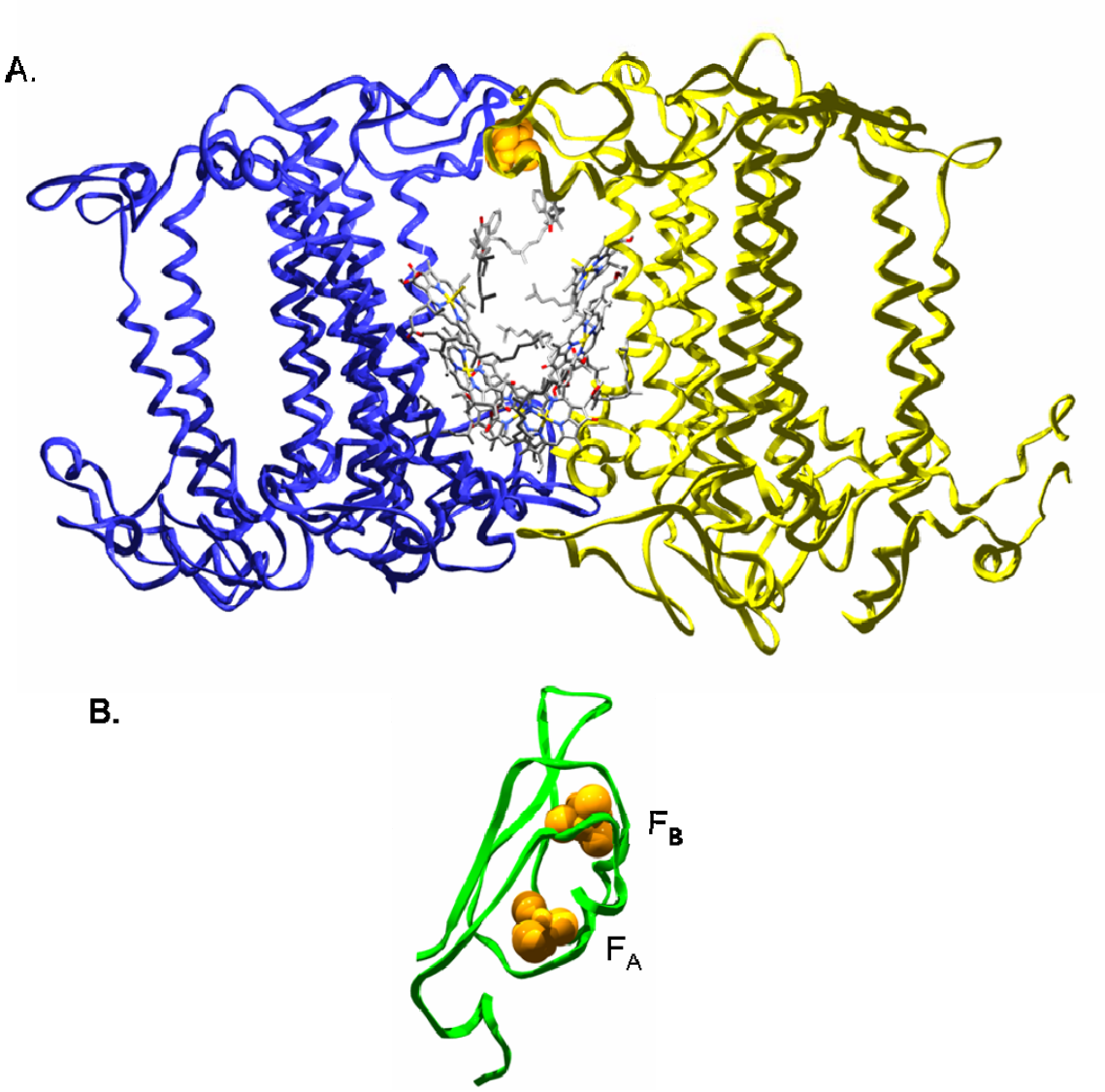

Figure 3. The arrangement of electron cofactors bound to PsaA, PsaB, or PsaC. (A). The PsaA and PsaB subunits that form the heterodimeric core of PSI and the electron transfer molecules bound to each subunit. PsaA is depicted in yellow and PsaB is depicted in blue. The electron transfer cofactors from the luminal side toward the stromal side of the membrane include P_{700}, eC_{A2}, eC_{B2}, eC_{B3}, eC_{A3}, A_{1A}, A_{1B} and F_X. The subscripts designate the subunit which binds the cofactor. F_X is bound to both the PsaA and PsaB subunits. (B). The terminal electron acceptors bound to the PsaC subunit located on the

Figure 3 continued

stromal side of PSI. F_A and F_B are depicted as spherical balls in yellow and the PsaC subunit is colored green. The figure is reproduced from the 2.5 Å resolution crystal structure of PSI from *S. elongatus* (PDB file accession number 1JB0 (Jordan et al. 2001)) using Swiss-Pdb viewer (v3.7; www.expasy.ch/spdbc) and rendered using POV-Ray (v3.5; www.povray.org).

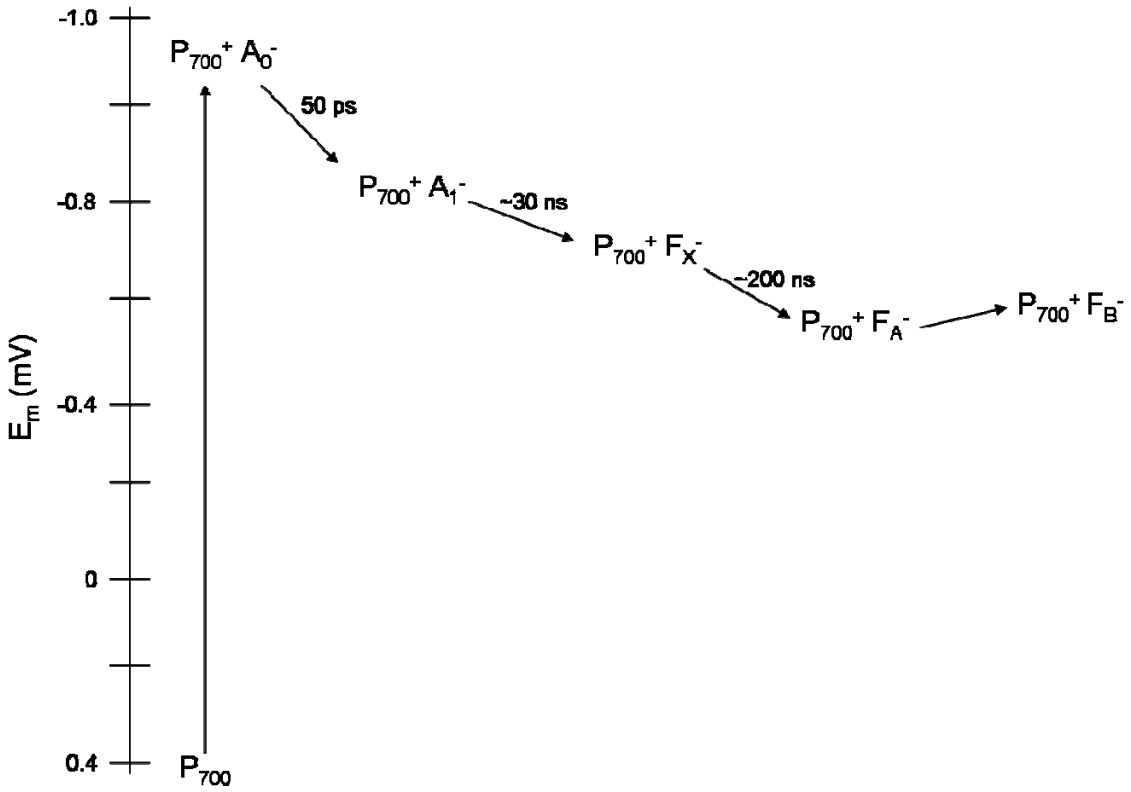

Figure 4. Electron transfer scheme in PSI starting with the radical pair $P_{700}^+ A_0^-$ (Brettel, K. et al. 2001; Vassiliev et al. 2001 and references therein).

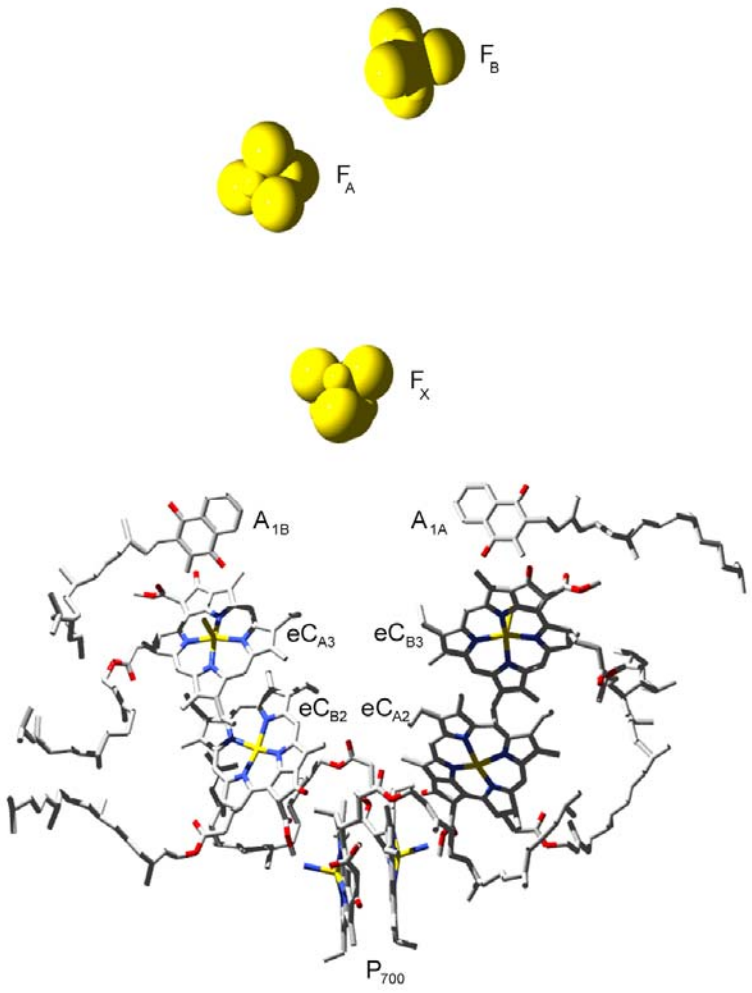

Figure 5. Arrangement of the electron cofactors of PSI. The figure is reproduced from the 2.5 Å resolution crystal structure of PSI from *S. elongatus* (PDB file accession number 1JB0 (Jordan et al. 2001)) using Swiss-Pdb viewer (v3.7; www.expasy.ch/spdbc) and rendered using POV-Ray (v3.5; www.povray.org). The nomenclature of the accessory chl comes from ref (Grotjohann et al. 2005). The subscripts indicate the subunit to which the cofactor is bound.

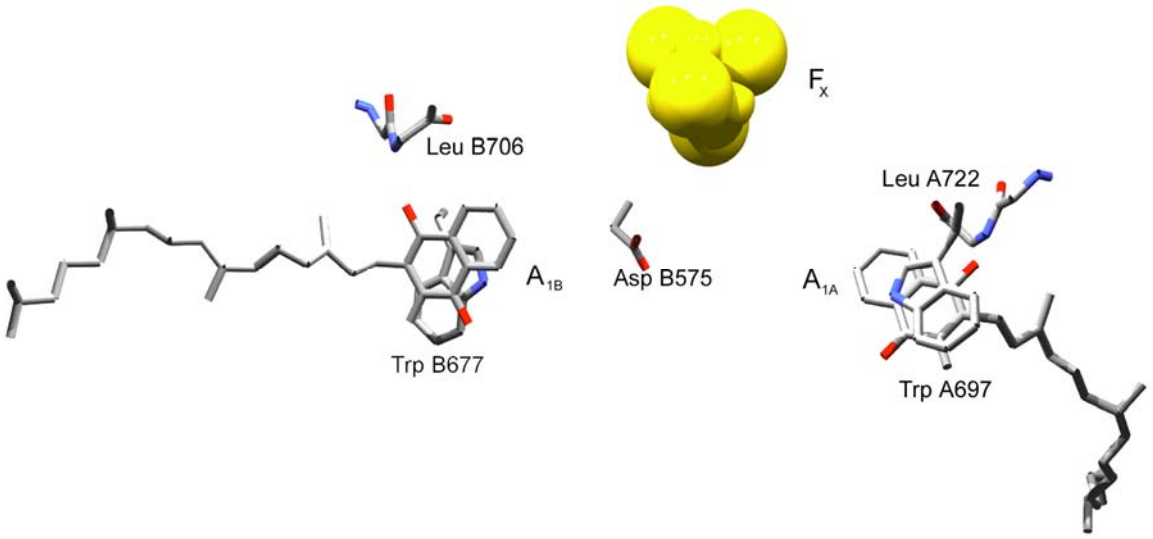

Figure 6. The prominent features of the A_1 binding pocket. Both A_1 molecules are in hydrogen bonding distance to the backbone of a leucine molecule as well as π-stacking distance to a tryptophan residue. The aspartate B575 residue has been implicated in the modulation of the redox potential of A_1.

CHAPTER 2

BIOSYNTHETIC PATHWAYS OF CHLOROPHYLL, PHYLLOQUINONE AND AROMATIC AMINO ACIDS

The research presented in the following chapters applies isotope labeling techniques to characterize protein dynamics during electron transfer in PSI. These labeling techniques utilize the biosynthetic pathways of chlorophyll, phylloquinone, and the aromatic amino acids to specifically isotope label hydrogen, carbon or oxygen atoms. In order to incorporate isotopes into specific positions of the molecules, the biosynthetic pathways were manipulated at precise steps. Here I present a brief overview of the biosynthetic pathways for chlorophyll, phylloquinone and the aromatic amino acids and outline the enzymatic steps that were utilized to incorporate the desired isotope**.**

2.1 Biosynthetic Pathway of Chlorophyll

Chlorophyll contains a tetrapyrrole ring structure known as a prophyrin, common to that found in the heme prosthetic group of hemoglobin and cytochrome. There are several biosynthetic steps shared by chlorophyll and heme, however chlorophyll contains a magnesium atom coordinated by four nitrogen atoms whereas heme binds an iron atom. The biosynthetic pathway of chlorophyll has been elucidated through the use of various biochemical techniques such as isotope labeling, enzyme biochemistry, and mutation studies.((Beale 1999) and references therein).

In all organisms that synthesize tetrapyrroles the universal precursor is aminolevulinic acid (ALA). In animals, the enzyme known as aminolevulinic acid synthase performs three enzymatic steps which convert glycine and succinyl-CoA to ALA (Gibson et al. 1958; Kikuchi et al. 1958). In plants, green algae, and cyanobacteria, there are three enzymes responsible for the production of ALA. The chl biosynthetic pathway begins with glutamic acid, ligated to a tRNA molecule (Beale et al. 1974; Beale et al. 1975; Kannangara et al. 1988). Glutamyl-tRNA synthatase (EC 6.1.1.17) activates glutamate by ligating it to a $tRNA^{glu}$ molecule. Glutamyl tRNA reductase reduces the activated carboxyl group of the $tRNA^{glu}$ to a formyl group; producing glutamate-1-semialdehyde. This step is followed by an amino-exchange reaction, to form δ-aminolevulinic acid (ALA), and is catalyzed by glutamate-1-semialdehyde aminotransferase (EC 5.4.3.8) (Beale 1999). These three enzymatic steps are outlined in Figure 1.

Two molecules of ALA are condensed to form a pyrrole molecule known as porphobilinogen. This step in the chlorophyll biosynthetic pathway is catalyzed by the enzyme ALA dehydratase (Schmidt et al. 1955; Calisson et al. 1966; Nandi et al. 1967). Four molecules of porphobilinogen are combined in the synthesis of 1-hydroxymethylbilane by the enzyme porphobilinogen deaminase; with four molecules of NH_3 being released (Frydman et al. 1970). The next step in the synthesis pathway is the production of the macrocycle ring. The macrocycle ring formation is carried out by the enzyme referred to as uroporphyrinogen III synthase (EC 4.2.1.75) (Hart et al. 1985). This enzyme has undergone intensive studies due to the proposed mechanism of cyclization (Crockett et al. 1991; Beale 1999) and references therein). Uroporphyrinogen

III synthase catalyzes a ring inversion, which interchanges of the carbons that constitute part of the tetrapyrrole ring From Figure 2, the acetate group and propionate group do not simply exchange; instead the enzyme catalyzes a ring flip and subsequent interchange. Uroporhyrinogen III decarboxylase decarboxylates the macrocycle ring, resulting in four molecules of CO_2 to be released. The formation of the macrocycle ring is shown in Figure 2.

Three enzymes are involved in the conversion of uroporphyrinogen III to protoporphyrin IX and are responsible for transforming the molecule from a hydrophilic and photochemically unreactive molecule to a hydrophobic, photochemically active molecule. These reactions are shown in Figure 3. The first two steps in the conversion require oxygen to oxidize multiple single bonds to double bonds on the macrocycle ring, resulting in the production of water and CO_2. These reactions are carried out by coporphyrinogen III oxidase (EC 4.1.1.37) and protoporphyrinogen IX oxidase (EC 1.3.34) to produce protoporphyrin IX (Jacobs et al. 1979; Hart et al. 1985; Robinson et al. 1985). The reactions outlined above to form protoporphyrin IX are common to both plants and animals. Although the synthesis of ALA differs, the reactions that convert ALA to protoporphyrin are common to both groups of organisms. To form a heme molecule, ferrochelatase (EC 4.99.1) inserts an iron atom into the center of protoporphyrin IX. In plants and cyanobacteria, magnesium chelatase is responsible for the addition of a magnesium atom into the center of protoporphyrin IX, as shown in Figure 3 (Gorchein 1972; Walker et al. 1991).

Once the magnesium has been incorporated into the macrocycle ring, a methyl group is added to the 13^2 carboxyl group to form an ester by the enzyme Mg-

protporphyrin IX methyltransferase (EC 2.1.1.11) (Figure 4) (Ellswort et al. 1972). This enzyme uses the substrate *S*-adenosylmethionine as the methyl donor. Previous studies have used this step to incorporate C^2H_3 at this carbon position (Kim et al. 2000). This was accomplished by growing methionine tolerant *Synechocystis* supplemented with *L*-C^2H_3-methionine. After the methyl group has been added to the macrocycle, the fifth ring is formed.

Figure 4 depicts the last steps of the chl biosynthesis pathway. The fifth ring is formed by an oxygen dependent cyclase; the mechanism of which is not well understood. The cyclase catalyzes carbon bond formation as well as the oxidation of the 13^1 carbon to a carbonyl, using O_2 as a substrate (Bollivar et al. 1995, 1996). Further processing of the macrocycle is accomplished by 8-vinyl reductase which reduces a double bond on the 8^2 carbon to a single bond to produce monovinyl protochlorophyllide a, and uses the oxidation of NADPH to $NADP^+$ to drive the reaction to completion. The reduction of ring IV by protochlorophyllide oxidoreductase (EC 1.3.1.33) requires light energy and NADPH to produce chlorophyllide a (Oliver et al. 1980). The final step in the formation of chlorophyll a is the attachment of the phytol tail, which is accomplished with the use of chlorophyll synthatase (EC 3.1.1.14) (Rudiger et al. 1980).

For the isotope labeling studies presented here, I was able to utilize the first three enzymatic steps in the production of ALA, which utilizes glutamate as the sole carbon source. Eight molecules of glutamate are used in the production of one molecule of chl. In order to specifically label the 13^1 keto group of chl, a glutamate-tolerant strain of *Synechocystis* PCC 6803 was cultured in glutamic -^{13}C-3-acid. Figures 1-4 illustrate the incorporation glutamic-^{13}C-3- acid with the green carbons showing the ^{13}C isotope.

A second set of studies were conducted to incorporate ^{18}O into chl. As outlined above, the chl synthesis pathway contains an oxygen-dependent cyclase that catalyzes the formation of ring V and the oxidation of the 13^1C to a carbonyl carbon. *Synechocystis* cultures were grown in the presence of $^{18}O_2$, bubbled through the media. Figure 4 depicts the cyclase reaction and the incorporation of molecular oxygen (colored blue) into chl.

2.2 Chorismate Biosynthesis

Synthesis of chorismate constitutes a common step in aromatic amino acids and quinone biosynthetic pathways in plants and microorganisms (Herrmann 1995, 1995). The seven enzymes involved in the production of chorismate have been studied extensively in plants and bacteria (Bentley 1990; Pittard 1996). The biosynthetic pathway for chorismate production, also referred to as the shikimate pathay, is depicted in Figure 5. The biosynthetic pathway begins with phosphoenolpyruvate, an intermediate in glycolysis, and erythrose-4-phosphate derived from the pentose phosphate pathway. 3-deoxy-D-arabino-heptulosonate-7-phosphate (DAHP) synthase catalyzes the condensation reaction to produce DAHP. DAHP synthase has similar kinetic properties in bacteria and plants, however the bacterial DAHP synthase is feedback inhibited by any of the three aromatic amino acids, whereas plant DAHP synthase is activated by tryptophan (Srinivasan et al. 1959; Smith 1962).

The second step in the biosynthetic pathway involves the formation of a six carbon ring, catalyzed by 3-dehydroquinate synthase to produce 3-dehydroquinate. This molecule is converted to 3-dehydroshikimate by a dehydration step catalyzed by 3-dehydroquinnate dehydratase. A reduction reaction utilizing NADPH and shikimate

dehydrogenase reduces 3-dehydroshikimate to shikimate (Balinsky et al. 1971). In plants, both these steps are catalyzed on the bifunctional enzyme shikimate:$NADP^+$ oxidoreductase (Bentley 1990).

Shikimate is phosphorlated by shikimate kinase to produce shikimate-3-phosphate (Gollube 1966, 1966; Koshiba 1979). Once this molecule is formed, 5-enolpyruvylshikimate-3-phosphate (EPSP) synthase catalyzes the transfer of enolpyruvate (PEP) to shikimate-3-phosphate to produce EPSP (Bondinell et al. 1971). This enzyme is the most studied of all the enzymes involved in chorismate biosynthesis and has been the target of many herbicides including glyphosphate (Roundup ™) and for novel antimicrobials (Marques et al. 2007). The final step of the pathway, the conversion of EPSP to chorismate, involves a 1,4-*trans* elimination of phosphate from EPSP. This reaction is catalyzed by chorismate synthase to produce chorismate (Gaertner et al. 1973). The reaction is considered unusual due to its absolute requirement for a reduced flavin mononucleotide, which is not consumed during the reaction (Macheroux et al. 1999).

2.3 Phylloquinone Biosynthesis

The biosynthetic pathway of the phylloquinone A_1 which functions as a secondary electron acceptor in PSI has not been fully investigated. The bacterial menoquinone biosynthesis pathway has been elucidated, and it believed that formation of the napthoquinone ring follows the same enzymatic steps for phylloquinone. The best studied system for menoquinone biosynthesis is *E. coli*, and the genes encoding the enzymes are designated as *men* genes. Genetic comparisons of *E. coli* genome to the *Synechocystis* sp. PCC 6803 genome have shown that all the expected *E. coli men* genes are present in *Synechocystis*. Furthermore, knockout mutants of the five genes for PhQ

biosynthesis have been created and disruption of four of them, *men*D, *men*E, *men*B, and *men*A, resulted in a complete absence of PhQ accumulation (Johnson et al. 2000; Johnson et al. 2001). The addition of exogenous phylloquinone and other naphthoquinones can partially restore the activity of PSI (Johnson, T.W. et al. 2000; Johnson, T. W. et al. 2001) confirming the biosynthetic pathway of phylloquinone in cyanobacteria. The proposed biosynthetic scheme for phylloquinone is shown in Figure 6.

The phylloquinone biosynthetic pathway begins with chorismate, a six membered ring synthesized through the shikimate biosynthetic pathway (as described previously). Isochorismate synthetase catalyzes the isomerization reaction of chorismate to isochorismate (Simantiras et al. 1989). Little research has been done on the mechanism of the enzyme in cyanobacteria and higher plants. The next enzymatic reaction involves the decarboxylation of isochorismate and the addition of 2-ketoglutarate by the enzyme known as 2-succinyl-6-hydroxy-2,4-cyclohexadiene-1-carboxylate synthase to form 2-succinyl-6-hydroxy-2,4-cyclohexadiene-1-carboxylate (Palaniappan et al. 1992). The following step in the phylloquinone biosynthetic pathway involves dehydration of the molecule to form *o*-succinyl benzoate by *o*-succinyl benzoate synthase (Sharma et al. 1993).

Formation of the quinone ring is catalyzed by 1,4-dihydroxy-2-naphthoyl-CoA synthase. In this enzymatic step, the napthoquinone ring structure is formed, and a CoA is attached via a sulfur bond to the ring structure. The CoA is released by thioesterase resulting in production of a 1,4-dihydroxy-2-napthoate molecule (Sharma et al. 1992; Meganathan 2001). Once CoA is removed from the ring structure, an isoprenyl tail is added, catalyzed by 1,4-dihydroxy-2-napthoate phytyltransferase, resulting in the

formation of demethylphylloquinone (Johnson et al. 2000). The last enzymatic step is the transfer of a methyl group from methionine to produce phylloquinone, which is catalyzed by the enzyme demethylphylloquinone methyl transferase (Suvarna et al. 1992; Koiki-Takeshita et al. 1997).

In order to incoporate C^2H_3 into the methyl group of phylloquinone, I utilzed the last step in the biosynthetic pathway. Methionine-tolerant *Synechocystis* PCC 6803 were grown in the presence of L- C^2H_3 -methionine. As outlined above, methionine is used as a methyl donor in the last enzymatic step of phylloquinone biosynthesis. The chlorophyll biosynthesis pathway also utlizes methionine as a methyl donor. Previous experiments have shown 42-68% incorporation of C^2H_3 into chl and plastoquinone using this experimental method (Barry 1995; Razeghifard et al. 1999; Bender et al. 2008)

2.4 Aromatic Amino Acid Biosynthesis

Tyrosine and phenylalanine are produced by the same pathway, branching at the last enzymatic step as shown in Figure 7. First, chorismate is converted to prephenate by the enzyme chorismate mutase. This enzymatic step catalyzes the intramolecular rearrangement of the enolpyruvyl side chain of chorismate, reducing the double bond, and moves the enolpyruval group in a Claisen rearrangement (Poulson et al. 1991). This is the committed step for phenylalanine and tyrosine synthesis. Chorismate mutase is feedback inhibited by each of the end products, phenylalanine and tyrosine, and is activated by tryptophan (Poulson et al. 1991).

In plants and cyanobacteria, prephenate aminotransferase is responsible for the production of arogenate, which contains the amide group common to both phenylalanine

and tyrosine. The enzyme uses glutamate to transfer the amino group to prephenate, producing alpha-ketoglutarate (Bonner et al. 1987). Arogenate is the last common precursor of phenylalanine and tyrosine. Arogenate dehydratase catalyzes the decarboxylation of arogenate to produce phenylalanine (Hall et al. 1982). Arogenate dehydrogenase uses $NADP^+$ as an oxidizing agent to oxidize arogenate to tyrosine through a two step process. First the enzyme oxidizes the alcohol group on the ring to a carbonyl, and then catalyzes a decarboxylation to form tyrosine and CO_2(Hall et al. 1982).

Figure 7 outlines the biosynthetic pathway and the structure of the intermediates involved in the synthesis of tryprophan from chorismate. Anthranilate synthase catalyzes the committing step in tryptophan biosynthesis. This enzyme catalyzes the amination of chorismate and the removal of the enolpyruvyl side chain to produce anthranilate. Anthranilate synthase utilizes either glutamine or ammonium as the amine donor, a Mg^{2+} as a cofactor and is feedback inhibited by the end product of the pathway, tryptophan (Braus 1991). The formation of anthranilate and the following biosynthetic pathway to produce tryptophan are identical in all the prokaryotes and eukaryotes that have been examined (Gilchrist et al. 1980).

The second step in the tryptophan biosynthesis pathway involves a transfer of a 5-phosphoribosyl pyrophosphate to anthranilate by the enzyme phosphoribosylanthranilate transferase. *N*-phosphoribosyl-anthranilate is converted to 1-(*o*-carboxyphenylamino)-1-deoxyribulose-5-phosphate by the enzyme known as phosphoribosylanthranilate isomerase. Relatively little is known about the previous two enzymes in plants; however,

both enzymes have been the focus of genetic and molecular testing and analysis (Furter et al. 1986; Hutter et al. 1986; Hommel et al. 1989).

The enzyme, indole-3-glycerol-phosphate (IGP) synthase catalyzes the decarboxylation and ring closure of carboxyphenylamino-l-deoxyribulose 5-phosphate (CDRP). This is the least well-studied step in the plant tryptophan synthesis pathway. The crystal structures of indole-3-glycerol-phosphate (IGP) synthase have been reported from *E. coli*, and research comparing the indole-3-glycerol-phosphate (IGP) synthase genes from various organisms has been performed (Priestle et al. 1987; Braus 1991). From these studies it is known that IGP synthase is bifunctional, and it is the second domain that catalyzes the second ring closure of IGP. Tryptophan synthase catalyzes the final step in tryptophan synthesis by converting indole-3-glycerol phosphate and serine to tryptophan. Tryptophan synthase from *E. coli* is the best studied enzyme of the biosynthetic pathway (Pittard 1996).

In order to incorporate ring-labeled $^{2}H_5$-tryptophan into PSI, I utilized feedback inhibition in *Synechocystis* PCC 6803 cells. Cultures were grown in the presence of millimolar concentrations of phenylalanine, tyrosine, with tryptophan or $^{2}H_5$-trpytophan. This method will inhibit DAHP synthase, an enzyme in the chorismate biosynthesis pathway (explained above). Chorismate is a common precursor to the aromatic amino acids. Previous studies using ring-labeled, $^{2}H_4$-tyrosine have shown little scrambling of the isotope into chlorophyll and plastoquinone (Barry et al. 1987).

The previous sections have outlined the biosynthetic approaches for incorporation of isotopes into cofactors and amino acids in PSI. These *in vivo* biochemical techniques allow precise assignments of the light-induced FT-IR difference spectrum of PSI. The

following chapters illustrate the usefulness of these techniques in identifying protein dynamics and protein-cofactor interactions during light-induced electron transfer.

2.5 References

Balinsky, D., A. W. Dennis and W. W. Cleland (1971). "Kinetic and isotope-exchange studies on shikimate dehydrogenase from *Pisumsativum*." *Biochemistry* **10**: 1947-1952.

Barry, B. A. (1995). "Tyrosyl radicals in photosystem II." *Methods Enzymol.* **258**: 303-319.

Barry, B. A. and G. T. Babcock (1987). "Tyrosine radicals are involved in the photosynthetic oxygen evolving system." *Proc. Natl. Acad. Sci. USA* **84**: 7099-7103.

Beale, S. I. (1999). "Enzymes of chlorophyll biosynthesis." *Photosynth. Res.* **60**: 43-73.

Beale, S. I. and P. A. Castefranco (1974). "The biosynthesis of delta-aminolevulinic acid in higher plants." *Plant Physiol.* **53**: 297-303.

Beale, S. I., S. P. Gough and S. Granik (1975). "Biosynthesis of delta-aminolevulinic acid from the intact carbon skeleton of glutamic acid in greening barley." *Proc. Natl. Acad. Sci. USA* **72**: 2719-2723.

Bender, S. L., J. Keough, S. E. Boesch, R. A. Wheeler and B. A. Barry (2008). "The vibrational spectrum of the secondary electron acceptor, A_1, in photosystem I." *J. Phys. Chem. B* **112**: 3844-3852.

Bentley, R. (1990). "The shikimate pathway - a metabolic tree with many branches." *CRC Critical Reviews of Biochemistry and Molecular Biology* **25**: 307-384.

Bollivar, D. W. and S. I. Beale (1995). "Formation of the isocyclic ring of chlorophyll by isolated *Chlamydomonas reinhardtii* chloroplasts." *Photosynth. Res.* **43**: 113-124.

Bollivar, D. W. and S. I. Beale (1996). "The chlorophyll biosynthetic enzyme Mg-protoporphyrin IX monomethyl ester (oxidative) cyclase. Characterization and partial purification from *Chlamydomonas reinhardtii* and *Synechocystis* sp. PCC 6803." *Plant Physiol.* **112**: 105-114.

Bondinell, W. E., J. Vnek, P. F. Knowles, M. Sprecher and D. B. Sprinson (1971). "On the mechanism of 5-enolpyruvylshikimate 3-phosphate synthetase." *J. Biol. Chem.* **246**: 6191-6196.

Bonner, C. and R. Jensen (1987). "Prephenate aminotransferase." *Methods Enzymol.* **142**: 479-487.

Braus, G. H. (1991). "Aromatic amino acid biosynthesis in the Yeast *Saccharomyces cerevisiae*: a model system for the regulation of eukaryotic biosynthetic pathway." *Microbiol. Rev.* **55**: 349-370.

Crockett, N., P. Alefounder, A. Battersby and C. Abell (1991). "Uroporphyrinogen III synthase: studies on its mechanism of action, molecular biology and biochemistry." *Tetrahedron* **47**: 6003-6014.

Ellswort, R. K. and J. P. Dullagha (1972). "Activity and properites of (-)-*S*-adenosyl-L-methionine: magnesium-protoporphyrin IX methyl transferase in crude homogenates from wheat seedlings." *Biochim. Biophys. Acta* **268**: 327-333.

Frydman, R. B. and B. Frydman (1970). "Purification and properites of porphobilinogen deaminase from wheat germ." *Arch. Biochem. Biophys.* **136**: 193-202.

Furter, R., G. Paravicini, M. Aebi, G. Braus, F. Prantl, P. Niederberger and R. Hutter (1986). "The TRP4 gene of *Saccharomyces cerevisiae*: isolation and structural analysis." *Nucleic Acids Res.* **14**: 6357-6373.

Gaertner, F. H. and K. W. Cole (1973). "Properties of chorismate synthase in *Neurospora crassa*." *J. Biol. Chem.* **248**: 4602-4609.

Gibson, K., W. Laver and A. Neuberger (1958). "Formation of delta-aminolevulinic acid in vitro from succinyl-conenzyme A and glycine." *Biochem. J.* **70**: 71-81.

Gilchrist, D. G. and T. Kosuge (1980). *The Biochemistry of Plants*. New York, Academic Press.

Gollube, E. (1966a). "Correlation of genes and enzymes and studies on regulation of aromatic pathway in *Salmonella*." *J. Biol. Chem.* **242**: 5323.

Gollube, E. (1966b). "Enzymes associated with unlinked genes of aromatic pathway in *Salmonella*." *Federation Proceedings* **25**: 337.

Gorchein, A. (1972). "Magnesium protoporphyrin chelatase activity in *Rhodopseudomonas spheroides*. Studies with whole cells." *Biochem. J.* **127**: 97-106.

Hall, G. C., M. B. Flick, R. L. Gherna and R. Jensen (1982). "Biochemical Diversity for biosynthesis of aromatic amino acids among the cyanobacteria." *J. Bacteriol.* **149**: 65-78.

Hart, G. and A. Battersby (1985). "Purification and properties of uroporphyrinogen II synthase (co-synthase) from *Euglena gracilis*." *Biochem. J.* **232**: 151-160.

Herrmann, K. M. (1995a). "The shikimate pathway as an entry to aromatic secondary metabolism." *Plant Physiol.* **107**.

Herrmann, K. M. (1995b). "The shikimate pathway; early steps in the biosynthesis of aromatic compounds." *Plant Cell* **7**: 909-917.

Hommel, U., A. Lustig and K. Kirschner (1989). "Purification and characterization of yeast anthranilate phosphoribosyltransferase." *Eur. J. Biochem.* **180**: 33-40.

Hutter, R., P. Niederberger and J. A. DeMoss (1986). "Tryptophan biosynthetic genes in eurkaryotic microorganisms." *Annu. Rev. Microbiol.* **40**: 55-77.

Johnson, T. W., G. Shen, B. Zybailov, D. Kolling, R. Reategui, S. Beauparlant, I. R. Vassiliev, D. A. Bryant, A. D. Jonesi, J. H. Golbeck and C. P.R. (2000). "Recruitment of a foreign quinone into the A_1 site of photosystem I. I. Genetic and physiological characterization of phylloquinone biosynthetic pathway mutants in *Synechocystis* sp. pcc 6803." *J. Biol. Chem.* **275**: 8523-8530.

Johnson, T. W., B. Zybailov, A. D. Jones, R. Bittl, S. Zech, D. Stehlik, J. H. Golbeck and P. R. Chitnis (2001). "Recruitment of a foreign quinone into the A_1 site of Photosystem I. *In vivo* replacement of plastoquinone-9 by media-supplemented naphthoquinones in phylloquinone biosynthetic pathway mutants of *Synechocystis* sp. PCC 6803." *J. Biol. Chem.* **276**: 39512-39521.

Kannangara, C. G., S. P. Gough, P. Bruyant, J. K. Hoober, A. Kahn and D. von Wettstein (1988). "$tRNA^{Glu}$ as a cofactor in delta-aminolevulinate biosyntheisis. Steps that regulate chlorophyl synthesis." *Trends Biochem. Sci.* **13**: 139-143.

Kikuchi, G., A. Kumar, P. Talmage and D. Shemin (1958). "The enzymatic synthesis of delta-aminolevulinic acid." *J. Biol. Chem.* **233**: 1214-1219.

Kim, S. and B. A. Barry (2000). "Identification of carbonyl modes of P_{700} and P_{700}^{+} by in situ chlorophyll labeling in photosystem I." *J. Am. Chem. Soc.* **122**: 4980-4981.

Koiki-Takeshita, A., T. Koyama and K. Ogura (1997). "Identification of a novel gene cluster participating in menaquinone (vitamin K_2) biosynthesis." *J. Biol. Chem.* **272**: 12380-12383.

Koshiba, T. (1979). "Alicyclic acid metabolism in plants. 12. Partial purification and some properties of shikimate kinase from Phaseolus-mungo seedlings." *Plant Cell Physiol.* **20**: 803-809.

Macheroux, P., R. Schmid, N. Amrhein and A. Schaller (1999). "A unique reaction in common pathway: mechanism and function of chorismate synthase in the shikimate pathway." *Planta* **207**: 325-334.

Marques, M. R., J. H. Pereira, J. S. Oliveira, L. A. Basso, W. F. de Azevedo, D. S. Santos and M. S. Palma (2007). "The inhibition of 5-enolpyruvylshikimate-3-phosphate synthase as a model for development of novel antimicrobials." *Curr. Drug Targets* **8**: 445-457.

Meganathan, R. (2001). "Biosynthesis of menoquinone (vitamin K2) and ubiquinone (coenzyme Q): a perspective on enzymatic mechanisms." *Vitamin and Hormones* **61**: 173-218.

Oliver, R. P. and W. T. Griffiths (1980). "Identification of the polypeptides of NADPH-protochlorophyllide oxidoreductase." *Biochem. J.* **191**: 277-280.

Palaniappan, C., V. Sharma, M. E. S. Hudspeth and R. Meganathan (1992). "Menoquinone (vitamin K_2) biosynthesis: evidence that the *Escherichia coli men*D gene encodes both 2-succinyl-6-hydroxy-2,4-cyclohexadiene-1-carboxylic acid synthase and alpha-ketoglutarate decarboxylase activities." *J. Bacteriol.* **174**: 8111-8118.

Pittard, A. J. (1996). Biosynthesis of the aromatic amino acids, in Escherichia coli and Salmonella. *Cell. Mol. Biol.* F. Neidardt, American Society of Bacteriology**:** 458-484.

Poulson, C. and R. Verpoorte (1991). "Roles of chorismate mutase, isochorismate synthase and anthranilate synthase in plants." *Phytochemistry* **30**: 377-386.

Priestle, J. P., M. G. Gruetter, J. White, M. G. Vincent, M. Kania, E. Wilson, T. S. Jardetzkey, K. Kirschner and J. N. Jansonius (1987). "3-dimensional structure of the bifunctional enzyme phosphoribosylanthranilate isomerase: indoleglycerol phosphate synthase from *Escherichia coli*." *Proc. Natl. Acad. Sci. USA* **84**: 5690-5694.

Razeghifard, M. R., S. Kim, J. Patzlaff, R. S. Hutchison, T. Krick, I. Ayala, J. Steenhuis, S. E. Boesch, R. A. Wheeler and B. A. Barry (1999). "In vivo, in vitro and calculated vibrational spectra of plastoquinone and the plastosemiquinone anion radical." *J. Phys. Chem. B* **103**: 9790-9800.

Rudiger, W., J. Benz and Guthoff, C. (1980). "Detection and partial characterization of activity of chlorophyll synthetase in etioplast membranes." *Eur. J. Biochem.* **109**: 193-200.

Sharma, V., R. Meganathan and M. E. S. Hudspeth (1993). "Menaquinone (vitamin K_2) biosynthesis: nucleotide sequence and expression of the menC gene from *Escherichia coli*." *J. Bacteriol.* **175**: 4917-4921.

Sharma, V., K. Suvarna, R. Meganathan and M. E. S. Hudspeth (1992). "Menaquinone (vitamin K2) biosynthesis: nucleotide sequence and expression of the menB gene from Eschericia coli." *J. Bacteriol.* **174**: 5057-5062.

Simantiras, M. and E. Leistner (1989). "Formation of o-succinylbenzoic acid from iso-chorismic acid in protein extracs from anthraquinone-producing plant cell suspensions." *Phytochemistry* **28**: 1381-1382.

Smith, L. C. (1962). "Control of 3-deoxy-D-arabino-heptulosonic acid 7-phosphate synthesis by phenylalanine and tyrosine." *J. Biol. Chem.* **237**: 3566-3570.

Srinivasan, P. R. and D. B. Sprinson (1959). "2-keto-3-deoxy-D-arabo-heptonic acid 7-phosphate synthetase." *J. Biol. Chem.* **234**: 716-722.

Suvarna, K., D. Stevenson, R. Meganathan and M. E. S. Hudspeth (1992). "Menoquinone (vitamin K_2) biosynthesis: localization and characterization of the menA gene from *Escherichia coli*." *J. Bacteriol.* **180**: 2782-2787.

Walker, C. J. and J. Wienstein (1991). "In vitro assay of the chlorophyll biosynthetic enzyme Mg-chelatase: resolution of the activity into soluble and membrane-bound fractions." *Proc. Natl. Acad. Sci. USA* **88**: 5789-5793.

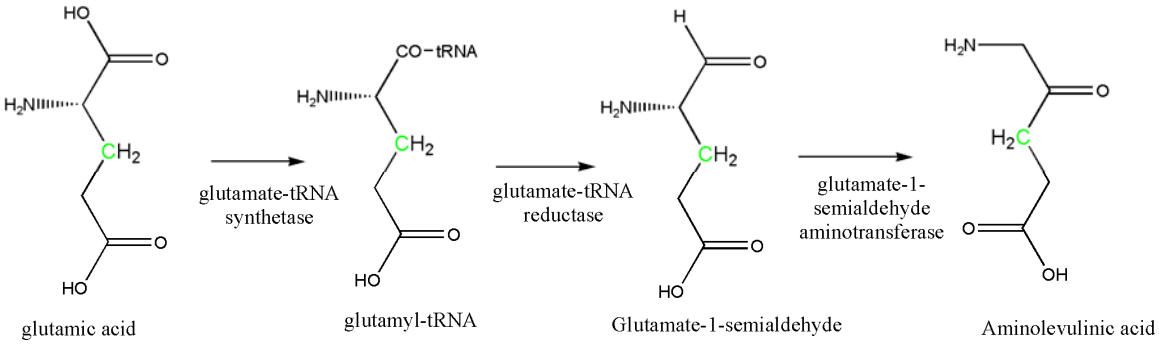

Figure 1. Formation of delta-aminolevulinic acid from L-glutamic acid. Carbon 3 (green) will be incorporated into eight positions of the tetrapyrrole ring of chlorophyll, including the 13^1 keto position.

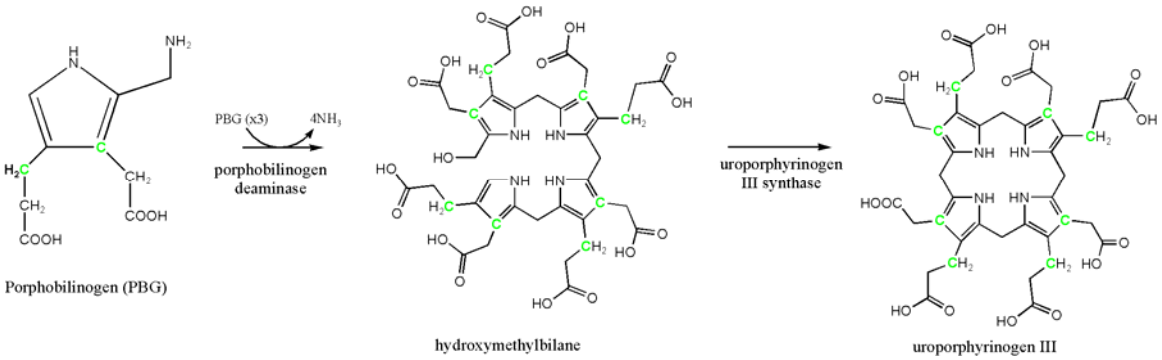

Figure 2. Formation of uroporphyrinogen III from porphobilinogen. The carbons in green are from L-glutamic-3-^{13}C-acid. Uroporphyrinogen is the branching point for heme synthesis and chlorophyll synthesis.

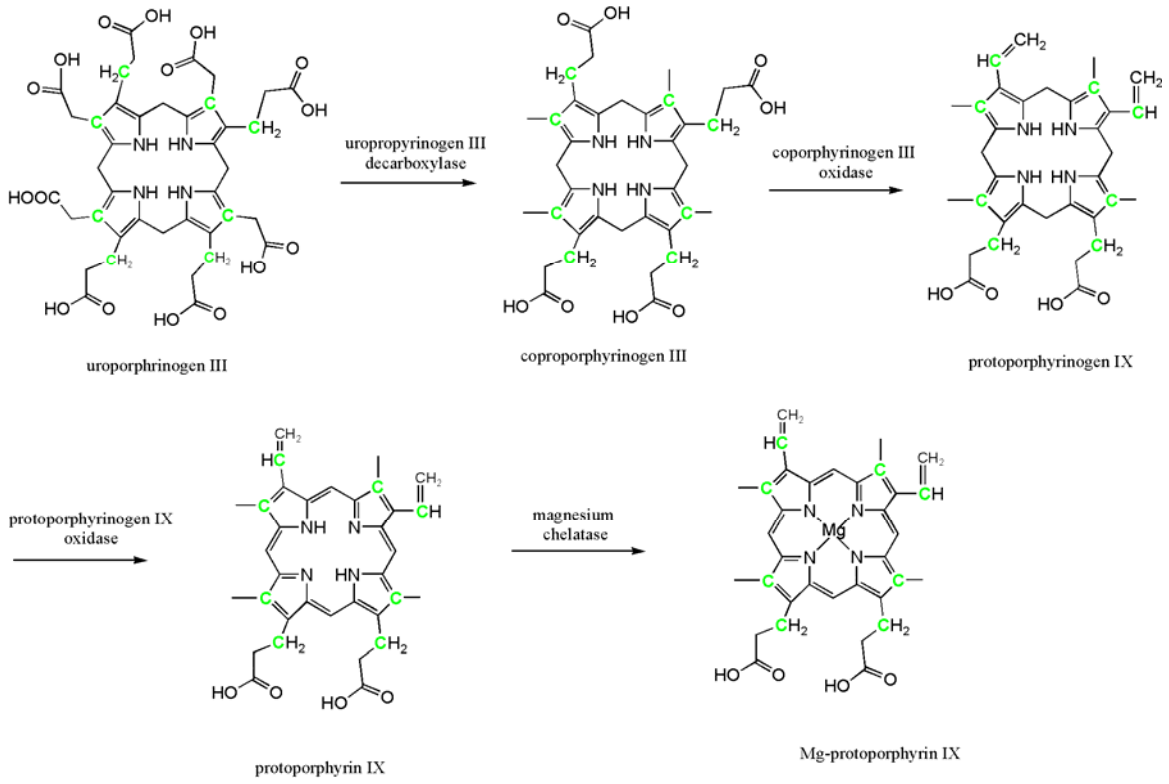

Figure 3. Enzymatic steps involved in synthesis of Mg-protophorphyrin IX. The carbons in green are from L-glutamic-3-^{13}C-acid.

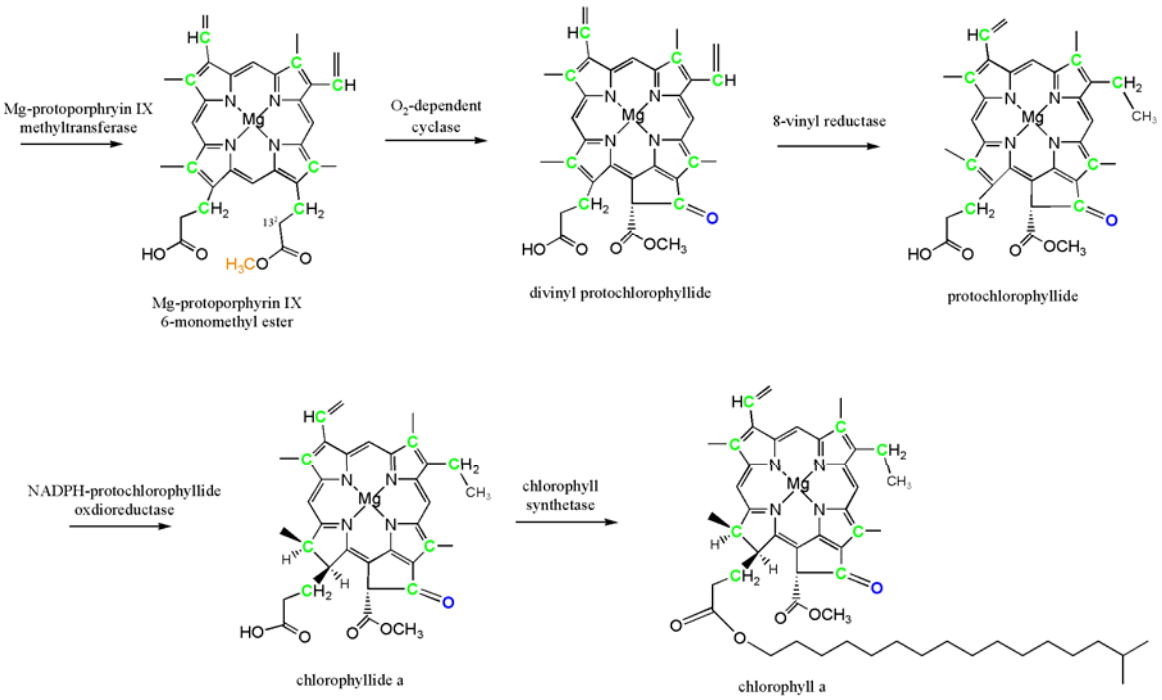

Figure 4. Final enzymatic steps in the formation of chlorophyll a including formation of ring V. The oxygen (blue) will be incorporated from O_2 by the cyclase enzymatic reaction. The carbons in green are from L-glutamic-3-^{13}C-acid.

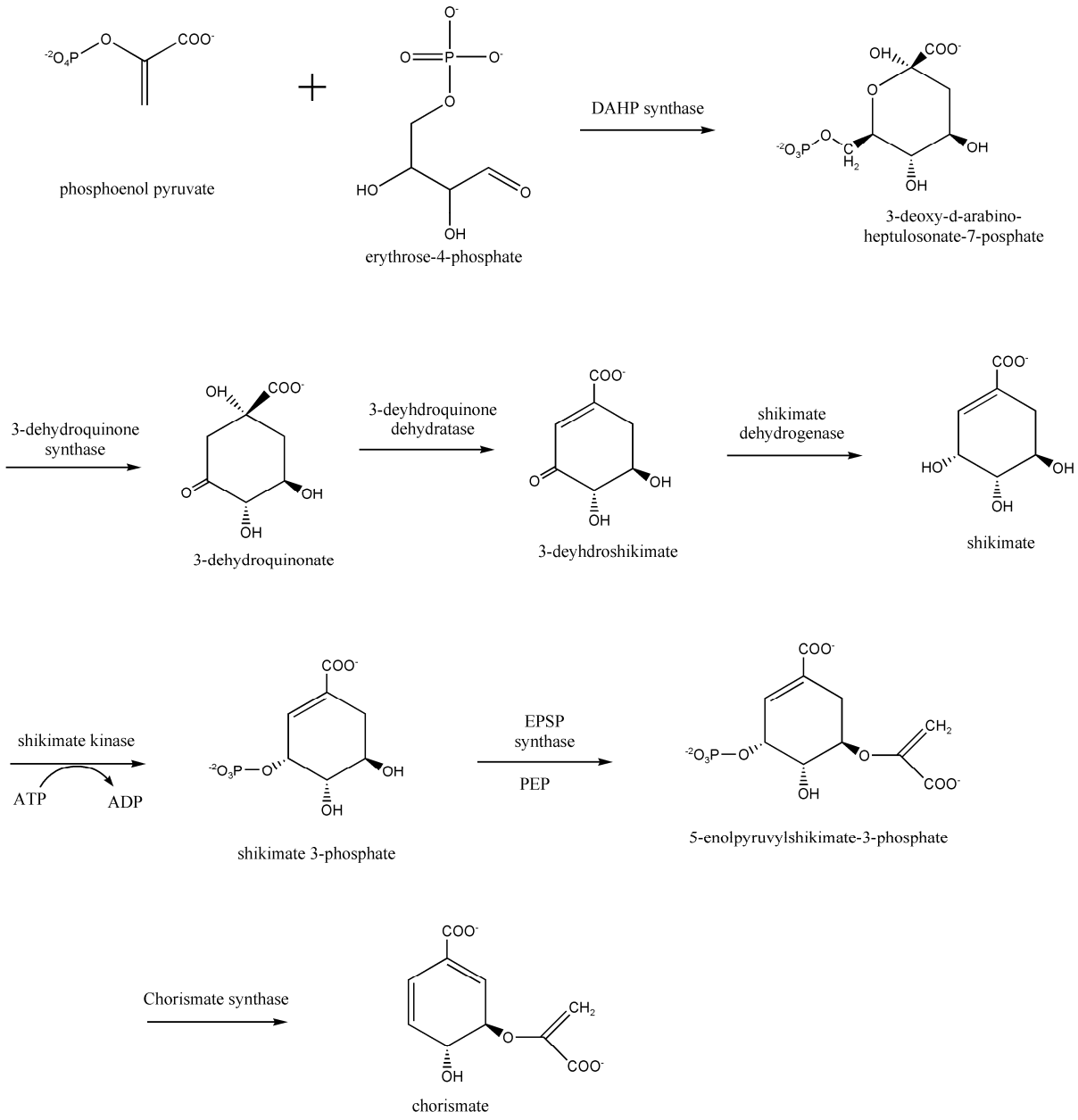

Figure 5. Biosynthetic steps involved in the production of chorismate from phosphoenolpyruvate and erythrose 4-phosphate.

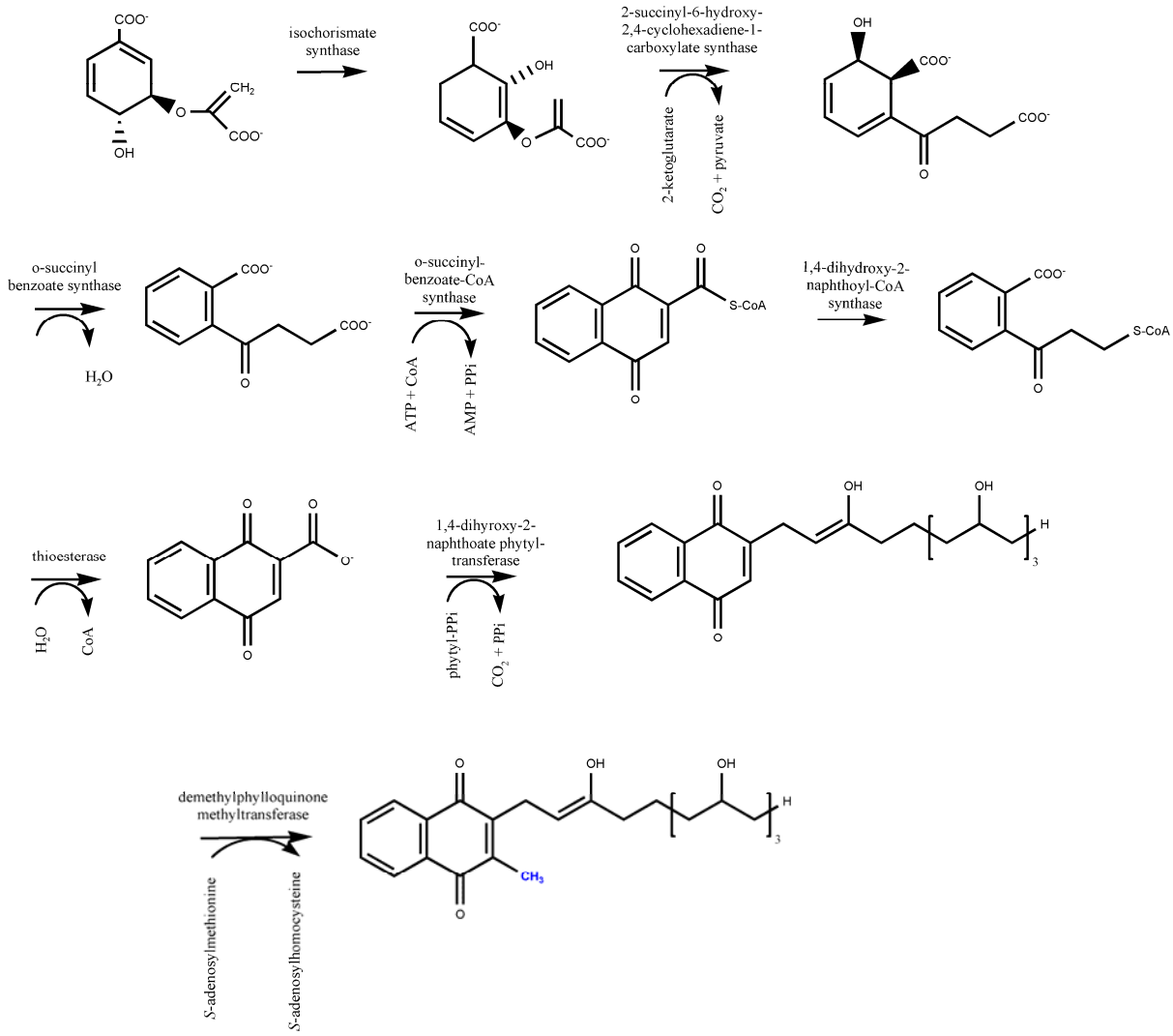

Figure 6. Enzymes and cofactors involved in the production of phylloquinone from chorismate. The methyl group (blue) will be incorporated from *S*-adenosylmethionine.

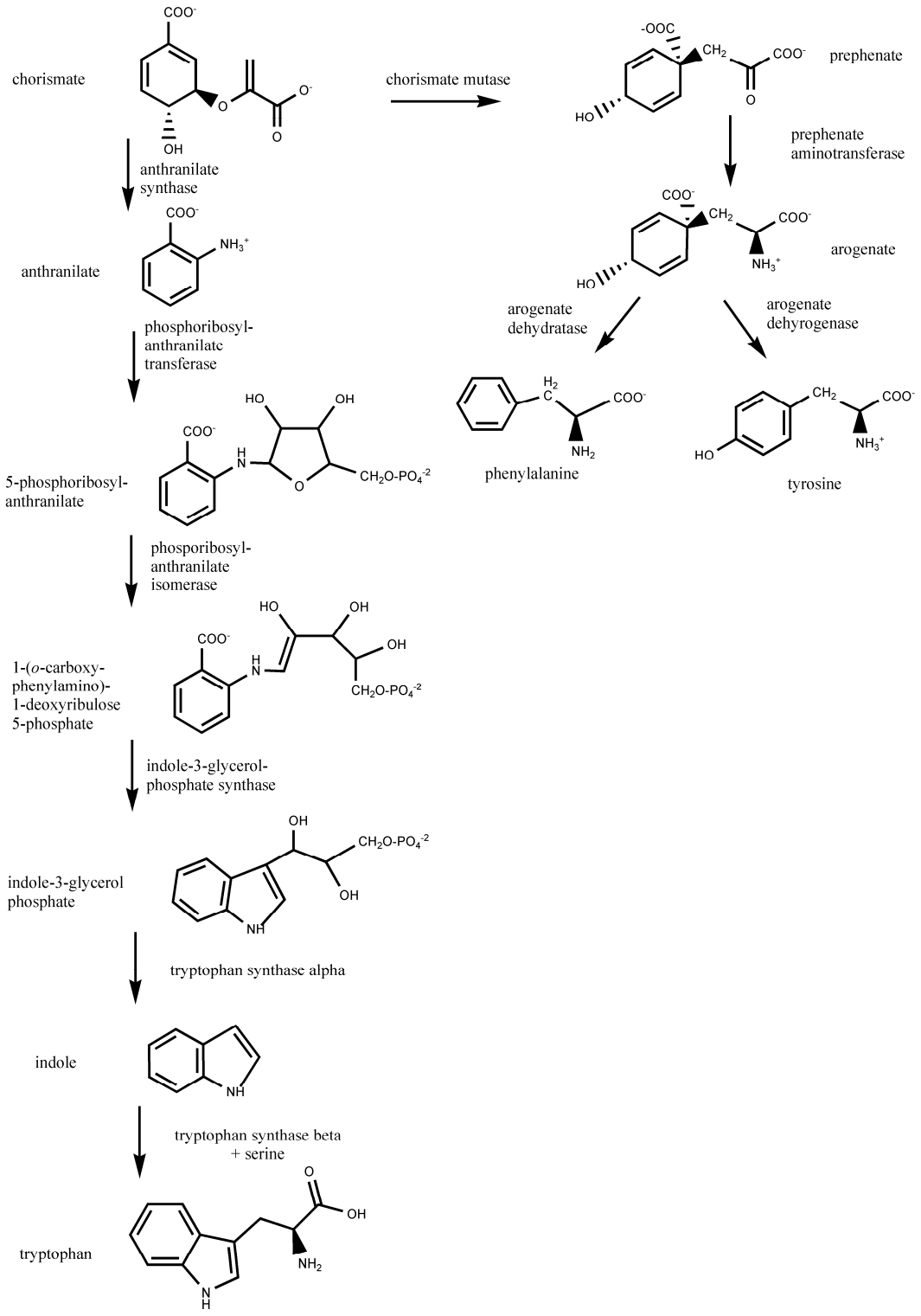

Figure 7. Biosynthetic pathway of the aromatic amino acids: phenylalanine, tryptophan, and tyrosine, starting with the common precursor, chorismate.

CHAPTER 3

THE VIBRATIONAL SPECTRUM OF THE SECONDARY ELECTRON ACCEPTOR, A_1, IN PHOTOSYSTEM I

3.1 Abstract

Photosystem I (PSI) is a multisubunit protein complex, which carries out light-induced, transmembrane charge separation in oxygenic photosynthesis. In PSI, the electron transfer pathway consists of chlorophyll and phylloquinone molecules, as well as iron-sulfur clusters. There are two phylloquinone molecules, which are located in structurally symmetric positions in the reaction center. It has been proposed that both phylloquinone molecules are active as the A_1 secondary electron acceptor in bi-directional electron transfer reactions. The PSI A_1 acceptors are of interest because they have the lowest reduction potential of any quinone found in nature. In this work using light-induced FTIR

spectroscopy, isotope-edited spectra are presented, which attribute vibrational bands to the carbonyl stretching vibrations of A_1 and A_1^- and the quinoid ring stretching vibration of A_1. Bands are assigned by comparison with hybrid Hartee-Fock density functional calculations, which predict vibrational frequencies, amplitudes, and isotope shifts for the phylloquinone singlet and radical anion states. The results are consistent with an environmental interaction increasing the frequency of the singlet CO vibration and decreasing the frequency of the anion radical CO vibration, relative to model compounds. This environmental interaction may be the asymmetric hydrogen bond to A_1/A_1^-, electrostatic interactions with charged amino acid side chains, or a pi-pi interaction with the indole ring of a nearby tryptophan. Such differential effects on the structure of A_1 and A_1^- may be associated with a destabilization of the anion radical. These studies give novel information concerning the effect of the protein matrix on the PSI electron transfer cofactor.

3.2 Introduction

In oxygenic photosynthesis, photosystem I carries out the light-driven oxidation of plastocyanin and the reduction of ferredoxin. These reactions lead to a charge separation across the thylakoid membrane. Electron transfer is initiated by photoexcitation of the photosystem I primary chlorophyll donor, which reduces the primary acceptor, A_0, a chl *a* monomer (Holzwarth et al. 2006). The resulting positive charge resides on P_{700}, a heterodimeric chlorophyll, which is composed of chl *a* and its epimer, chl *a*' (Fromme et al. 2001; Jordan et al. 2001). A_0 reduces the secondary electron acceptor, A_1, which is a phylloquinone (Rustandi et al. 1990). Sequential electron transfer reactions then lead to the reduction of F_X, F_A and F_B, which are iron-sulfur clusters. F_A and F_B are bound to the extrinsic PsaC subunit, while the other electron transfer cofactors are bound to the intrinsic, membrane-associated PsaA and PsaB subunits (Fromme et al. 2001; Jordan et al. 2001).

The structure of PSI from *Synechococcus elongates* has been solved at 2.5 Å resolution by X-ray diffraction (Jordan et al. 2001). There are two phylloquinone acceptor molecules, which are located in C_2 structurally symmetric positions. The two phylloquinone cofactors will be designated here as A_{1A} and A_{1B}, where the subscripts designate the subunit to which the phylloquinone molecule is bound. It has been proposed that both sets of phylloquinone cofactors are reduced in PSI electron transfer reactions, but with different time constants (Rigby, S. E. et al. 1996; Joliot et al. 1999; Boudreaux et al. 2001; Guergova-Kuras et al. 2001; Purton et al. 2001; Rigby, S. E. J. et al. 2002; Ramesh et al. 2004; Bautista et al. 2005; Poluektov et al. 2005; Santabarbara et al. 2005a; Santabarbara et al. 2005b; Ali et al. 2006; Li et al. 2006; Santabarbara et al. 2006; Ramesh et al. 2007). In *Chlamydomonas*

reinhardtii, electron transfer has been deduced to be bidirectional with a 1:1 ratio of the kinetic phases (Joliot et al. 1999; Guergova-Kuras et al. 2001). In cyanobacteria, electron transfer is more unidirectional along the PsaA branch with ratios of 1:2-3 (Klughammer et al. 1999; Guergova-Kuras et al. 2001; Xu et al. 2003a; Xu et al. 2003b; Cohen et al. 2004; Dashdorj et al. 2005). In particular, PSI from *Synechocystis PCC 6803* shows a fast phase (time constant 11 ns) and slow phase, which have been assigned to electron transfer down the B and A branch, respectively. The slow phase was observed to have a 340 ns time constant at 295 K and to slow upon cooling, with an activation energy of 110 meV (Aglarov et al. 2003). The minor fast phase was observed to be temperature independent.

The structure of phylloquinone is shown in Figure 1, along with its IUPAC numbering scheme. Figure 2 displays the binding pockets of A_{1A} (left) and A_{1B} (right) from the 2.5 Å PSI structure (Jordan et al. 2001). A predominant feature of both binding pockets is a tryptophan residue, which is within π-stacking distance of each A_1 acceptor. These two conserved tryptophans are located on the stromal side of A_{1A} and A_{1B}. The distances between the indole ring and the quinone are approximately 3 Å for A_{1A} and 3.5 Å for A_{1B}. Another striking feature of the A_1 protein environment is an asymmetric hydrogen bond from the amide NH groups of LeuA722 and LeuB706 respectively, to the C_4=O groups of each A_1 molecule (Jordan et al. 2001; Pushkar, Y. et al. 2004; Teutloff et al. 2004). The lack of a second hydrogen bond to C_1=O distinguishes the A_1 binding site, when compared to the Q_A binding site in bacterial reaction centers, in which two hydrogen bonds are formed to Q_A^-. A tryptophan-Q_A pi-pi interaction also occurs in the bacterial reaction center (Allen et al.; Deisenhofer et al. 1989; Kamlowski et al. 1998; Fromme et al. 2001; Pushkar, Y. et al. 2004).

A_1 has the lowest known redox potential of any quinone found in nature. Measurements for the A_1 redox potential range from -750 to -810 mV (Brettel, Klaus 1997). Previous studies in which A_1 has been exchanged for various quinone molecules, such as benzoquinone, have shown a -0.3 V change in the redox potential compared to the measured reduction potential in solution (Itoh et al. 2001). These results indicated that specific protein-cofactor interactions, such as the NH...CO asymmetric hydrogen bond (Pushkar, Y. et al. 2004; Li et al. 2006; Feldman et al. 2007) and possibly the pi-pi interaction, modulate the redox potential of quinones bound to the A_1 binding site (van der Est 2001). Recent work has also implicated an electrostatic interaction with an aspartate as a modulator of A_1 redox potential (Karyagina et al. 2007).

To understand the structure of A_1/A_1^- and their interaction with the protein environment, we have used FTIR spectroscopy. Vibrational spectroscopy supplies dynamic structural information concerning the electron transfer cofactors in vivo. Previously, A_1^-/A_1 spectra have been constructed, and multiple assignments have been suggested for the A_1 and A_1^- vibrational bands (Hastings et al. 2001; Sivakumar et al. 2005; Bandaranayake, K. M.; et al. 2006; Bandaranayake, K. M. et al. 2006a; Bandaranayake, K. M. et al. 2006b). However, there are discrepancies in these assignments, and different spectroscopic methods have yielded contradictory results.

In this study, we have used isotopic labeling of phylloquinone in order to identify the vibrational modes of A_1 and A_1^-, under conditions in which A_1 is the terminal electron acceptor in PSI. When the iron-sulfur clusters, F_x, F_A, and F_B are removed, the $P_{700}^+A_1^-$ state can be photo-generated (Warren et al. 1990; Van der Est et al. 1994; Shen et al. 2002a). We have incorporated C^2H_3 into the methyl group of A_1 using a methionine-tolerant strain of the

cyanobacterium, *Synechocystis sp.* PCC 6803. This approach has been used previously to assign bands to the plastoquinone acceptors, Q_A and Q_A^-, in cyanobacterial photosystem II (Razeghifard et al. 1999). In our current work, light-minus-dark FT-IR spectroscopy identifies C^2H_3-sensitive bands of A_1 and A_1^-. The data presented here support the interpretation that an asymmetric hydrogen bond, electrostatic interactions, and/or a pi-pi interaction shifts the CO stretching and quinone ring stretching frequencies of A_1 and A_1^-, relative to model compounds.

3.3 Materials and Methods

3.3.1 Isotopic labeling and PSI purification. A methionine-tolerant strain of *Synechocystis PCC* 6803 was grown on solid media, containing 90 μM methionine BG-11, 5 mM TES-NaOH, pH 8.0, and 6 mM NaS_2O_3 (Rippka et al. 1979; Barry, B.A. 1995). Liquid cultures (15 L) were supplemented either with 200 μM natural abundance C^1H_3-methionine or C^2H_3-methionine (98% enrichment, Cambridge Isotope Laboratories, Andover, MA) (Razeghifard et al. 1999). Trimeric PSI was purified as described previously (Kim et al. 2001). Purified trimeric PSI samples were dialyzed overnight in 5 mM HEPES-NaOH pH 7.5, 0.04% dodecyl-β-D-maltoside (LM) and were concentrated using an Amicon (Bedford, MA) Ultra 100,000 MWCO centrifugal filter device to a final concentration of 4.6 mg chl/ml.

3.3.2 Apo-F_x preparations. PSI (0.25 mg chl/ml) was incubated in a buffer containing 6.8 M urea, 50 mM Tris, 10 mM glycine-NaOH, pH 10 for 70 minutes as previously described (Parrett, K. G. et al. 1989). The PSI sample was then dialyzed overnight against 50 mM Tris-HCl, pH 8.3. The sample was incubated in 3 M urea, 5 mM Ke_3FeCN_6

50 mM Tris-HCl, pH 8.3 for 2 hours to remove the F_x cluster (Warren et al. 1990). The sample was dialyzed overnight against 50 mM Tris-HCl, pH 8.3, and then again overnight against a buffer containing 50 mM Tris-HCl, pH 8.3, 5 mM 4,5-dihydroxy-1,3-benzene-disulfonic acid, which was supplied as the disodium salt. The sample was dialyzed a third night against 50 mM Tris, pH 8.3, 0.035% LM (Parrett, K. G.; et al. 1990; Warren et al. 1990; Warren et al. 1993). The sample was buffer exchanged with 5 mM HEPES-NaOH, pH 7.5 and concentrated using an Amicon Ultra 100,000 MWCO centrifugal filter device. The final chl concentration was 3 mg/ml.

Transient absorption spectroscopy, monitoring the decay of the P_{700}^+ signal at 820 nm, was performed to verify iron-sulfur cluster removal, as previously described (Warren et al. 1990). The PSI concentration was 41-58 micrograms chl/ml, and the samples were in 50 mM Tris pH 8.3, and 0.035% LM. Sodium ascorbate (5 mM) and dichloroindophenol (DCPIP, 4 μM) were added as exogenous electron donors. The 532 nm photolysis laser had an energy of 1.5-1.8 mJ/cm^2. SDS gel electrophoresis was also used to verify PsaC removal (Piccioni et al. 1982; Kruip et al. 1997).

3.3.3 Assessment of isotope enrichment through mass spectrometry. Previous quantitative work has shown that both the 13^4-methyl of chl (Kim et al. 2000a) and the phylloquinone ring C_2 methyl group (Barry, B. A. et al. 1987; Kim et al. 2001) are labeled from C^2H_3-methionine, which is a methyl group donor to both cofactors. Therefore, phylloquinone isotopic enrichment can be monitored indirectly by measuring the amount of chl isotopic labeling in cyanobacterial cultures grown on C^2H_3-methionine (Kim et al. 2000b). The control sample was isolated from cyanobacteria grown on natural abundance methionine. Chlorophyll was extracted from PSI with a solution of 80% acetone/20%

methanol. The extracted pigments were vortexed, sonicated, centrifuged, and filtered as previously described (Patzlaff et al. 1996). Chlorophyll was concentrated and dried using a Thermo-savant SpeedVac concentrator with VLP120 pump and RVT 400 refrigerated vapor trap (Thermo Electron Corporation, Waltham, MA). Chlorophyll samples were stored at -70°C until use. Matrix assisted laser desorption ionization mass spectrometry on a 4700 Proteomics Analyzer (Applied Biosystems Foster City, CA) was performed to determine the amount of C^2H_3 incorporation. Immediately before the measurement, chlorophyll was dissolved in a mixture of 80% methanol, 19% water, and 1% acetic acid; this treatment removes the central Mg^{+2} ion of chlorophyll and generates pheophytin. The matrix used was alpha-cyano-4-hydroxy cinnamonic acid. The 871.5 *m/z* peak of pheophytin [M+H] was used for quantitation. Data were analyzed using IGOR (Wavemetrics, Lake Oswego, OR) software. The data were normalized to the [M+H] peak, and the isotope distribution was calculated. This approach showed 40 $\pm$ 1% labeling of the chlorophyll methyl group from C^2H_3-methionine and implies a similar amount of phylloquinone labeling (Barry, B. A. et al. 1987; Kim et al. 2000b). Previous work has shown that there is no significant scrambling into other amino acids besides methionine, suggesting that there will be no detectable labeling of the peptide backbone (Razeghifard et al. 1999).

3.3.4. FTIR Spectroscopy: FT-IR spectra were collected at -10°C (Kim et al. 1998) or at room temperature (20°C). Samples contained 3 mM potassium ferricyanide and 3 mM potassium ferrocyanide and were concentrated at room temperature under a steady flow of nitrogen gas. Concentration times were 20-30 minutes. Spectral conditions were as follows: resolution, 4 cm^{-1}; zero filling, 1; data acquisition time, 4.0 min. Difference spectra (light-minus-dark) were generated by taking the ratio of single beam spectra collected before and

during illumination and converting to absorbance. A_1^-/A_1 spectra were generated by subtraction of data from intact and apo-Fx PSI. The A_1^-/A_1 isotope edited spectra were generated by subtracting difference FT-IR spectra, acquired from C^2H_3-PSI samples, from difference FT-IR spectra, acquired from natural abundance, C^1H_3-PSI samples (Kim et al. 2000b; Kim et al. 2001; Sacksteder et al. 2005). FT-IR spectra were obtained in the dark or under continuous illumination with red- and heat-filtered light, as previously described (Kim et al. 2001; Sacksteder et al. 2005). A 90 min dark relaxation time was used between successive illuminations. The final averaged difference FT-IR spectra were an average of 45 spectra and were normalized for small differences in sample concentration and path length, using the amplitude of the amide II band in the infrared absorption spectrum. The infrared absorption spectrum was created using a dark and a background scan, which were acquired with infrared windows, but no PSI sample. Previous studies have found that changes in hydration levels alter the details of PSI charge separation (Sacksteder et al. 2005). Therefore, water content in all the FTIR samples was held constant, as assessed by the ratio (1.1-1.3) of the 3300 cm^{-1} band to the amide I band at 1656 cm^{-1} (Kim et al. 2001).

3.3.5 Density Functional Calculations. Density functional methods were used to predict the vibrational frequencies, IR intensities, and isotopic frequency shifts for the normal modes of models for phylloquinone and the phylloquinone anion radical. Figure 1 displays the structure of phylloquinone, and for the model the isoprenyl chain of phylloquinone was truncated to a single isoprenyl unit for ease in computation. The methyl group on the quinone ring was completely deuterated in order to estimate the maximum isotopic frequency shifts.

The B3LYP hybrid Hartree-Fock density functional (HF/DF) method (Becke 1993) was used to calculate the vibrational frequencies for a model of phylloquinone and its radical anion. The B3LYP method was chosen because it is known to give harmonic vibrational frequencies within approximately 4% of experiment, for approximately the same computer time investment as a Hartree-Fock calculation, in which estimated frequencies vary from experiment by more than 10% (Scott et al. 1996). The three-parameter B3LYP method uses a weighted sum of Hartree-Fock, local DF, and gradient-corrected DF expressions for the exchange and correlation energies where (E_X^{Slater}) is Slater's local spin density functional for exchange, (Slater 1974) E_X^{Becke} is Becke's gradient correct exchange functional, (Becke 1988) E_C^{VWN} is the local density correlation functional of Vosko, Wilk, and Nusair, (Vosko et al. 1980) and E_C^{LYP} is the gradient-corrected correlation functional of Lee, Yang, and Parr (Lee et al. 1988). Coefficients giving the relative weights of various approximations for the exchange and correlation energies in this method were optimized to reproduce thermochemical data for a variety of small molecules (Becke 1993). All calculations reported here were performed using the 6-31G(d) split-valence plus polarization basis set (Hehre et al. 1986; Helgaker et al. 1995). This basis set was chosen because it reproduces the properties of medium-sized organic molecules, including a variety of *p*-benzoquinones and their radical anions and is small enough for rapid calculations (Boesch et al. 1995, 1997a, 1997b; Wise et al. 1997; Grafton et al. 1998a, 1998b).

The quantum chemistry program Gaussian 03 (Frisch et al. 2004) was used for all calculations. Berny's optimization algorithm was used to perform full geometry optimizations in C1 symmetry using internal coordinates (Schlegel 1986). Frequency calculations were performed for the optimized geometries. It has been customary to scale

calculated vibrational frequencies, and we adopt the scaling factor of 0.9614 suggested by Scott and Radom (Scott et al. 1996).

Vibrational mode assignments were performed by animating each mode using the program XMOL (Wasikowski et al. 1993) and comparing the modes of one molecule to another using the program ViPA, an acronym for Vibrational Projection Analysis (Grafton et al. 1998a, 1998b). The ViPA program (Grafton et al. 1998a, 1998b) exploits the vector properties of vibrational normal modes to assess the similarity between modes of an object molecule and a structurally similar basis molecule. The program first aligns the two molecules and calculates each molecule's normal modes and vibrational frequencies. For each molecule, each of the normal vibrational modes is a column vector, which is orthonormal to all other normal modes of the same molecule. The vector projection operation is done by sequentially projecting each normal mode of the object molecule to the modes of the basis molecule. The similarity of any mode of the object molecule to any mode of the basis molecule can then be expressed as a percentage by calculating the sum of the squares of the matrix elements and multiplying by 100. Vibrational projection analysis has been exploited to compare normal modes modified by isotopic substitution, oxidation/reduction, as well as covalent (Grafton et al. 1998a; Wise et al. 1999) and non-covalent (Razeghifard et al. 1999) modifications.

3.4 Results

Transient absorption experiments were performed to verify the removal of the iron-sulfur clusters in the apo-Fx samples. In the absence of F_X, F_A, and F_B, P_{700}^+ recombines with A_1^-, and an acceleration in the decay rate of P_{700}^+, is expected (Parrett, K. G.; et al.

1990; Warren et al. 1990; Golbeck 1994; Brettel, Klaus 1997; Brettel, K. et al. 2001; Shen et al. 2002a; Shen et al. 2002b). P_{700}^{+} decay can be detected at 820 nm (Figure 3) after a 532 nm flash. At the low 532 nm excitation energies employed here, previous work has shown that chl triplets do not make a significant contribution to 820 nm decay kinetics either in intact or apo-F_X PSI (Vassiliev et al. 1997). Therefore, the decay of 820 nm absorbance is attributed to P_{700}^{+} recombination with PSI electron acceptors (Vassiliev et al. 1997). Note that the effects of changes in 532 nm excitation energy on intact and apo-Fx PSI have been previously described (Vassiliev et al. 1997).

Figures 3A and 3B show P_{700}^{+} decay kinetics in intact PSI samples, which contain F_X, F_A, and F_B. Figure 3A was obtained from cells cultured on C^1H_3 methionine; Figure 3B was obtained from cells cultured on C^2H_3 methionine. These intact samples show the expected P_{700}^{+} F_A^{-}/F_B^{-} recombination kinetics (Parrett, K. G.; et al. 1990; Warren et al. 1990) with lifetimes of 15-17 ms and 84-95 ms. A third slower phase (lifetime 3-6 s) is assigned to the reduction of P_{700}^{+} by the exogenous electron donor, DCPIP. Figure 3C and 3D exhibit the P_{700}^{+} decay kinetics, which were measured in apo-F_X PSI. Figure 3C was obtained from cells cultured on C^1H_3 methionine, and Figure 3D was obtained from cells cultured on C^2H_3 methionine. In Figures 3C and 3D, the lifetime of P_{700} has decreased dramatically, as predicted for samples with A_1 as the terminal electron acceptor. The slow phases of 15-17 and 84-96 ms have been replaced by faster biphasic kinetics with lifetimes of 11-13 μs and 69-115 μs (Brettel, K. et al. 1995). These results demonstrate that F_A, F_B, and F_X have been removed in the apo-F_X preparation.

In Figure 4, we present difference (light-minus-dark) FT-IR spectra acquired either from apo-F_X (Figure 4A) or intact PSI (Figure 4B) at room temperature (solid lines) or at -

10°C (dotted lines). The data in Figure 4A correspond to $P_{700}^{+}A_1^{-}$-minus-$P_{700}A_1$ spectra, and the data in Figure. 4B correspond to $P_{700}^{+}F_B^{-}$-minus-$P_{700}F_B$ spectra. The spectrum in Figure 4A is in good agreement with previous published time-resolved spectra of P_{700}^{+}/A_1, confirming the accumulation of the A_1^{-} species (Sivakumar et al. 2005; Bandaranayake, K. M. et al. 2006a) and the generation of P_{700}^{+} and not the P_{700} triplet, $^3P_{700}$ (Breton et al. 1999; Sivakumar et al. 2005).

In Figure 4C (room temperature) and Figure 4D, (-10°C), construction of the double difference spectrum, A_1^{-}-minus-A_1, was performed by subtraction of data in Figure 4B from Figure 4A. In construction of these double difference spectra, data in Figure 4A were divided by a factor of 3 to account for an overall difference in spectral amplitude in the two PSI preparations. The increased spectral amplitude in Figure 4B, compared to Figure 4A, may be attributable to an increased efficiency of charge separation in intact PSI, compared to apo-F_X PSI, under the low intensity, continuous, red-filtered illumination used for the FT-IR measurements.

In the resulting double difference spectra (Figures 4C and 4D), unique vibrational bands of A_1 appear as negative signals; unique vibrational contributions from A_1^{-} are positive bands. The reduction spectrum of F_B is not expected to contribute significantly in this spectral region (Breton et al. 1999). Figure 4 demonstrates that the A_1^{-}-minus-A_1 spectra acquired at room temperature and -10°C are similar (Figure 4C and 4D), except for an increased amplitude at ~1620 cm^{-1} in the room temperature data, which may be due to an increased contribution from water at the higher temperature (Figure 4C). Previously, the difference FT-IR A_1^{-}-minus-A_1 spectrum has been reported in apo-F_X PSI preparations at room temperature. Comparison of our data with this previously reported work is difficult

due to the use of ^2H_2O buffers in ref (Hastings et al. 2001). However, the spectra in Figure 4C and 4D do show similarities to the transient spectrum, attributed to A_1^--minus-A_1, in intact cyanobacterial PSI. The transient spectrum was acquired by microsecond, time resolved, step-scan FT-IR techniques in ^1H_2O buffers at 77K (Sivakumar et al. 2005).

In Figure 5, we present difference (light-minus-dark) FT-IR spectra obtained from apo-Fx PSI samples and attributable to $P_{700}^+A_1^-$-minus-$P_{700}A_1$. Figure 5A shows the difference spectrum acquired from the natural abundance, C^1H_3 phylloquinone control, which was isolated from cells cultured on C^1H_3-methionine. Figure 5B shows the spectrum acquired from C^2H_3 phylloquinone labeled samples. The isotope-edited C^1H_3-minus-C^2H_3 double difference spectrum (Figure 5C) was constructed by subtraction of Figure 5B from 5A and was multiplied by a factor of ten for presentation. C^2H_3-induced shifts are observed as derivative-shaped spectral features. To appear in the isotope-edited spectrum, the frequencies must be perturbed by charge separation (for example, by the reduction of A_1) and by isotope-incorporation. Figure 5D shows a control subtraction that was generated by subtracting one-half of the C^1H_3-PSI data set from the other half of the data set. The spectrum will not contain any vibrational bands and allows an estimate of the noise in the averaged data. Comparison of Figure 5C and Figure 5D demonstrates that the vibrational frequencies observed in Figure 5C are significant. Figure 5E is the dark-minus-dark spectrum, showing that the observed spectra in A and B are dependent on illumination of the sample.

Both the 13^4-methyl of chl and the phylloquinone ring C_2 methyl group (Figure 1) are labeled from methionine (Barry, B. A. et al. 1987; Kim et al. 2000b). Chl methyl labeling has been shown to shift the ester and keto vibrational bands of P_{700}^+-minus-P_{700} (Kim et al.

2000a). The ester vibrational bands of P_{700}^{+}-minus-P_{700} have been previously assigned to spectral features observed between 1760 and 1700 cm^{-1}, (Kim et al. 2000a) and in Figure 5C, the expected spectral shifts due to the P_{700}/P_{700}^{+} ester bands are observed. Therefore, the isotope-edited spectrum in Figure 5C exhibits contributions from isotope labeling of P_{700}, as well as from labeling of A_1.

To identify isotope shifts due to A_1/A_1^{-}, the C^2H_3-spectrum derived from intact PSI (Figure 6B) was subtracted from the C^2H_3-edited spectrum derived from apo-F_X PSI (Figure 6A), after normalization for the chl ester bands. This normalization accounts for the lower amplitude of the difference spectrum, acquired from the apo-F_X preparation. This lower amplitude may be due to a smaller amount of charge separation in the apo-F_X preparation, as described above. The resulting isotope-edited spectrum (Figure 6C) will reflect isotope-induced shifts in vibrational bands of A_1 and A_1^{-}. Unique vibrational bands of A_1 appear as negative signals, with the corresponding isotope-shifted components appearing as positive bands. Unique vibrational contributions from A_1^{-} are positive bands; the corresponding isotope-shifted components are negative bands. Figure 6D shows a negative control, in which no vibrational bands are expected.

To assign spectral features in Figure 6C to normal modes of the phylloquinone singlet and anion radical, DFT calculations were used to predict the frequencies, intensities, and C^2H_3 isotope shifts. The predicted frequencies and intensities are in reasonable agreement with those reported previously (Bandaranayake, K. M. et al. 2006a). Of particular interest are the carbonyl and quinone ring stretching vibrations (Table 1), which have frequencies and intensities that may respond to environmental perturbations, such as hydrogen bonding, electrostatic interactions, and pi-pi stacking. Table 1 shows that only the CO stretching and

CC quinoid ring stretching vibrations are predicted to have vibrational frequencies that are sensitive to phylloquinone reduction. Aromatic ring modes are expected to cancel approximately in the difference spectrum, due to the lack of reduction induced frequency shift, and are not considered further. The CO antisymmetric stretching vibration is predicted to be the most intense band both in the singlet and the anion spectrum (Table 1). Although in principle, two CO bands are expected, the symmetric CO vibrational mode is predicted to be significantly less intense compared to the antisymmetric mode, and the frequencies are predicted to be similar (Table 1). Therefore, the two CO bands may overlap. Upon phylloquinone reduction, the CO band is predicted to downshift 174 cm^{-1}. The most intense quinoid CC stretching vibration is predicted to downshift by 100 cm^{-1} and to change from a "symmetric" stretch (predominantly C_2C_3 stretching) to an "antisymmetric" stretch (mainly C_9C_{10} stretching). The predicted isotope shifts in Table 1 are accurate only to approximately 5 cm^{-1} and, therefore, the expected isotope-induced downshifts for these bands are similar and less than 8 cm^{-1}. The CO and quinoid normal modes are predicted to have similar intensities both in the singlet and in the anion spectrum, and thus should be observable in the isotope-edited spectrum.

Based on comparison to these DFT calculations, bands in Figure 6C are assigned to A_1^- and A_1 in Table 1. For comparison, previous experimental assignments of phylloquinone singlet and anion radical bands are summarized in Table 2 (Bauscher et al. 1992; Breton et al. 1994; Breton 1997; Bandaranayake, K. M. et al. 2006a). In our isotope-based assignments, a negative-positive-negative complex spectral feature is observed with frequencies of 1695 (neg.), 1655 (pos.) and 1637 (neg.) cm^{-1}. The data were simulated by the generation of Gaussian curves (data not shown). These simulations were dominated by two bands centered

at 1688(-) cm^{-1} and 1685(+) cm^{-1}, which we assign to the singlet CO stretching vibration and its induced isotope shift. The complexity of the observed spectral lineshape may be due to overlapping contributions from the CO antisymmetric and symmetric stretching vibrations in each of two A_1 molecules (Table 1). Our scaled DFT calculations predict a frequency of 1672 cm^{-1} for the CO antisymmetric vibrational mode, supporting this assignment.

The singlet quinoid CC stretching mode is predicted in Table 1 with reasonable intensity at 1610 (scaled) cm^{-1}. Therefore, the negative spectral feature at 1557 cm^{-1} in Figure 6C is assigned to the A_1 quinoid ring stretching vibration. The corresponding isotope-shifted component is shifted in the predicted direction, but the magnitude of the shift is larger than predicted (Table 1). This observation suggests significant motion of the methyl group in these singlet CO and quinoid normal modes. This is supported by the fact that the calculated mode also contains some methyl group motion.

As discussed above, the CO stretching vibration is predicted to be the most intense A_1^- band (Table 1). In Figure 6C, the only positive band, which is assignable to the A_1^- CO, is at 1393 cm^{-1}. Therefore, the broad spectral features (Figure 6C) at positive 1393 cm^{-1} and negative 1371 cm^{-1} are assigned to the CO vibration of the anion and its isotope-shifted component (Table 1). Broadening of these bands may be due to overlapping contributions from two A_1^- molecules and from the antisymmetric and symmetric CO bands. The scaled CO antisymmetric stretching frequency (Table 1) predicts a frequency of 1498 cm^{-1} for this mode. We speculate that the lower than expected intensity and frequency for the CO band (Table 1) may be due to the asymmetric hydrogen bond, an electrostatic interaction, or to the pi-pi interaction with the quinone binding site tryptophan (see discussion below). In Figure 6C, candidates for the quinoid CC stretching vibrations are not observed in the expected

1500-1400 cm^{-1} spectral region, perhaps because the isotope shifts are small and the bands have low intrinsic intensity (Table 1).

3.5 Discussion

In this work, we have incorporated C^2H_3 into the C_2 methyl group of the A_1 electron acceptor, and we have used this approach to assign vibrational bands to A_1^- and A_1. This experiment was performed in apo-F_X PSI preparations, in which A_1 is the terminal electron acceptor (Warren et al. 1990; Warren et al. 1993). Previous studies have shown that inactivation of the rubA gene resulted in PSI complexes lacking the stromal subunits, PsaC, PsaD and PsaE. Furthermore, this mutant was unable to assemble F_X (Shen et al. 2002a). This work led to the conclusion that removal of the iron-sulfur clusters does not appreciably alter the orientation of A_1^- or the distance between A_1^- and P_{700}^+. However, that study did find that the motion of A_1 in the mutants may be greater due to the absence of F_X and the stromal subunits (Shen et al. 2002b). Previous work studying chemically extracted P_{700}-A_1 core proteins have concluded that there is a change in the A_1 hydrogen bonding environment (Warren et al. 1990; Warren et al. 1993; Van der Est et al. 1994; Shen et al. 2002a). However, our approach of using apo-F_X samples has the advantage of simplifying the spectrum, increasing the amplitude of A_1^- spectral contributions, and avoiding complex spectral deconvolution techniques, which are required to study A_1^- in intact PSI, where the anion radical has a short (microsecond) lifetime (Brettel, K. et al. 2001).

The PSI crystal structure (Figure 2) reveals that the C_1O groups of the A_1 acceptors do not participate in hydrogen bonding. However, the C_4O groups accept a hydrogen bond from the backbone NH group of LeuA722 for A_{1A} or LeuB706 for A_{1B} (Fromme et al. 2001;

Jordan et al. 2001; Pushkar, Y. et al. 2004; Grotjohann et al. 2005). EPR studies have shown asymmetric hydrogen bonding to A_1^- and an asymmetric distribution of spin density (Shen et al. 2002b; Pushkar, Y. et al. 2004; Teutloff et al. 2004; Pushkar, Y. N. et al. 2005). This result suggests that the hydrogen bond to C_4O is sustained upon reduction of A_1. Evidence for a pi-pi stacking interaction with a nearby tryptophan comes from analysis of the PSI structure and from EPR and mutational studies (Hanley et al. 1997; Fromme et al. 2001; Guergova-Kuras et al. 2001; Jordan et al. 2001; Purton et al. 2001).

Our assignments, which are presented in Table 1, are based on DFT calculations as well as isotope labeling of the phylloquinone molecule. An analysis of these results and comparison to previous work is presented below.

3.5.1 Comparison to previous A_1^-/A_1 assignments in apo-F_X PSI. Our results, based on phylloquinone labeling, are congruent with previous interpretations of the apo-F_X A_1/A_1^- spectrum at room temperature (Table 2) (Hastings et al. 2001). In those experiments, a 1680 cm^{-1} band was assigned to the C_1O stretching of A_1; the hydrogen bonded C_4O group was assigned at 1643 cm^{-1}. The previously assigned 1680 cm^{-1} band may correspond to our 1688 cm^{-1} band. The previous 1643 cm^{-1} assignment may correspond to the negative 1637 cm^{-1} band, which we observe in our data. The A_1^- CO stretching frequencies were assigned at 1455 and 1445 cm^{-1} in that previous work (Table 2). A band at 1396 cm^{-1} was observed, but assigned to a CC stretching vibration of the anion radical. Because our DFT calculations indicate that the most intense A_1^- band will be the CO antisymmetric stretching vibration, we favor the assignment of our 1393 cm^{-1} band to a carbonyl stretching vibration. Other, previously reported bands in the 1500-1400 cm^{-1} region (Table 2) are predicted by our calculations to be less isotope-sensitive and are not observed here with significant intensity.

3.5.2 Comparison to previous A_1^-/A_1 assignments in intact PSI. Recently, A_1^-/A_1 spectra were generated using time-resolved FTIR measurements at 77 K in intact PSI. Overall, the spectra exhibit similarities to the A_1^-/A_1 data reported here. However, in this previous time-resolved work, bands at 1655 and 1607 cm^{-1} were identified as the A_1 CO stretching vibrations (Table 2), consistent with two distinct carbonyl stretching vibrations for A_1. Quinoid CC stretching and benzene aromatic stretching vibrations were assigned at 1651 and 1634 cm^{-1}. Upon anion formation, the CO stretching and CC stretching vibrational bands were assigned at 1495 and 1414 cm^{-1}, respectively (Sivakumar et al. 2005). These assignments are in contrast to ours (Table 1), as well as to previous assignments derived from FT-IR studies of apo-F_X PS1 (Table 2 and (Hastings et al. 2001)). These differences could arise from the deconvolution of the complex, time resolved FT-IR spectra, which was interpreted to contain chl A_0 keto vibrational bands in the 1680 cm^{-1} region (Sivakumar et al. 2005). It is also possible that removal of the polypeptides PsaC, PsaD, and PsaE, and F_X causes subtle changes in the binding pocket of A_1, which are reflected in the vibrational frequencies of A_1 and A_1^- in the apo-Fx preparation.

3.5.3 Comparison to previous studies of model phylloquinone and phylloquinone anion radicals in vitro. Previous electrochemical FTIR studies of phylloquinone *in vitro* assigned two singlet CO stretching vibrations at 1658 and 1616 cm^{-1} (Table 2) and an aromatic ring stretching vibration at 1596 cm^{-1}. Upon quinone reduction, the anion CO stretching band was observed at 1488 cm^{-1}, and the quinoid stretching was not assigned (Bauscher et al. 1992). However, other FTIR studies of phylloquinone (Table 2) have observed only one singlet CO stretching band at 1661 cm^{-1}, in agreement with our

predictions (Table 1). In this second study, the quinoid stretching was assigned at 1618 cm^{-1}, and the aromatic ring stretching band was assigned at 1597 cm^{-1} (Breton et al. 1994).

We assign the A_1 CO vibration at 1688 cm^{-1}, the A_1 quinoid stretching vibration at 1557 cm^{-1}, and the A_1^- CO vibration at 1393 cm^{-1} (Table 1). Compared to previous model compound work (Table 2), these data suggest significant environmental perturbations of A_1 and A_1^- in PSI. This environmental perturbation upshifts the singlet CO stretching vibration (by ~30 cm^{-1}), downshifts the singlet quinoid ring vibration (by ~40 cm^{-1}), and downshifts the radical CO vibration (by ~95 cm^{-1}).

3.5.4 Comparison to previous studies of phylloquinone in the bacterial reaction center. In the bacterial reaction center, phylloquinone can be substituted and can function as the primary quinone acceptor, Q_A. In contrast to the PSI A_1 acceptor, in the bacterial reaction center, two hydrogen bond bonds are formed, one to each Q_A carbonyl oxygen. In *R. viridis*, it has been reported that the Q_A carbonyl oxygens are hydrogen bonded to the peptide NH of Ala M258 and to a non-heme iron histidine ligand (Deisenhofer et al. 1989). In *R. sphaeroides*, it has been reported that the quinone carbonyl oxygens are hydrogen bonded to the peptide NH of Ala M258 and to Thr M222 (Breton et al. 1997). The indole group of a tryptophan is nearly parallel to the Q_A ring at a distance of 3.1 Å (Deisenhofer et al. 1989; Breton et al. 1997).

When phylloquinone was substituted into Q_A binding site in the bacterial reaction center, (Breton et al. 1994; Breton 1997) two CO bands were observed, with frequencies at ~1650 and 1640 cm^{-1} (Table 2). These bands were attributed to the asymmetric CO vibration of the two different carbonyl groups, which have different frequencies due to differential

hydrogen bonding (Breton et al. 1994; Breton 1997). The anion CO band was assigned either at 1438 or 1444 cm^{-1}, ~40 cm^{-1} lower than frequency compared to *in vitro* phylloquinone studies and ~50 cm^{-1} higher in frequency compared to our assignments for A_1^- (Table 1 and 2).

3.5.5 Rationalization of environmental perturbations to the A_1 and A_1^- vibrational spectra. We suggest that observed perturbations, when PSI is compared to model compounds or to phylloquinone-substituted bacterial reaction centers, are due to a combination of the asymmetric hydrogen bonding pattern, electrostatic interactions, and the pi-pi stacking interaction with a tryptophan (Figure 2). We propose that these protein-quinone interactions have differential effects on the anion and singlet CO vibrational bands (see below).

From the crystal structure, the secondary electron acceptor A_1 is known to be in pi-pi stacking distance with a tryptophan residue. The distance between the aromatic ring system of the Trp residues, TrpA697 and TrpB677, and the quinone A_{1A} and A_{1B} range between 3-3.5 Å respectively (Fromme et al. 2001). Previous ESEEM studies have suggested a quinone-tryptophan interaction, because it was shown that the unpaired electron on A_1^- is coupled to the nitrogen of tryptophan (Hanley et al. 1997; Van der Est et al. 1997). An increase in the g_x value of A_1^-, compared to phylloquinone in solution, has been interpreted to imply that A_1 exists in a negative electrostatic environment (MacMillan et al. 1997; Karyagina et al. 2007). Quantum chemical calculation have suggested that a fixed pi-stacked arrangement, as observed in the PSI structure, may lower the redox potential of the A_1 electron acceptor (Kaupp 2002). A charged aspartate may also modify the quinone redox potential (Karyagina et al. 2007).

It should be noted that in model studies, symmetric hydrogen bonding in protic solvents had little effect on phylloquinone ring or CO frequencies (Bauscher et al. 1992). In phylloquinone-substituted bacterial reaction centers, two hydrogen bonds to phylloquinone produced a splitting of only 10 cm^{-1} in the CO vibrational bands (Breton et al. 1994; Breton 1997). In addition, DFT calculations have predicted only small splittings and shifts of the CO vibrational bands (6-14 cm^{-1}), when an asymmetric hydrogen bond to phylloquinone and the phylloquinone anion radical is included in a simple model system. Therefore, prediction of the spectral changes due to the introduction of an unusual, asymmetric hydrogen bond awaits more detailed theoretical approaches based on the PSI structure, which must also include the effect of electrostatic or Stark interactions on the vibrational spectrum (Suydam et al. 2003).

Pi-pi interactions have complex effects on vibrational frequencies, perhaps due to difficulties in separating the effects of hydrogen bonding, geometry, dispersive, and electrostatic interactions in many biologically relevant systems (McCarthy et al. 1997; Plokhotnichenko et al. 1998; Hobza et al. 2000; Hermansson 2002; Sacksteder et al. 2005; Lee et al. 2006; Saeki et al. 2006). Therefore, the expected effects of pi-pi interactions on quinone and tryptophan vibrational frequencies and amplitudes must also be addressed in future studies. Currently, DNA base stacking provides one possible model system for assessing the effect of pi-pi interactions. IR studies of poly-uracil/poly-adenine have shown that shifts of IR bands occur with helix formation. The uracil CO stretching frequency increased 19 cm^{-1}, and the uracil ring stretching vibration decreased in frequency (Miles et al. 1978). The transition from non-ordered to ordered structures was observed to shift the carbonyl vibration towards higher frequency (Liquier et al. 1996). Studies of 1,3-

dimethyluracil, cytidine, caffeine, inosine and 2'-deoxyadenosine found that stacking of these molecules also had an effect on the IR spectra. The carbonyl stretching band increased in frequency, and a decrease in the intensity of the skeletal ring stretching vibrational bands were observed (Maevsky et al. 1980). These experimental results concerning the effect of pi stacking on nucleobases are congruent with our A_1/A_1^- assignments.

3.6 Acknowledgments

Supported by NIH GM43273 (B.A.B.) and the Oklahoma Supercomputing Center for Education and Research (OSCER). The authors thank Dr. J. Golbeck and Dr. R. Agalarov for performing the transient absorption measurements.

3.7 References

Aglarov, R. and B. Klaus (2003). "Temperature dependence of biphasic forward electron transfer from the phylloquinone(s) A_1 in Photosystem I: only the slower phase is activated." *Biochim. Biophys. Acta* **1604**: 7-12.

Ali, K., S. Santabarbara, P. Heathcote, M. C. W. Evans and S. Purton (2006). "Bidirectional electron transfer in photosystem I: replacement of the symmetry-breaking tryptophan close to the PsaB-bound phylloquinone A_{1B} with a glycine residue alters the redox properties of A_{1B} and blocks forward electron transfer at cryogenic temperatures." *Biochim Biophys Acta* **1757**: 1623-1633.

Allen, J. P., G. Feher, T. O. Yeates, H. Komiya and D. C. Rees (1988). "Structure of the reaction center from *Rhodabacter sphaeroides* R-26: protein-cofactor (quinones and F^{2+}) interactions." *Proc. Natl. Acad. Sci. USA* **85**: 8481-8491.

Bandaranayake, K. M., V. Sivakumar, R. Wang and G. Hastings (2006). "Modeling the A_1 binding site in Photosystem I. Density functional theory for the calculation of "anion-neutral" FTIR difference spectra of phylloquinone." *Vib. Spectrosc* **42**: 78-87.

Bandaranayake, K. M., R. Wang and G. Hastings (2006a). "Modification of the phylloquinone in the A_1 binding site in photosystem I studied using time-resolved FTIR difference spectroscopy and density functional theory." *Biochemistry* **45**: 4121-4127.

Bandaranayake, K. M., R. Wang, T. W. Johnson and G. Hastings (2006b). "Time-resolved FTIR difference spectroscopy for the study of photosystem I particles with plastoquinone-9 occupying the A_1 binding site." *Biochemistry* **45**: 12733-12740.

Barry, B. A. (1995). "Tyrosyl radicals in photosystem II." *Methods Enzymol.* **258**: 303-319.

Barry, B. A. and G. T. Babcock (1987). "Tyrosine radicals are involved in the photosynthetic oxygen evolving system." *Proc. Natl. Acad. Sci. USA* **84**: 7099-7103.

Bauscher, M. and W. Maentele (1992). "Electrochemical and infrared-spectroscopic characteriziation of redox reaction of p-quinones." *J.Phys.Chem.* **96**: 11101-11108.

Bautista, J. A., F. Rappaport, M. Guergova-Kuras, R. O. Cohen, J. H. Golbeck, J. Y. Wang, D. Beal and B. A. Diner (2005). "Biochemical and biophysical characterization of photosystem I from phytoene desaturase and zeta-carotene desaturase deletion mutants of *Synechocystis* Sp. PCC 6803: evidence for PsaA- and PsaB-side electron transport in cyanobacteria." *J. Biol. Chem.* **280**: 20030-20041.

Becke, A. D. (1988). "Density-functional exchange-energy approximation with correct asymptotic behavior." *Phys. Rev. A* **38**: 3098-3100.

Becke, A. D. (1993). "A new mixing of Hartree-Fock and local density functional theories." *J. Chem. Phys.* **98**: 1372-1377.

Boesch, S. E. and R. A. Wheeler (1995). "Pi-donor substituent effects on calculated structures and vibrational frequencies of p-benzoquinone, p-fluoranil, and p-chloranil." *J. Phys. Chem.* **99**: 8125-8134.

Boesch, S. E. and R. A. Wheeler (1997a). "Pi-Donor Substituent effects on calculated structures, spin properties, and vibrations of radical anions of p-chloranil, p-fluoranil, and p-benzoquinone." *J. Phys. Chem. A* **101**: 8351-8359.

Boesch, S. E. and R. A. Wheeler (1997b). "Structures and properties of ubiquinone-1 and its radical anion from hybrid Hartree-Fock/density functional studies." *J. Phys. Chem. A* **101**: 5799-5804.

Boudreaux, B., F. MacMillan, C. Teutloff, R. Agalarov, F. Gu, S. Grimaldi, R. Bittl, K. Brettel and K. Redding (2001). "Mutations in both sides of the photosystem I reaction center identify the phylloquinone observed by electron paramagnetic resonance spectroscopy." *J. Biol. Chem.* **276**: 37299-37306.

Breton, J. (1997). "Efficient exchange of the primary quinone acceptor Q_A in isolated reaction centers of *Rhodopsuedomonas viridis*." *Proc. Natl. Acad. Sci. USA* **94**: 11318-11323.

Breton, J., C. Boullais, J. R. Burie, E. Nabedryk and C. Mioskowski (1994). "Binding sites of quinones in photosynthetic bacterial reaction centers investigated by light-induced FTIR difference spectroscopy: assignment of the interactions of each carbonyl of Q_A in *Rhodobacter sphaeroides* using site-specific ^{13}C-labeled ubiquinone." *Biochemistry* **33**: 14378-14386.

Breton, J., E. Nabedryk, J. P. Allen and J. C. Williams (1997). "Electrostatic influence of Q_A reduction on the IR vibrational mode of the 10a-ester C==O of HA demonstrated by mutations at residues Glu L104 and Trp L100 in reaction centers from Rhodobacter sphaeroides." *Biochemistry* **36**: 4515-4525.

Breton, J., E. Nabedryk and W. Leibl (1999). "FTIR study of the primary electron donor of Photosystem I (P_{700}) revealing delocalization of the charge in P_{700}^+ and localization of the triplet character in $^3P_{700}$." *Biochemistry* **38**: 11585-11592.

Brettel, K. (1997). "Electron transfer and arrangement of the redox cofactors in Photosystem I." *Biochim. Biophys. Acta* **1318**: 322-373.

Brettel, K. and J. H. Golbeck (1995). "Spectral and kinetic characterization of electron acceptor A_1 in a Photosystem I core devoid of iron-sulfur centers F_X F_B and F_A." *Photosynth. Res.* **45**: 183-193.

Brettel, K. and W. Leibl (2001). "Electron transfer in Photosystem I." *Biochim. Biophys. Acta* **1507**: 100-114.

Cohen, R. O., G. Shen, J. H. Golbeck, W. Xu, P. R. Chitnis, A. I. Valieva, A. van der Est, Y. Pushkar and D. Stehlik (2004). "Evidence for asymmetric electron transfer in cyanobacterial photosystem I: analysis of a methionine-to-luecine mutation of the ligand to the primary electron acceptor A_0." *Biochemistry* **43**: 4741-4754.

Dashdorj, N., W. Xu, R. O. Cohen, J. H. Golbeck and S. Savikhin (2005). "Asymmetric electron transfer in cyanobacterial Photosystem I: charge separation and secondary electron transfer dynamics of mutations near the primary electron acceptor A_0." *Biophys. J.* **88**: 1238-1249.

Deisenhofer, J. and H. Michel (1989). "The photosynthetic reaction center from the purple bacterium *Rhodopseudomonas viridis*." *Science* **245**: 1463-1473.

Feldman, K. S., D. K. Hester 2nd and J. H. Golbeck (2007). "A relationship between amide hydrogen bond strength and quinone reduction potential: Implications for photosystem I and bacterial reaction center quinone function." *Bioorg. Med. Chem. Lett.* **In press**.

Frisch, M. J., G. W. Trucks, H. B. Schlegel, G. E. Scuseria, M. A. Robb, J. R. Cheeseman, J. A. Montgomery, T. Vreven, K. N. Kudin, J. C. Burant, J. M. Millam, S. S. Iyengar, J. Tomasi, V. Barone, B. Mennucci, M. Cossi, G. Scalmani, N. Rega, G. A. Petersson, H. Nakatsuji, M. Hada, M. Ehara, K. Toyata, J. Fukuda, M. Hasegawa, T. Ishida, T. Nakajima, Y. Honda, O. Kitao, H. Nakai, M. Klene, X. Li, J. E. Knox, H. P. Hratchian, J. B. Cross, V. Bakken, C. Adamo, J. Jaramillo, R. Gomperts, R. E. Stratmann, O. Yazyev, A. J. Austin, R. Cammi, C. Pomelli, J. W. Ochterski, P. Y. Ayala, K. Morokuma, G. A. Voth, P. Salvador, J. J. Dannenberg, V. G. Zakrzewski, S. Dapprich, A. D. Daniels, M. C. Strain, O. Farkas, D. K. Malick, A. D. Rabuck, K. Raghavachari, J. B. Foresman, J. V. Ortiz, Q. Cui, A. G. Baboul, S. Clifford, J. Cioslowski, B. B. Stefanov, G. Liu, A. Liashenko, P. Piskorz, I. Komaromi, R. L. Martin, D. J. Fox, T. Keith, M. A. Al-Laham, C. Y. Peng, A. Nanayakkara, M. Challacombe, P. M. W. Gill, B. Johnson, W. Chen, M. W. Wong, C. Gonzalez and J. A. Pople (2004). Gaussian 03, Revision D.01. Wallingfort, CT, Gaussian, Inc.

Fromme, P., P. Jordan and N. Krauss (2001). "Structure of photosystem I." *Biochim Biophys Acta* **1507**: 5-31.

Golbeck, J. H. (1994). *In The Molecular Biology of Cyanobacteria*. Dordrecht, Kluwer Academic Publishers.

Grafton, A. K. and R. A. Wheeler (1998a). "Vibrational projection analysis: new tool for quantitatively comparing vibrational normal modes of similar molecules." *J. Comput. Chem.* **19**: 1663-1674.

Grafton, A. K. and R. A. Wheeler (1998b). "ViPA: A computer program for vector projection analysis of normal vibrational modes of molecules." *Comput. Phys. Commun.* **113**: 78-84.

Grotjohann, I. and P. Fromme (2005). "Structure of cyanobacterial photosystem I." *Photosynth. Res.* **85**: 51-72.

Guergova-Kuras, M., B. Boudreaux, A. Joliot, P. Joliot and K. Redding (2001). "Evidence for two active branches for electron transfer in photosystem I." *Proc. Natl. Acad. Sci. USA* **98**: 4437-4442.

Hanley, J., Y. Deligiannakis, F. MacMillan, H. Bottin and A. W. Rutherford (1997). "ESEEM study of the phyllosemiquinone radical A_1^- in ^{14}N- and ^{15}N-labeled Photosystem I." *Biochemistry* **36**: 11543-11549.

Hastings, G. and V. Sivakumar (2001). "A fourier transform infrared absorption difference spectrum associated with the reduction of A_1 in Photosystem I: are both phylloquinones involved in electron transfer?" *Biochemistry* **40**: 3681-3689.

Hehre, W. J., L. Radom, P. v. R. Schleyer and J. A. Pople (1986). *Ab initio Molecular Orbital Theory*. New York, John Wiley & Sons.

Helgaker, T. and P. R. Taylor (1995). Modern electronic structure theory, Part II. D. R. Yarkony. Singapore, *World Scientific*. **2:** 725-856.

Hermansson, K. (2002). "Blue-shifting hydrogen bonds." *J. Phys. Chem. A* **206**: 4695-4702.

Hobza, P. and Z. Havlas (2000). "Blue-shifting hydrogen bonds." *Chem. Rev.* **100**: 4253-4264.

Holzwarth, A. R., M. G. Muller, J. Niklas and W. Lubitz (2006). " Ultrafast transient absorption studies on photosystem I reaction centers from *Chlamydomonas reinhardtii*. 2: Mutations near the P_{700} reaction center chlorophylls provide new insight into the nature of the primary electron donor." *Biophys. J.* **90**: 552-565.

Itoh, S., M. Iwaki and I. Ikegami (2001). "Modification of photosystem I reaction center by the extraction and exchange of chlorophylls and quinones." *Biochim. Biophys. Acta* **1507**: 115-138.

Joliot, P. and A. Joliot (1999). "In vivo analysis of the electron transfer within Photosystem I: are the two phylloquinones involved?" *Biochemistry* **38**: 11130-11136.

Jordan, P., P. Fromme, H. T. Witt, O. Klukas, W. Saenger and N. Krauss (2001). "Three-dimensional structure of cyanobacterial photoystem I at 2.5 Å resolution." *Nature* **411**: 909-917.

Kamlowski, A., B. Altenberg-Greulich, A. van der Est, S. G. Zeck, R. Bittl, P. Fromme, W. Lubitz and D. Stehlik (1998). "The quinone acceptor A_1 in Photosystem I: binding site, and comparison to Q_A in purple bacteria reaction centers." *J. Phys. Chem. B* **102**: 8278-8287.

Karyagina, I., Y. Pushkar, D. Stehlik, A. Van der Est, H. Ishikita, E. W. Knapp, B. Jagannathan, R. Agalarov and J. Golbeck (2007). "Contribution of the protein environment to the midpoint potentials of the A_1 phylloquinones and the F_X iron-sulfur cluster in Photosystem I." *Biochemistry* **46**: 10804-10816.

Kaupp, M. (2002). "The function of Photosystem I. Quantum chemical insights into the role of tryptophan-quinone interactions." *Biochemistry* **41**: 2895-2900.

Kim, S. and B. A. Barry (1998). "The protein environment surrounding tyrosyl radicals D• and Z• in photosystem II: a difference Fourier-transform infrared spectroscopic study." *Biophys. J.* **74**: 2588-2600.

Kim, S. and B. A. Barry (2000a). "Identification of carbonyl modes of P_{700} and P_{700}^+ by in situ chlorophyll labeling in photosystem I." *J. Am. Chem. Soc.* **122**: 4980-4981.

Kim, S., J. S. Patzlaff, T. Krick, I. Ayala, R. K. Sachs and B. A. Barry (2000b). "Isotope-based discrimination between the infrared modes of plastosemiquinone anion radicals and neutral tyrsoyl radicals in photosystem II." *J. Phys. Chem. B* **104**: 9720-9727.

Kim, S., C. A. Sacksteder, K. A. Bixby and B. A. Barry (2001). "A reaction-induced FT-IR study of cyanobacterial photosystem I." *Biochemistry* **40**: 15384-15395.

Klughammer, C., B. Klughammer and R. Pace (1999). "Deuteration effects on the in vivo EPR spectrum of the reduced secondary photosystem I electron acceptor A_1 in cyanobacteria." *Biochemistry* **38**: 3726-3732.

Kruip, J., P. Chitnis, B. Lagoutte, M. Rogner and E. J. Boekema (1997). "Structural organization of the major subunits in cyanobacterial Photosystem I." *J. Biol. Chem.* **272**: 17061-17069.

Lee, C., K. H. Park and M. Cho (2006). "Vibrational dynamics of DNA I. Vibrational basis modes and couplings." *Journal of Chemical Physics* **125**: 114508.

Lee, C., W. Yang and R. G. Parr (1988). "Development of the Colle-Salvetti correlation-energy formula into a functional of the electron density." *Phys. Rev. B* **37**: 785-789.

Li, Y., A. van der Est, M. G. Lucas, V. M. Ramesh, F. Gu, A. Petrenko, S. Lin, A. N. Webber, F. Rappaport and K. Redding (2006). "Directing electron transfer within Photosystem I by breaking H-bonds in the cofactor branches." *Proc. Natl. Acad. Sci. USA* **103**: 2144-2149.

Liquier, J. and E. Taillandier (1996). *Infrared Spectroscopy of Biomolecules*. New York, Wiley-Liss.

MacMillan, F., J. Hanley, L. van der Weerd, M. Knupling, S. Un and A. W. Rutherford (1997). "Orientation of the phylloquinone electron acceptor anion radical in Photosystem I." *Biochemistry* **36**: 9297-9303.

Maevsky, A. A. and B. I. Sukhorukov (1980). "IR study of base stacking interactions." *Nucleic Acids Res.* **8**: 3029-3042.

McCarthy, W., J. Smets, L. Adamowicz, A. M. Plokhotnichenko, E. D. Radechenko, G. G. Sheina and S. G. Stepanian (1997). "Competition between H-bonded and stacked dimers of pyrimidine: IR and theoretical ab-initio study." *Mol. Phys.* **91**: 513-525.

Miles, H. T. and J. Frazier (1978). "Infrared spectroscopy of polynucleotides in the carbonyl region in H_2O solution: A-U systems." *Biochemistry* **17**: 2920-2927.

Parrett, K. G., T. Mehari and J. H. Golbeck (1990). "Resolution and reconstitution of the cyanobacterial Photosystem I complexes." *Biochim. Biophys. Acta* **1015**: 341-352.

Parrett, K. G., T. Mehari, P. G. Warren and J. H. Golbeck (1989). "Purification and properties of the intact P_{700} and F_X containing Photosystem I core protein." *Biochim Biophys Acta* **973**: 324-332.

Patzlaff, J. S. and B. A. Barry (1996). "Pigment quantitation and analysis by HPLC reverse phase chromatography: a characterization of antenna size in oxygen-evolving photosystem II preparations from cyanobacteria and plants." *Biochemistry* **35**: 7802-7811.

Piccioni, R., G. Bellemare and N. Chua (1982). Methods of polyacrylamide gel electrophoresis in the analysis and preparation of plant polypeptides. *Methods in Chloroplast Molecular Biology.* H. Edelman, R. B. Hallick and N.-H. Chua. Amsterdam, Elsevier**:** 985-1014.

Plokhotnichenko, A. M., E. D. Radechenko, S. G. Stepanian and L. Adamowicz (1998). "Hydrogen-bonded and stacked homo and heterodimers of systems modeling nucleic acid base pairs." *Recent Res. Devel. in Physical Chem.* **2**: 1087-1104.

Poluektov, O. G., S. V. Paschenko, L. M. Utschig, K. V. Lakshmi and M. C. Thurnauer (2005). "Bidirectional electron transfer in photosystem I: direct evidence from high-frequency time-resolved EPR spectroscopy." *J. Am. Chem. Soc.* **127**: 11910-11911.

Purton, S., D. R. Stevens, I. P. Muhiuddin, M. C. W. Evans, S. Carter, S. E. J. Rigby and P. Heathcote (2001). "Site-directed mutagenesis of PsaA residue W693 affects phylloquinone binding and function in the photosystem I reaction center of *Chlamydomonas reinhardtii*." *Biochemistry* **40**: 2167-2175.

Pushkar, Y., D. Stehlik, M. Van Gastel and W. Lubitz (2004). "An EPR/ENDOR study of the asymmetric hydrogen bond between the quinone electron acceptor and the protein backbone in Photosystem I." *Journal of Molecular Structure* **700**: 233-241.

Pushkar, Y. N., I. Karyagina, D. Stehlik, S. Brown and A. van der Est (2005). "Recruitment of a foreign quinone into the A_1 site of Photosystem I." *J. Biol. Chem.* **280**: 12382-12390.

Ramesh, V. M., K. Gibasiewicz, S. Lin, S. E. Bingham and A. N. Webber (2004). "Bidirectional electron transfer in photosystem I: accumulation of A_0^- in A-side or B-side mutants of the axial ligand to chlorophyll A_0." *Biochemistry* **43**: 1369-1375.

Ramesh, V. M., K. Gibasiewicz, S. Lin, S. E. Bingham and A. N. Webber (2007). "Replacement of the methionine axial ligand to the primary electron acceptor A0 slows the A0- reoxidation dynamics in photosystem I." *Biochim Biophys Acta* **1767**: 151-160.

Razeghifard, M. R., S. Kim, J. Patzlaff, R. S. Hutchison, T. Krick, I. Ayala, J. Steenhuis, S. E. Boesch, R. A. Wheeler and B. A. Barry (1999). "In vivo, in vitro and calculated vibrational spectra of plastoquinone and the plastosemiquinone anion radical." *J. Phys. Chem. B* **103**: 9790-9800.

Rigby, S. E., M. C. Evens and P. Heathcote (1996). "ENDOR and Special Triple Resonance Spectroscopy of A1- of Photosystem I." *Biochemistry* **35**: 6651-6656.

Rigby, S. E. J., I. P. Muhiuddin, M. C. W. Evans, S. Purton and P. Heathcote (2002). "Photoaccumulation of the PsaB phyllosemiquinone in photosystem I of *Chlamydomonas* reinhardtii." *Biochim. Biophys. Acta* **1556**: 13-20.

Rippka, R., J. Deruelles, J. B. Waterbury, M. Herdman and R. Y. Stanier (1979). "Generic assignments, strain histories and properties of pure cultures of cyanobacteria." *Journal of General Microbiology* **111**: 1-61.

Rustandi, R. R., S. W. Snyder, L. L. Feezel, T. J. Michalski, J. R. Norris, M. C. Thurnauer and J. Biggins (1990). "Contribution of vitamin K_1 to the electron spin polarization in spinach photosystem I." *Biochemistry* **29**: 8030-8032.

Sacksteder, C. A., S. L. Bender and B. A. Barry (2005). "Role for bound water and CH-pi aromatic interactions in photosynthetic electron transfer." *J. Am. Chem. Soc.* **127**: 7879-7890.

Saeki, M., H. Akagi and M. Fujii (2006). "Theoretical study on the structure and the frequency of isomers of the naphthalene dimer." *Journal of Chemical Theory and Computation* **2**: 1176-1183.

Santabarbara, S., P. Heathcote and M. C. Evans (2005a). "Modeling of the electron transfer reactions in Photosystem I by electron tunnelling theory: the phylloquinones bound to the PsaA and the PsaB reaction centre subunits of PSI are almost isoenergetic to the iron-sulfur cluster F(X)." *Biochim Biophys Acta* **1708**: 283-310.

Santabarbara, S., I. Kuprov, W. V. Fairclough, S. Purton, P. J. Hore, P. Heathcote and M. C. W. Evans (2005b). "Bidirectional electron transfer in photosystem I: determination of two distances between P_{700}^+ and A_1^- in spin-correlated radical pairs." *Biochemistry* **44**: 2119-2128.

Santabarbara, S., I. Kuprov, P. J. Hore, A. Casal, P. Heathcote and M. C. Evans (2006). "Analysis of the spin-polarized electron spin echo of the [P_{700}^{+} A_1^{-}] radical pair of photosystem I indicates that both reaction center subunits are competent in electron transfer in cyanobacteria, green algae, and higher plants." *Biochemistry* **45**: 7389-7403.

Schlegel, H. B. (1986). "Optimization of equilibrium geometries and transition structures." *J. Comput. Chem.* **3**: 214-218.

Scott, A. P. and L. Radom (1996). "Harmonic Vibrational Frequencies: An evaluation of Hartree-Fock, Moller-Plesset, quadratic configuration interaction, density functional theory, and semiemperical scale factors." *J. Phys. Chem.* **100**: 16502-16513.

Shen, G., M. L. Antonkine, A. Van der Est, I. R. Vassiliev, K. Brettel, R. Bittl, S. G. Zech, J. Zhao, D. Stehlik, D. A. Bryant and J. H. Golbeck (2002a). "Assembly of photosystem I. II. Rubredoxin is required for the in vivo assembly of $F_{(X)}$ in *Synechococcus* sp. PCC 7002 as shown by optical and EPR spectroscopy." *J Biol Chem* **277**: 20355-20366.

Shen, G., J. Zhao, S. K. Reimer, M. L. Antonkine, Q. Cai, S. M. Weiland, J. H. Golbeck and D. A. Bryant (2002b). "Assembly of photosystem I. I. Inactivation of the rubA gene encoding a membrane-associated rubredoxin in the cyanobacterium *Synechococcus* sp. PCC 7002 causes a loss of photosystem I activity." *J Biol Chem* **277**: 20343-20354.

Sivakumar, V., R. Wang and G. Hastings (2005). "A_1 reduction in intact cyanobacterial photosystem I particles studied by time-resolved step-scan Fourier transform infrared difference spectroscopy and isotope labeling." *Biochemistry* **44**: 1880-1893.

Slater, J. C. (1974). *Quantum Theory of Molecules and Solids*. New York, McGraw-Hill.

Suydam, I. T. and S. G. Boxer (2003). "Vibrational stark effects calibrate the sensitivity of vibrational probes for electric fields in proteins." *Biochemistry* **42**.

Teutloff, C., R. Bittl and W. Lubitz (2004). "Pulse ENDOR studies on the radical pair $P_{700}^{+}A_1^{-}$ and the photoaccumulated quinone acceptor A_1^{-} of Photosystem I." *Appl. Magn. Reson.* **26**: 5-21.

van der Est, A. (2001). "Light-induced spin polarization in type I photosynthetic reaction centres." *Biochim. Biophys. Acta* **1507**: 212-225.

Van der Est, A., C. Bock, J. H. Golbeck, K. Brettel, P. Setif and D. Stehlik (1994). "Electron transfer from the acceptor A_1 to the iron-sulfur centers in Photosystem I as studies by transient EPR sepctroscopy." *Biochemistry* **33**: 11789-11797.

Van der Est, A., T. Prisner, R. Bittl, P. Fromme, W. Lubitz, K. Mobius and D. Stehlik (1997). "Time-resolved X-, K-, and W-band EPR of the radical pair state $P_{700}^{+}A_1^{-}$ of

Photosystem I in comparison with $P_{865}^{+}Q^{-}$ in bacterial reaction centers." *J. Phys. Chem. B* **101**: 1437-1443.

Vassiliev, I. R., Y.-S. Jung, M. D. Mamedov, A. Y. Semenov and J. H. Golbeck (1997). "near-IR absorbance changes and electrogenic reactions in the microsecond-to-second time domain in Photosystem I." *Biophys. J.* **72**: 301-315.

Vosko, S. H., L. Wilk and M. Nusair (1980). "Accurate spin-dependent electron liquid correlation energies for local spin density calculations: a critical analysis." *Can. J. Phys.* **58**: 1200-1211.

Warren, P. V., J. H. Golbeck and J. T. Warden (1993). "Charge recombination between P_{700}^{+} and A_1^{-} occurs directly to the ground state of P_{700} in a Photosystem I core devoid of F_X F_B and F_A." *Biochemistry* **32**: 849-857.

Warren, P. V., K. G. Parrett, J. T. Warden and J. H. Golbeck (1990). "Characterization of a photosystem I core containing P_{700} and intermediate electron acceptor A_1." *Biochemistry* **29**: 6545-6550.

Wasikowski, C. and S. Klemm (1993). XMOL Version 1.3.1, Research Equipment, Inc. d.b.a. Minnesota Supercomputer Center, Inc.

Wise, K. E., A. K. Grafton and R. A. Wheeler (1997). "Trimethyl-p-benzoquinone provides excellent structural spectroscopic and thermochemical models for plastoquinone-1 and its radical anion." *J. Phys. Chem. A* **101**: 1160-1165.

Wise, K. E., J. B. Pate and R. A. Wheeler (1999). "Phenoxyl, (methylthio) phenoxyl, and (methylthio) cresyl radical models for the structures, vibrations, and spin properties of the cysteine-Linked tyrosyl radical in galactose oxidase." *J. Phys. Chem. B* **103**: 4764-4772.

Xu, W., P. Chitnis, A. Valieva, A. van der Est, Y. N. Pushkar, M. Krzystyniak, C. Teutloff, S. G. Zech, R. Bittl, D. Stehlik, B. Zybailov, G. Shen and J. H. Golbeck (2003a). "Electron transfer in cyanobacterial photosystem I: I. Physiological and spectroscopic characterization of site-directed mutants in a putative electron transfer pathway from A_0 through A_1 to F_x." *J. Biol. Chem.* **278**: 27864-27875.

Xu, W., P. R. Chitnis, A. Valieva, A. van der Est, K. Brettel, M. Guergova-Kuras, Y. N. Pushkar, S. G. Zech, D. Stehlik, G. Shen, B. Zybailov and J. H. Golbeck (2003b). "Electron transfer in cyanobacterial photosystem I: II. Determination of forward electron transfer rates of site-directed mutants in a putative electron transfer pathway from A_0 through A_1 to F_x." *J. Biol. Chem.* **278**: 27876-27887.

Table 1. Assignments of A_1 and A_1^- Vibrational Bands, Based on Isotopic Labeling of the Phylloquinone Acceptor and DFT Calculations

Singlet	Frequency[#] C^1H_3	Frequency C^2H_3	Δ C^2H_3	Predicted[‡] Frequency	Predicted[‡]* Δ C^2H_3	Predicted[‡] Intensity
CO antisymmetric stretching	1688	1685	3	1672	0	279
CO symmetric stretching	NA[∫]	NA	----	1666	0	26
Aromatic ring stretching	NA	NA	----	1584	1	52
Quinoid "symmetric" stretching**	1557	1544	13	1610	3	42
Quinoid "antisymmetric" stretching**	NA	NA	----	1571	1	2
Anion radical	**Frequency C^1H_3**	**Frequency C^2H_3**	**Δ C^2H_3**	**Predicted[‡] Frequency**	**Predicted[‡] CΔ $^2H_3$**	**Predicted[‡] Intensity**
Quinoid antisymmetric stretching	NA	NA	----	1510	1	35
Quinoid symmetric stretching	NA	NA	----	1576	1	3
Aromatic ring stretching	NA	NA	----	1585	0	3
CO antisymmetric stretching	1393	1371	22	1498	1	310
CO symmetric stretching	NA	NA	----	1483	8	17

[#]Frequencies reported in wavenumber (cm^{-1})

[‡]Predicted frequencies (scaled by 0.9614), isotope shifts (Δ $^2H_3$), and intensities from DFT calculations

*Predicted shifts accurate to $\pm$ 5 cm^{-1}

[∫]NA, not assigned

**Although singlet quinoid stretching modes are labeled "symmetric" and "antisymmetric", the modes are mixed and highly localized. Thus, the "symmetric" mode contains predominantly C2C3 stretching, whereas the "antisymmetric" stretch contains predominantly C9C10 stretching.

Table 2. Previous Assignments of Phylloquinone Singlet and Anion Radical IR Bands

In vitro phylloquinone vibrational assignments			
Description of normal mode	Solvent and sample type	Singlet (cm^{-1})	Anion Radical (cm^{-1})
carbonyl stretching	CH_2Cl_2 (Bauscher et al. 1992)	1658, 1616	1488
quinoid stretching	CH_2Cl_2 (Bauscher et al. 1992)	1596	[j]NA
aromatic ring stretching	CH_2Cl_2 (Bauscher et al. 1992)	1596	NA
carbonyl stretching	Film (Breton et al. 1994)	1661	NA
quinone stretching	Film (Breton et al. 1994)	1618	NA
aromatic stretching	Film (Breton et al. 1994)	1597	NA
Bacterial reaction center vibrational assignments			
Description of normal mode	Bacterial reaction center sample	Singlet (cm^{-1})	Anion Radical (cm^{-1})
carbonyl stretching	*Rb. viridis* (Breton 1997)	1653,1637	1438
quinoid stretching	*Rb. viridis* (Breton 1997)	NA	NA
aromatic ring stretching	*Rb. viridis* (Breton 1997)	1590	NA
carbonyl stretching	*Rb. sphaeroides* (Breton et al. 1994)	1651, 1640	1444
quinoid stretching	*Rb. sphaeroides* (Breton et al. 1994)	1608	1478, 1394-1388
aromatic ring stretching	*Rb. sphaeroides* (Breton et al. 1994)	1588	1478, 1394-1388
Photosystem I vibrational assignments			
Description of normal mode	Photosystem I sample	Singlet (cm^{-1})	Anion Radical (cm^{-1})
carbonyl stretching	Intact (Sivakumar et al. 2005)	1655, 1607	1495
quinoid stretching	Intact (Sivakumar et al. 2005)	1651, 1634	1414
aromatic ring stretching	Intact (Sivakumar et al. 2005)	1651, 1634	1414
carbonyl stretching	Apo-F_X (Hastings et al. 2001)	1680, 1643	1455, 1445
quinoid stretching	Apo-F_X (Hastings et al. 2001)	NA	1396, 1381
aromatic ring stretching	Apo-F_X (Hastings et al. 2001)	NA	1396, 1381

[j]NA, not assigned

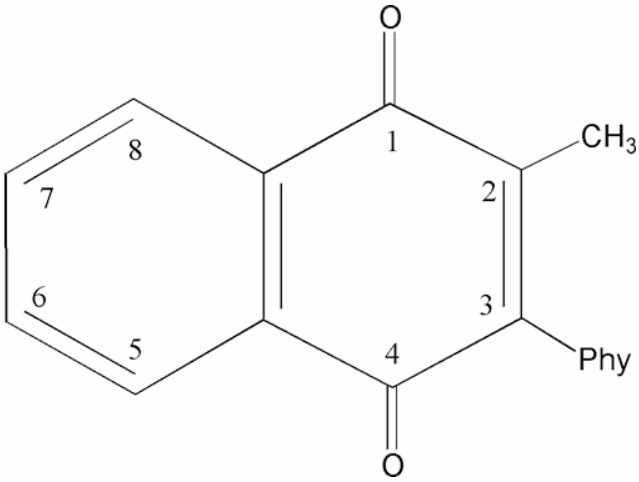

Figure 1. The structure of the secondary electron acceptor A_1 in photosystem I. Numbering is according to IUPAC nomenclature. Phy represents the phytol tail bonded to carbon 3.

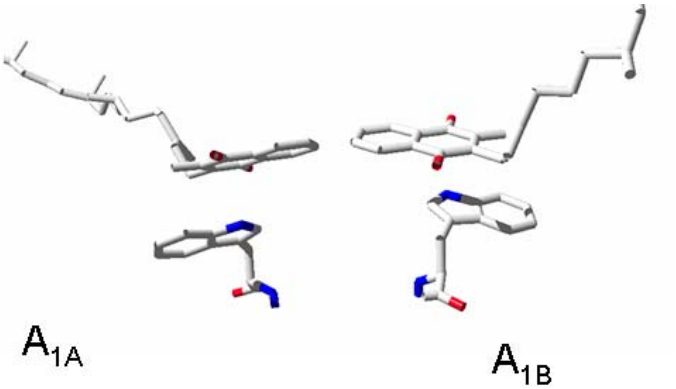

Figure 2. The binding site of A_{1A} *left* and A_{1B} *right* in Photosystem I from the PSI crystal structure at 2.5Å.resolution (Jordan et al. 2001) The tryptophan residues are within π-stacking distance (3-3.5 Å) of the quinone ring.

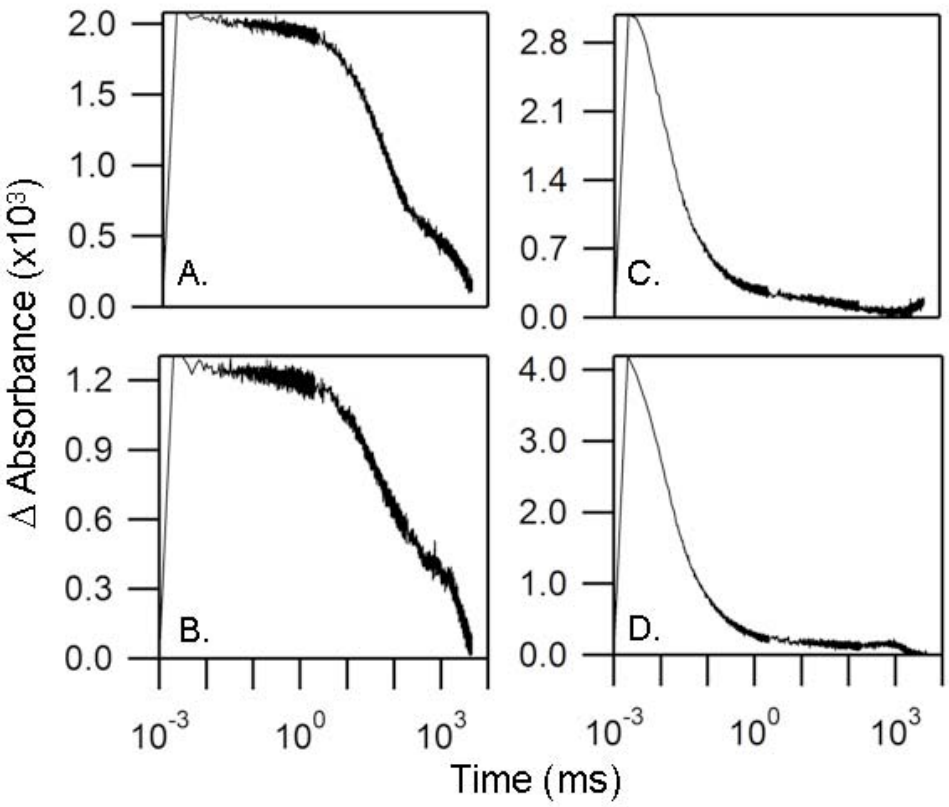

Figure 3. Decay of P_{700}^{+}, as assessed by 820 nm kinetic measurements, in (A) natural abundance, C^1H_3-A_1 intact PSI, (C) natural abundance, C^1H_3-A_1 apo-F_X PSI, (B) labeled C^2H_3-A_1 intact PSI, and (D) labeled C^2H_3 apo-F_X PSI. The reaction medium contained 50 mM Tris buffer (pH 8.3), 0.04% n-dodecyl-β-D-maltoside, 4 μM DCPIP, and 5 mM sodium ascorbate. See Materials and Methods for additional experimental details.

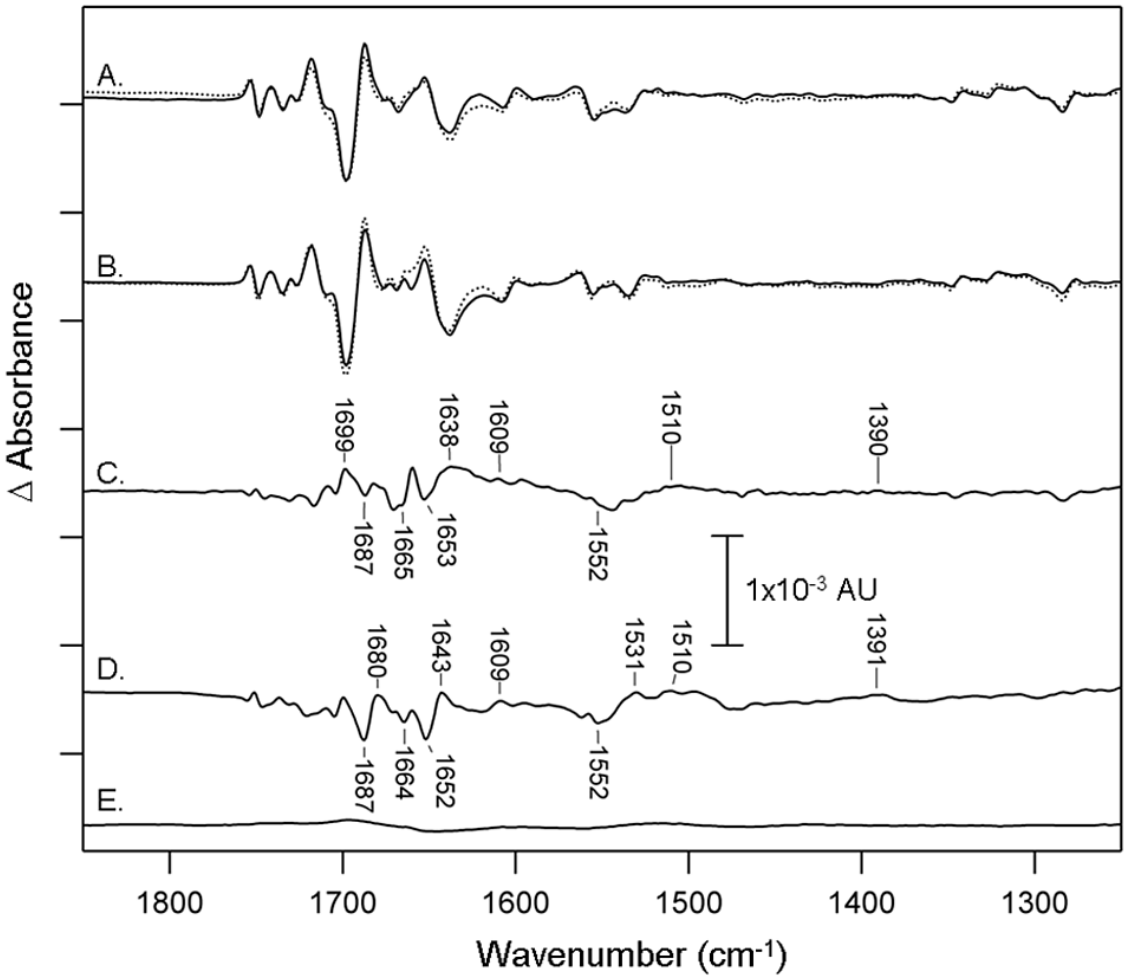

Figure 4. Light-induced FT-IR difference spectra of (A) natural abundance, apo-F_X and (B) natural abundance, intact PSI. Spectra were recorded either at room temperature (20°C, solid lines) or at -10°C (dotted lines). The data in (B) were divided by a factor of 3 to correct for a difference in the amount of stable charge separation. The room temperature A_1^--minus-A_1 spectrum in (C) was constructed by subtracting (B, solid line) from (A, solid line). The -10°C A_1^--minus-A_1 spectrum in (D) was constructed by subtracting (B, dotted line) from (A, dotted line). Spectrum (E) is room temperature, dark-minus-dark control, which was derived from the apo-F_X PSI data set. The solid lines in A, B, and E are the average of 21, 22, and 21 spectra, respectively. The dotted lines in A and B are the average of 45 and 27 spectra respectively. See Materials and Methods for additional experimental details.

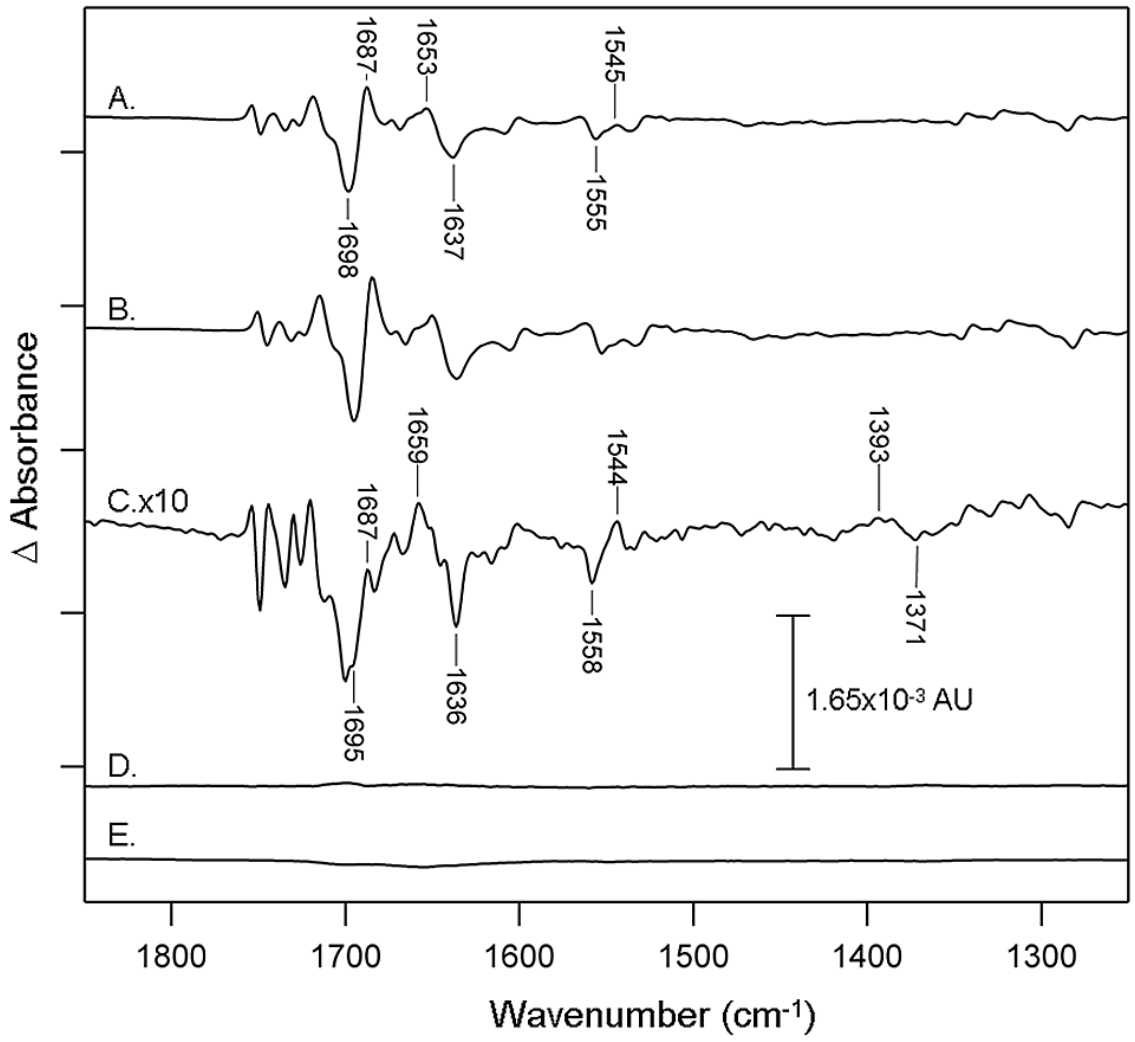

Figure 5. Light-induced FTIR difference spectra of (A) natural abundance C^1H_3-A_1, apo-F_X PSI and (B) labeled C^2H_3-A_1, apo-F_X PSI. The isotope-edited spectrum shown in (C) is a C^1H_3-minus-C^2H_3 double difference spectrum created by subtraction of (B) from (A) and multiplying by a factor of 10. Spectrum (D) is a control double difference spectrum generated by taking one-half of the data in A, subtracting the other half of the data set, and dividing by √2. Spectrum (E) is a dark-minus-dark control. A, B, D, and E are the average of 45 spectra. See Materials and Methods for additional experimental details.

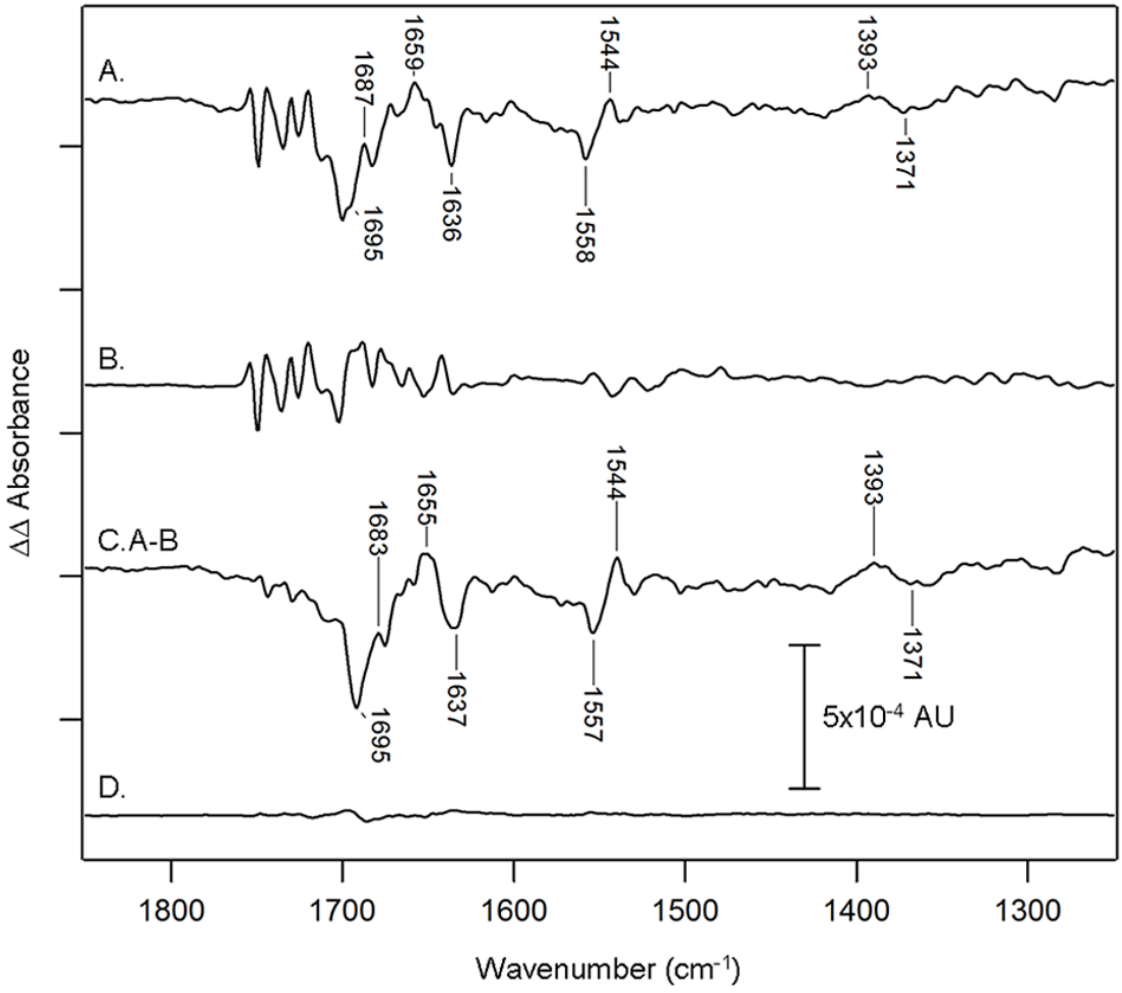

Figure 6. Isotope-edited FT-IR spectra of PSI. (A) shows the C^1H_3-minus-C^2H_3 double difference spectrum, acquired from apo-F_X PSI, (B) shows the C^1H_3-minus-C^2H_3 double difference spectrum, acquired from intact PSI, and (C) shows a subtraction of (A) minus (B), revealing isotopic shifts in A_1^- (positive) and A_1 (negative) bands. The spectra in A and B were normalized to give the same intensity in the P_{700}^+ ester vibrational bands between 1752 and 1748 cm^{-1}. Spectrum (D) is a control double difference spectrum generated by taking one-half of the data in A, subtracting the other half of the data set, and dividing by √2. See Materials and Methods for additional experimental details.

CHAPTER 4

LIGHT-INDUCED DYNAMICS IN PHOTOSYSTEM I ELECTRON TRANSFER

4.1 Abstract

Protein dynamics are likely to play important, regulatory roles in many aspects of photosynthetic electron transfer, but a detailed description of these coupled protein conformational changes has been lacking. In oxygenic photosynthesis, photosystem I (PSI) catalyzes the light-driven oxidation of plastocyanin or cytochrome c and the reduction of ferredoxin. A chl a/a' heterodimer, P_{700}, is the secondary electron donor, and the two P_{700} chl, are designated P_A and P_B. In this work, we have used specific chl isotopic labeling and reaction-induced FT-IR spectroscopy to assign chl keto vibrational bands to P_A and P_B. In the cyanobacterium, *Synechocystis sp.* PCC 6803, the chl keto carbon was labeled from ^{13}C-labeled glutamate, and the chl keto oxygen was labeled from $^{18}O_2$. These isotope-based assignments provide new information concerning the structure of P_A^+. P_A^+ is found to give rise to two chl keto vibrational bands, with frequencies at 1653 and 1687 cm^{-1}. In contrast, P_A gives rise to one chl keto band at 1638

cm^{-1}. Observation of two P_A^+ keto frequencies is consistent with a protein relaxation-induced distribution in P_A^+ hydrogen bonding. These results suggest a light-induced conformational change in PSI, which may regulate the oxidation of soluble electron donors and other electron transfer reactions. This work provides novel information concerning the role of protein dynamics in oxygenic photosynthesis.

4.2 Introduction

In oxygenic photosynthesis, Photosystem I (PSI) is a multi-subunit, membrane protein complex, which carries out the light-induced reduction of ferredoxin and the oxidation of plastocyanin or cytochrome c (Golbeck et al. 1991). These redox events are initiated by light-induced electron transfer, which leads to the oxidation of a chlorophyll dimer, P_{700}, and the reduction of an iron sulfur cluster, F_B.(Brettel et al. 2001; Jordan et al. 2001) Other electron transfer cofactors include the primary chlorophyll donor (eC-2 or eC-3), two A_0 chlorophyll and two A_1 phylloquinone electron acceptors, and two additional iron-sulfur clusters, F_X and F_A. The PSI reaction center contains two large intrinsic polypeptides, PsaA and PsaB (Jordan et al. 2001). The 2.5 Å resolution crystal structure reveals a pseudo-C_2 symmetric arrangement of the accessory chl molecules and of the two A_0 and the two A_1 electron acceptors. These two branches of electron transfer cofactors are referred to as the PsaA and PsaB branches (Jordan et al. 2001). Studies have suggested that both branches carry out light-induced electron transfer (Joliot et al. 1999; Guergova-Kuras et al. 2001).

Recent studies have suggested that charge separation begins on an accessory chl monomer (either eC-2 or eC-3), which donates its electron to an A_0 acceptor (Holzwarth et al. 2006). This primary donor is reduced by P_{700}, a chl a/a' heterodimer, which is the terminal electron donor in the PSI reaction center (Webber et al. 2001). P_{700} is present in the dark, and P_{700}^+ is produced under illumination. P_{700} is composed of a chl a molecule, designated P_B, and of a chl a' molecule, designated P_A. While the X-ray structure supports the interpretation that P_A has hydrogen bonding interactions with its protein

environment, P_B does not appear to be hydrogen bonded (Jordan et al. 2001; Grotjohann et al. 2005).

The soluble copper-containing protein, plastocyanin, acts as the electron donor to P_{700}^+ in plants, algae, and cyanobacteria. Under copper limiting conditions, a cytochrome c can replace plastocyanin as the electron donor in cyanobacteria (Merchant et al. 1986). In plants and algae, plastocyanin docks with the luminal side of PSI to form an interaction complex, in which electron transfer from the reduced copper to P_{700}^+ occurs on the microsecond time scale (Bottin et al. 1985; Hippler et al. 1997). In cyanobacteria, the cytochrome, but not plastocyanin, has been proposed to form an electron transfer complex in vivo (Durán et al. 2004). In both cyanobacteria and algae, mutations in a hydrophobic region near P_{700}^+, which contains luminal PsaA and PsaB helices and a conserved tryptophan dimer, disrupt electron transfer (Sun et al. 1999; Sommer et al. 2002; Sommer et al. 2004). It has been proposed that conformational rearrangements may regulate electron transfer in the interaction complex {(Bottin et al. 1985; Sigfridsson et al. 1997), but see (Drepper et al. 1996)}.

Previously, site-directed mutagenesis and various spectroscopic techniques have been used to study the interaction of the cation radical, P_{700}^+, with its protein environment (Breton 2001; Brettel et al. 2001; van der Est 2001; Webber et al. 2001; Grotjohann et al. 2005). EPR studies have concluded that the unpaired spin is localized mainly on P_B, while FT-IR studies have concluded that the spin-density is evenly distributed over the dimer (Breton et al. 1999; Kaess et al. 2001). This discrepancy may be due to unsolved questions concerning the assignment of the FT-IR vibrational bands, as described below.

Recent experimental (Wang et al. 2007) and previous theoretical (Warshel et al. 1989; Gehlen et al. 1994; Parson et al. 2004) studies have underscored the role of protein dynamics in the control of primary electron transfer in the bacterial reaction center. In the chl-containing reaction center, photosystem II, an influence of protein dynamics on the photosynthetic water-splitting cycle has also been suggested by vibrational spectroscopic experiments on different time scales (Halverson et al. 2003; Barry et al. 2006; De Riso et al. 2006). In PSI, conformational dynamics have the potential to regulate bidirectionality of electron transfer in the reaction center and also to control the mechanism of plastocyanin/cytochrome c oxidation. The effect of light-induced dynamics on P_{700} and P_{700}^{+} can be detected in real time using vibrational spectroscopic techniques, such as FT-IR spectroscopy. Previously, evidence for structural heterogeneity in P_{700}/P_{700}^{+} has been obtained by methyl ester labeling of chl (Kim et al. 2000).

The light-minus-dark, P_{700}^{+}-minus-P_{700}, FT-IR spectrum is dominated by keto vibrational bands from chl and chl^{+}, which, in model compounds, are upshifted in frequency by oxidation (Nabedryk et al. 1990; Breton et al. 1999; Hastings et al. 2001). Keto vibrational frequencies are expected to reflect changes in polarity, hydrogen bonding, and electrostatics (Bellamy 1980). Previously keto vibrational bands have been assigned to P_A, P_A^{+}, P_B, and P_B^{+} in the P_{700}^{+}-minus-P_{700} spectrum. The observation of four keto vibrational bands has been attributed to the oxidation-induced change in force constant, as well as differences in hydrogen bonding interactions between the two halves of the dimer, P_A and P_B (Breton et al. 1999; Hastings et al. 2001; Witt et al. 2002; Li et al. 2004; Pantelidou et al. 2004). However, there has also been controversy over the

assignment of the keto FT-IR bands of P_{700} and P_{700}^{+} (Breton et al. 1999; Hastings et al. 2001), and the spectrum still contains unassigned bands. Therefore, the development of methods to specifically isotopically label chl, with minimal interference from protein labeling, is of particular importance.

In this work, we describe methods to ^{13}C and ^{18}O label the chl keto position (Figure 1) through manipulation of the cyanobacterial chl biosynthetic pathway (Beale 1999; Porra et al. 2001). These isotopically labeled samples were used to assign the 13^{1}-keto stretching bands of the P_{700}^{+}-minus-P_{700} FT-IR spectrum. These data reveal unexpected cofactor-protein relaxation events, which accompany light-induced electron transfer in PSI.

4.3 Materials and Methods

For ^{13}C chl labeling, glutamate-tolerant *Synechocystis* PCC 6803 cultures were grown on solid media containing BG-11 (Rippka et al. 1979), 250 μM L-glutamic acid buffered with 1mM TES-NaOH pH 8.0, 5 mM TES-NaOH, pH 8.0, and 6 mM $Na_2S_2O_3$ (Barry 1995). Liquid cultures (400 ml) were grown in BG-11, 5 mM TES-NaOH, pH 8.0, and 5 μg/ml kanamycin and were bubbled with sterile air. The cultures were supplemented with 1 mM L-glutamic acid or L-glutamic-3-^{13}C acid (99% enrichment, Isotec Inc., Miamisburg, OH), which were buffered with 1 mM TES-NaOH, pH 8.0. Cultures were harvested at an OD_{730} nm of 1.1-1.4.

For ^{18}O chl labeling, *Synechocystis* PCC 6803 cultures were grown on solid media containing BG-11, 5 mM TES-NaOH, pH 8.0, 6 mM $Na_2S_2O_3$, and 5 mM glucose.. Liquid cultures were grown as described above, except that the cultures were

continuously shaken on a cell culture agitator (New Brunswick Scientific, Edison, NJ). CO_2 was bubbled into the cell cultures at a rate of 1 ml/min for 5 minutes daily. Immediately following this, $^{16}O_2$ or $^{18}O_2$ (99% enrichment, Isotec Inc., Miamisburg, OH) was bubbled into the cell cultures at a rate of 1 ml/min for 5 minutes. Cultures were grown a total of 10 days. The OD_{730} for the cultures ranged from 1.0-1.1.

4.3.1 Purification of PSI. Thylakoid membranes were solubilized (Noren et al. 1991), and trimeric PSI was purified by ion exchange liquid chromatography using a Mono Q™ HR 5/5 column (Amersham Biosciences, Arlington, IL) and an ÄKTA explorer instrument (Amersham Biosciences, Arlington, IL) (Barry 1995). The fraction size collected was 0.5 ml, and the visible absorption spectrum of each fraction was recorded on a Hitachi (San Jose, CA) U-3000 UV-visible spectrophotometer using 1cm path length cuvettes. Fractions with absorption maxima greater than 679 nm were pooled. Purified trimeric PSI was dialyzed overnight in 5 mM HEPES-NaOH pH 7.5, 0.04% dodecyl-ß-D-maltoside (LM) and then concentrated using an Amicon (Bedford, MA) Ultra 100,000 MWCO centrifugal filter device to a final concentration of 2-3 mg chl/ml.

*4.3.2 FTIR Spectroscopy***.** FT-IR spectra were collected at -10 °C as described previously (Sacksteder et al. 2005; Bender et al. 2008). Samples contained 2 mM potassium ferricyanide and 2 mM potassium ferrocyanide and were concentrated at room temperature under a steady flow of nitrogen gas. Concentration times were 20-30 minutes. Spectral conditions were as follows: resolution, 4 cm^{-1}; zero filling, 1; data acquisition time, 4.0 min. Difference spectra (light-minus-dark) were generated by taking the ratio of single beam spectra collected before and during illumination and

converting to absorbance. FT-IR spectra were obtained in the dark or under continuous illumination with red and heat-filtered light, as previously described (Kim et al. 2001; Sacksteder et al. 2005; Bender et al. 2008). A 60 min dark relaxation time was used between successive illuminations. Spectra were normalized to account for small differences in sample concentration and path length, using the amplitude of the amide II band in the infrared absorption spectrum. All spectra were normalized to 0.5 AU. Infrared absorption spectra were created by use of a background.

Isotope-edited spectra were generated by subtracting the isotope-labeled difference spectrum from the natural abundance difference spectrum. For the ^{18}O-isotope edited spectrum (Fig. 3C), a direct one-to-one subtraction (C, dotted line), as well as an interactive subtraction (C, solid line), were performed. A subtraction factor of 0.9663 was chosen (Fig. 3C, solid line) in the interactive subtraction to minimize ester contributions, relative to the keto vibrational bands. For the ^{13}C-isotope edited spectrum (Fig. 4C), a direct one-to-one subtraction (C, dotted line) as well as an interactive subtraction (C, solid line) were performed. A subtraction factor of 0.9584 was chosen (Fig. 4C, solid line) in the interactive subtraction to minimize ester contributions relative to the keto vibrational bands. In Figs. 3C and Fig. 4C, the ^{18}O-isotope edited spectrum was multiplied by 8 and the ^{13}C-isotope edited spectrum was multiplied by 5 to equalize spectral amplitudes for comparison. In Figure 5, the interactive subtractions are displayed. To estimate the level of noise in the isotope-edited spectra, control double difference spectra (Figs. 3D and 4D) were generated by taking one-half of the control data set (either ^{12}C or ^{16}O-chl PSI), subtracting from it the second half of the data set, and dividing by the $\sqrt{2}$. Dark-minus-dark spectra were generated from data recorded before

illumination (Figs. 3E and Fig. 4E). Fig. 6A shows an overlay of Fig. 3A (blue, natural abundance) and Fig. 3B (black, ^{18}O-labeled); Fig. 6B shows an overlay of Fig. 4A (blue, natural abundance) and Fig. 4B (black, ^{13}C-labeled).

4.3.3 Assessment of chlorophyll (chl) isotopic enrichment. To determine the amount of isotope incorporation into chl from cell cultures grown with L-glutamic-3-^{13}C-acid or $^{18}O_2$, matrix-assisted laser desorption/ionization mass spectrometry was employed. The control samples were cultures grown in the presence of natural abundance L-^{12}C-glutamic acid or $^{16}O_2$. Chl was extracted from PSI samples with a solution of 80% acetone/20% methanol. The extracted pigments were vortexed, sonicated, centrifuged, and filtered as previously described (Patzlaff et al. 1996; Bender et al. 2008). For NMR spectroscopy, chl was HPLC purified (Patzlaff et al. 1996). Chl was concentrated and dried using a Thermo-Savant SpeedVac concentrator with VLP120 pump and RVT 400 refrigerated vapor trap (Thermo Electron Corporation, Waltham, MA). Chl samples were stored at -70°C until use. A 4700 Proteomics Analyzer (Applied Biosystems Foster City, CA) was used for the mass spectral measurements (Bender et al. 2008). Immediately before the measurement, chl was dissolved in a mixture of 80% methanol, 19% water, and 1% acetic acid; this treatment removes the Mg^{+2} ion of chl and generates pheophytin. The matrix used was alpha-cyano-4-hydroxy cinnamonic acid. The 871.5 *m/z* peak of pheophytin was used for quantitation. Data were analyzed using IGOR (Wavemetrics, Lake Oswego, OR) and Excel (Microsoft, Redmond, WA) software. The data were normalized to the [M+H] peak before the isotope distribution was calculated. Measurements were repeated twice for ^{12}C-chl and ^{13}C-chl, three times

for ^{18}O-chl, and four times for ^{16}O-chl, the error in the measurements was estimated from the range or standard deviation of the measurements.

4.3.4 ^{18}O labeling of chl. Mass spectral data from the $^{16}O_2$ control were subtracted from data derived from the $^{18}O_2$ labeled sample. Analysis of the remaining 873.5 peak {M+H+2} amplitude showed that 15 ± 6% of chl was labeled from $^{18}O_2$.

4.3.5 ^{13}C labeling of chl. In order to calculate the amount of ^{13}C incorporation, mass spectral data derived from the natural abundance sample (Table 1, column 2) were subtracted from the ^{13}C labeled data (Table 1, column 3). The resulting values are given in Table S1, column 4. The 872.5 *m/z* [M+H+1] peak amplitude gives the amount of the $^{+}1$ chl isotopomer, generated by ^{13}C-glutamate labeling (43 $\pm$ 8%). Because eight positions are expected to be labeled from ^{13}C glutamate, the probability the 13^{1} keto position is labeled in the $^{+}1$ isotopomer was derived by dividing by eight (5%, column 13).

To calculate the amount of simultaneous labeling at two chl positions, generating the $^{+}2$ isotopomer, the 873.5 [M+H+2] peak amplitude was employed. The $^{+}1$ isotopomer makes a significant contribution to the +2 isotopomer peak amplitude, which was factored out using the relative, natural abundance peak intensities (Table 4, column 2). Note that the observed, natural abundance and the predicted isotope distributions are similar (Table 4, compare column 2 and Table legend). This subtraction shows that ^{13}C glutamate labeling generated the $^{+}2$ chl isotopomer in 27 $\pm$ 7% of the sample (Table 4, column 6). Because eight positions are expected to be labeled, the probability that the keto position is labeled in the $^{+}2$ isotopomer is calculated by division by 2/8 (Table 4,

column 13). These calculations were repeated for all observed ion signals between 873.5-877.5 *m/z*, and the probabilities were summed to estimate the total amount of ^{13}C label at the keto position.

4.3.6 GC/MS analysis of ^{13}C isotope incorporation into PSI amino acids. To determine the amount of ^{13}C incorporation into amino acids, PSI samples were acid hydrolyzed, derivatized, and subjected to GC/MS as previously described (Kitson et al. 1996; Sachs et al. 2003). The derivatized amino acids were identified by retention time, and the characteristic ions for each amino acid were monitored (Table 4) (Kitson et al. 1996). The extent of isotope incorporation was determined by comparison to natural abundance PSI samples. The analysis was performed in duplicate, and the error in the measurement was estimated from the range.

4.4 Results

To label the oxygen of the 13^1 chl keto group, *Synechocystis* sp. PCC 6803 cyanobacterial cultures were grown in the presence of $^{18}O_2$. The formation of the chl *a* isocyclic ring is an aerobic process, in which the 13^1 oxo group (Figure 1) is derived from molecular oxygen using an oxygenase (Wong et al. 1985; Walker et al. 1989; Schneegurt et al. 1992; Bollivar et al. 1995, 1996). The amount of ^{18}O labeling was measured by mass spectrometry and found to be 15 $\pm$ 6% (Figure 2A and Materials and Methods). The keto position of chl (Figure 1) is the only group that is labeled by this protocol (Wong et al. 1985; Walker et al. 1989; Schneegurt et al. 1992; Bollivar et al. 1995).

Reaction-induced FT-IR spectra were acquired from control and ^{18}O-labeled PSI samples (Figure 3). The difference spectra, constructed by subtraction of data recorded

under illumination and in the dark, are attributable to $P_{700}^{+}F_B^{-}$-minus-$P_{700}F_B$ (Breton et al. 1999; Bender et al. 2008). Figure 3A shows the difference spectrum from ^{16}O-chl PSI and Figure 3B shows the difference spectrum from ^{18}O-chl PSI. The isotope-edited spectrum presented in Figure 3C exhibits keto stretching contributions from P_{700} (negative) and P_{700}^{+} (positive) (Nabedryk et al. 1990; Breton et al. 1999; Breton 2001; Hastings et al. 2001). Spectral changes associated with the labeling of the chl keto oxygen can be identified by an interactive subtraction of control and ^{18}O-labeled data. This interactive subtraction minimizes any small contributions from the chl ester 1754(+)/1749(-) cm^{-1} bands (Kim et al. 2000). Small differences in amplitude in this region can arise from minor alterations in the amount of stable charge separation (Figure 3). The resulting isotope-edited spectrum (Figure 3C) will have contributions only from vibrational bands perturbed by P_{700} oxidation and by the incorporation of the ^{18}O isotope at the keto position. In the isotope-edited spectrum, natural abundance P_{700} bands are negative, and natural abundance P_{700}^{+} bands are positive. The isotope-shifted components for each vibrational band have the opposite sign. Observed spectral features in Figure 3C are significant compared to the noise, which is estimated from a control-minus-control spectrum (Figure 3D).

To interpret the ^{18}O isotope-edited spectrum, incorporation of ^{13}C at the 13^1 carbon (Figure 1) is advantageous, because $13^1/^{13}$C labeling will also shift spectral bands assignable to the keto stretching vibration. In cyanobacterial chl biosynthesis, aminolevulinic acid, the first universal tetrapyrrole precursor, is formed from glutamate, which is activated by ligation to a tRNA molecule (Beale et al. 1975; Porra et al. 1983; Huang et al. 1986; Schön et al. 1986; Rieble et al. 1988). In our experiments, carbon

labeling at the chl 13^1 position was accomplished by growth of a glutamate-tolerant strain of *Synechocystis sp.* PCC 6803 in the presence of 1 mM glutamate, which was ^{13}C labeled at the third carbon (Table 1). Uptake of this isotope is expected to label the 13^1 carbon of chl (Figure 1) and seven other chl carbons (Figure 1) (Beale 1999). The vibrational bands, which are altered by labeling at the non-keto positions, are expected to be distinct in frequency from the keto vibrational bands (Boldt et al. 1987). Further, only a keto vibrational band will be shifted by both ^{18}O and $13^1/^{13}C$ labeling, and CO vibrational bands will be in common between the two types of isotope-edited spectra. Gas chromatography-mass spectral analysis on hydrolyzed PSI demonstrated that there was little scrambling of the ^{13}C glutamate label into other amino acids (Table 2 (Sachs et al. 2003)). Mass spectrometry (Figure 2B and Table 1) revealed that singly, doubly, and triply ^{13}C-labeled chl isotopomers were generated in significant yield (78%). For example, the yield of the $^{+}1$, $^{+}2$, and $^{+}3$ ^{13}C isotopomers was determined to be $43 \pm 8\%$, $27 \pm 7\%$, and $8 \pm 5\%$. Only $2 \pm 4\%$ of the $^{+}4$ isotopomer was detected (Table 2). Using these measured values, the total probability of labeling at the keto carbon position can be estimated as 16% (Table 1 and Materials and Methods). NMR spectroscopy on purified, extracted ^{13}C-labeled chlorophyll in organic solvents (Patzlaff et al. 1996) confirmed the incorporation of label into the keto position (data not shown).

Reaction induced FT-IR spectra were acquired from these ^{13}C labeled PSI samples (Figure 4). Figure 4A is the difference spectrum acquired from ^{12}C-chl PSI and Figure 4B is the difference spectrum acquired from ^{13}C-chl PSI. Figure 4.4C is the ^{13}C isotope-edited spectrum, which exhibits significant features relative to the noise (Figure 4D) and was produced from an interactive subtraction. In Figure 4C, related natural abundance

and isotopomer keto bands, which are expected to be of opposite sign, are labeled with the same color code. Figure 5 compares the ^{18}O isotope-edited spectrum (Figure 5A, solid line) and the ^{13}C isotope-edited spectrum (Figure 5B solid line). Bands assigned to natural abundance P_B and P_B^+ are filled with vertical lines, and bands assigned to natural abundance P_A and P_A^+ are filled with horizontal lines (Figure 5). The assignment of bands in the ^{18}O and ^{13}C isotope-edited spectra is summarized in Table 3.

Bands at (+) 1718 and (-) 1698 cm^{-1} are observed in Figure 5A and 5B, consistent with an assignment to a chl keto vibrational band, which is upshifted by light-induced electron transfer. Based on the signs, the positive 1718 cm^{-1} band would be assignable to P_{700}^+; the negative 1698 cm^{-1} band would be assignable to P_{700}. For these bands, an isolated, CO harmonic oscillator approximation predicts frequency downshifts of ~40 cm^{-1} either with ^{13}C or ^{18}O labeling. The isotope-shifted components for the (+) 1718 cm^{-1} band are observed at (-) 1681 cm^{-1} in the ^{18}O labeled samples (Figure 5A, red labels) and (-) 1679 cm^{-1} in the ^{13}C labeled samples (Figure 5B, red labels), respectively. The isotope-shifted components for the (-) 1698 cm^{-1} band are observed at (+) 1666 cm^{-1} in the ^{18}O labeled (Figure 5A, blue labels) and (+) 1663 cm^{-1} in the ^{13}C labeled samples (Figure 5B, blue labels), respectively. Therefore, the derived ^{13}C and ^{18}O isotope shifts for the 1718 and 1698 cm^{-1} bands are 37-39 cm^{-1} and 32-35 cm^{-1} (Figure 5) respectively, in reasonable agreement with the harmonic oscillator predictions for an isolated CO vibrational mode. In previous studies, spectral features at (+) 1717 and (-) 1698 cm^{-1} were assigned to the non-hydrogen bonded, keto band of P_B^+ and P_B, respectively (Breton et al. 1999; Hastings et al. 2001), and our isotope-based assignments are consistent with that previous work.

Bands at (+) 1653 and (-) 1638 cm^{-1} are observed in Figure 5A and Figure 5B, consistent with an assignment to a chl keto vibrational band, which is perturbed by light-induced electron transfer. Based on the signs, the positive 1653 cm^{-1} band would be assignable to P_{700}^{+}; the negative 1638 cm^{-1} band would be assignable to P_{700}. For these bands, the harmonic oscillator approximation predicts frequency downshifts of ~40 cm^{-1}. The isotope-shifted components for the (+) 1653 cm^{-1} band are observed at (-) 1608 cm^{-1} (Figures 5A and 5B, black labels). The isotope-shifted components for the (-) 1638 cm^{-1} band are observed at (+) 1602 (Figure 5A, orange labels) and (+) 1593 (Figure 5B, orange labels) cm^{-1}. Therefore, the derived ^{13}C and ^{18}O isotope shifts for the (+) 1653 and (-) 1638 cm^{-1} bands are 45 cm^{-1} and 36-45 cm^{-1}, respectively, in reasonable agreement with the harmonic oscillator predictions. In previous studies, spectral features at (+) 1653/4 and (-) 1638 cm^{-1} were assigned to hydrogen bonded, keto bands of P_A^{+} and P_A, respectively (Breton et al. 1999; Hastings et al. 2001), and our isotope labeling work is consistent with those assignments.

Based on model compounds (Nabedryk et al. 1990), P_A, P_A^{+}, P_B, P_B^{+} would be expected to give rise to one chl keto vibrational band each. Four keto bands with distinct frequencies are assigned in Table 3, based on the arguments described above. However, in each of the isotope-edited spectra presented in Figures 5A and 5B, there is still an unassigned positive band at 1687 cm^{-1} and an unassigned negative band at 1644/3 cm^{-1} (green labels). If the 1687 cm^{-1} band arises from a chl keto vibration, a harmonic oscillator treatment predicts a frequency of 1645 and 1648 cm^{-1} for the ^{18}O and ^{13}C isotopically labeled vibrational band, respectively. This comparison supports the interpretation that the positive 1687 cm^{-1} band is a keto vibrational band of P_{700}^{+} and that

the 1644/3 cm^{-1} band is its isotope-shifted component. Therefore, we assign the 1687 cm^{-1} spectral feature to a second keto vibrational band of P_B^+ or P_A^+. Based on previous site-directed mutagenesis work, we favor the assignment of this band to P_A^+ (see discussion below). The observation of two bands for P_A^+, one at 1687 cm^{-1} and one at 1653 cm^{-1}, and one band for P_A, at 1638 cm^{-1}, suggests that light-induced electron transfer leads to a structural change in the PSI reaction center. This structural change results in at least two distinct protein environments for the P_A half of the P_{700} dimer.

4.5 Discussion

In this paper, we employ methods to incorporate ^{13}C and ^{18}O isotopic labels specifically into the chl 13^1 keto group. Cyanobacterial cultures were used, and ^{13}C glutamate and $^{18}O_2$ were the source of the two labels. The amount of labeling at the keto position was found to be 15-16%, which is sufficient for detection using FT-IR spectroscopy. Figure 6 shows a comparison of the 1730-1590 cm^{-1} region in light-induced FT-IR spectra, associated with the oxidation of P_{700}. Amplitude changes are observed when the difference spectra of natural abundance and isotope labeled PSI are overlaid. In addition, chl labeling occurred with minimal scrambling into amino acid biosynthetic pathways.

Figure 7A shows the amino acids within 4 Å of the 13^1 keto group of P_A and P_B (Jordan et al. 2001). Ring V of P_A is not planar with the rest of molecule, and the 13^1 keto group of P_A is predicted to participate in a hydrogen bond with a conserved threonine residue, Thr 743 (*S. elongatus* numbering). There are no analogous hydrogen bonds predicted on the P_B half of the P_{700} dimer (Figure 7A). Therefore, the keto

vibrational bands of P_A/P_A^+ should be distinguishable from P_B/P_B^+ bands. Previous assignments of the 13^1 keto stretching vibrations of P_B, P_A, P_B^+, and P_A^+ have been based on mutagenesis studies, global ^2H incorporation, global ^{15}N incorporation, and comparison to model compounds (Nabedryk et al. 1990; Breton et al. 1999; Hastings et al. 2001). These approaches have led to some discrepancies in the interpretation of the PSI difference spectrum. Specific isotopic labeling, as performed here, has clarified the assignments. Four of our isotope-based P_B, P_B^+, P_A, and P_A^+ assignments are consistent with previous work (Table 3). However, we have identified an additional positive band at 1687 cm^{-1}, which is a chl keto vibration, based on its ^{13}C and ^{18}O isotope-induced downshifts. The sign of this band indicates that it arises from P_B^+ or P_A^+. This positive band has been observed previously in wild type PSI (Nabedryk et al. 1990; Breton et al. 1999) and either was unassigned or was assigned to a P_A^+ keto vibration, which was rationalized to downshift from 1695 cm^{-1} with oxidation (Hastings et al. 2001). However, model compound studies predict an oxidation-induced upshift (Nabedryk et al. 1990; Breton et al. 1999).

We favor the assignment of the 1687 cm^{-1} spectral band to the chl keto vibrational band of P_A^+, which upshifts from 1638 cm^{-1} with light-induced oxidation. This interpretation is consistent with previous site-directed mutagenesis studies. In this work, mutations at the conserved threonine were used to disrupt the hydrogen-bonding network of P_A, and an increase in the amplitude of a positive 1687 cm^{-1} band was observed (Witt et al. 2002; Li et al. 2004; Pantelidou et al. 2004). This increase in amplitude was attributed to an increased population of a more weakly hydrogen-bonded P_A^+ in the mutant (Witt et al. 2002). However, there was no significant change in amplitude of the

1687 cm^{-1} band when mutations were used to introduce hydrogen bonds to P_B (Breton et al. 2005).

Based on these previous investigations, we suggest that the 1687 cm^{-1} band arises from a state in which the P_A^+ hydrogen bond to Thr has been weakened by a light-induced protein structural change. In this interpretation, there are two populations of P_A^+, which are generated under illumination, a strongly hydrogen-bonded version, which contributes to the 1653 cm^{-1} band, and a less strongly hydrogen-bonded version, which contributes to the difference spectrum at 1687 cm^{-1}. Observation of only one P_A chl keto band, at 1638 cm^{-1}, demonstrates that the conformational change is light-induced. Thus, our work suggests a light-induced protein relaxation event, which weakens the hydrogen bond between P_A and Thr, most likely by a change in distance or angle between the 13^1 keto group of P_A and the Thr side chain. To explain the observation of the 1653 cm^{-1} band, this change in hydrogen bonding must occur in only a subset of PSI reaction centers.

In our experiments, PSI vibrational spectra were recorded under continuous, low intensity, red-filtered, illumination. The data acquisition time was 4 minutes. In PSI, forward electron transfer from the primary donor to the terminal electron acceptor, F_B, occurs with a time constant of ~500 nanoseconds, and $P_{700}^+F_B^-$ recombination events occur on the tens of milliseconds time scale (Brettel et al. 2001). Therefore, our experiment is expected to generate a photosteady state. In this photosteady state, protein relaxation events, which are coupled to the initial charge separation, will have the opportunity to accumulate under illumination and to influence the spectrum of P_{700}^+.

In our previous chl ester labeling experiments, P_{700}^{+}/P_{700} (Kim et al. 2000) was demonstrated to have more than four ester frequencies. Multiple, distributed ester frequencies are likely to be caused by the protein structural changes under discussion here. It was suggested that these multiple ester frequencies could reflect a distribution in keto-enol tautomerization. Such a structural change is expected to be coupled with alterations in hydrogen bonding, which will also alter the double bond character in the isocyclic ring of P_A (Kim et al. 2000). Comparison to this previous work suggests that both keto and ester vibrational bands can be used as reporters for light-induced protein relaxation events in PSI.

In PSI, two rates are observed for oxidation of A_1^- by F_X, which have been attributed to oxidation of the A_{1A}^- and A_{1B}^- species (Joliot et al. 1999; Guergova-Kuras et al. 2001). The rates of the two processes are ~20 and 200 nanoseconds, although the relative amplitudes of the two kinetic phases differ in different organisms (Brettel et al. 2001; Xu et al. 2003a; Xu et al. 2003b) and references therein}. In the bacterial reaction center, however, electron transfer to the intermediate acceptor, bacteriopheophytin, is unidirectional in wild type preparations (Heller et al. 1995; Kirmaier et al. 1999). Our observation of a P_A side structural change raises the question whether this protein relaxation event alters the rates and amplitudes of the A and B side electron transfer. From mutation studies, it was concluded that the midpoint potential of P_{700} decreases by 30-60 mV when a non-hydrogen bonding substitution is made at the conserved Thr residue (Witt et al. 2002; Li et al. 2004). While it was concluded that the disruption of the hydrogen bond to P_A does not alter the rates or relative amplitudes of A_{1B}^- and A_{1A}^- oxidation by F_X (Li et al. 2004), Thr mutations induced a shift of spin density from P_B

toward P_A (Witt et al. 2002). This result suggests that changes in the strength of the P_A^+ hydrogen bond can alter electronic coupling in the P_{700} dimer, and thus influence electron transfer rate from soluble electron carriers to P_{700}^+.

Changes in P_A^+ hydrogen bond strength may also influence cytochrome/plastocyanin oxidation through structural changes in the protein backbone. Figure 7B shows the luminal PsaA and PsaB helices in close proximity to P_{700}. This region of PSI has been demonstrated to be important in the facilitation of electron transfer from plastocyanin and cytochrome c to P_{700}^+ (Sun et al. 1999; Brettel et al. 2001; Sommer et al. 2002; Sommer et al. 2004). As suggested in Figure 7, changes in the angle or distance of the Thr-P_A^+ hydrogen bond are likely to influence the orientation and conformation of these luminal PsaA and PsaB helices. In the cyanobacterium, *Synechocystis*, such a change in orientation may alter the rate or mechanism of cytochrome c oxidation *in vivo* (Durán et al. 2004). For example, it has been proposed that a rate-limiting conformation change may occur to regulate oxidation (Bottin et al. 1985; Sigfridsson et al. 1997). A redox-linked conformational change may also regulate the binding affinity of the oxidized and reduced forms of the soluble electron carriers (Drepper et al. 1996).

In photosynthetic reaction centers, the protein environment is an inhomogeneous matrix, which relaxes after charge separation on many time scales. A complete understanding of photosynthetic electron transfer necessitates a description of these coupled protein conformational changes. Our work provides a new, detailed description of a protein relaxation event, which is coupled to light-induced electron transfer in PSI.

We propose that this light-induced change in P_A^+ hydrogen bonding regulates PSI electron transfer reactions.

4.6 Acknowledgments.

This work was supported by NIH GM 43273 (B.A.B). The authors thank Dr. L. Gelbaum for assistance with NMR data acquisition and Prof. Hugo Scheer for helpful discussion.

4.7 References

Barry, B. A. (1995). "Tyrosyl radicals in photosystem II." *Methods Enzymol.* **258**: 303-319.

Barry, B. A., I. Cooper, A. De Riso, S. H. Brewer, D. M. Vu and R. B. Dyer (2006). "Time-resolved vibrational spectroscopy detects protein-based intermediates in the photosynthetic oxygen-evolving cycle." *Proc. Natl. Acad. Sci. USA* **103**: 7288-7291.

Beale, S. I. (1999). "Enzymes of chlorophyll biosynthesis." *Photosynth. Res.* **60**: 43-73.

Beale, S. I., S. P. Gough and S. Granik (1975). "Biosynthesis of delta-aminolevulinic acid from the intact carbon skeleton of glutamic acid in greening barley." *Proc. Natl. Acad. Sci. USA* **72**: 2719-2723.

Bellamy, L. J. (1980). Advances in infrared group frequencies: the infrared spectra of complex molecules. *Advances in infrared group frequencies: The infrared spectra of complex molecules*. London; New York, Chapman and Hall. **2:** 263-275.

Bender, S. L., J. Keough, S. E. Boesch, R. A. Wheeler and B. A. Barry (2008). "The vibrational spectrum of the secondary electron acceptor, A_1, in photosystem I." *J. Phys. Chem. B* **112**: 3844-3852.

Boldt, N. J., R. J. Donohoe, R. R. Birge and D. F. Bocian (1987). "Chlorophyll model compounds: effects of low symmetry on the resonance Raman spectra and normal mode descriptions of nickel (II) dihydroporphyrins." *J. Am. Chem. Soc.* **109**: 2284-2298.

Bollivar, D. W. and S. I. Beale (1995). "Formation of the isocyclic ring of chlorophyll by isolated *Chlamydomonas reinhardtii* chloroplasts." *Photosynth. Res.* **43**: 113-124.

Bollivar, D. W. and S. I. Beale (1996). "The chlorophyll biosynthetic enzyme Mg-protoporphyrin IX monomethyl ester (oxidative) cyclase. Characterization and partial purification from *Chlamydomonas reinhardtii* and *Synechocystis* sp. PCC 6803." *Plant Physiol.* **112**: 105-114.

Bottin, H. and P. Mathis (1985). "Interaction of plastocyanin with the photosystem I reaction center: a kinetic study by flash absorption spectroscopy " *Biochemistry* **24**: 6453-6460.

Breton, J. (2001). "Fourier transform infrared spectroscopy of primary electron donors in type I photosynthetic reaction centers." *Biochim. Biophys. Acta* **1507**: 180-193.

Breton, J., P. R. Chitnis and M. Pantelidou (2005). "Evidence for hydrogen bond formation to the PsaB chlorophyll of P_{700} in photosystem I mutants of *Synechocystis* sp. PCC 6803." *Biochemistry* **44**: 5402-5408.

Breton, J., E. Nabedryk and W. Leibl (1999). "FTIR study of the primary electron donor of photosystem I (P_{700}) revealing delocalization of the charge in P_{700}^{+} and localization of the triplet character in $^{3}P_{700}$." *Biochemistry* **38**: 11585-11592.

Brettel, K. and W. Leibl (2001). "Electron transfer in photosystem I." *Biochim. Biophys. Acta* **1507**: 100-114.

De Riso, A., D. L. Jenson and B. A. Barry (2006). "Calcium exchange and structural changes during the photosynthetic oxygen evolving cycle." *Biophys. J.* **91**: 1999-2008.

Drepper, F., M. Hippler, W. Nitschke and W. Haehnel (1996). "Binding dynamics and electron transfer between plastocyanin and photosystem I." *Biochemistry* **35**: 1282-1295.

Durán, R. V., M. Hervás, M. A. De la Rosa and J. A. Navarro (2004). "The efficient functioning of photosynthesis and respiration in *Synechocystis* sp. PCC 6803 strictly requires the presence of either cytochrome c6 or plastocyanin." *J. Biol. Chem.* **279**: 7229-7233.

Gehlen, J. N., M. Marchi and D. Chandler (1994). "Dynamics affecting the primary charge transfer in photosynthesis." *Science* **263**: 499-502.

Golbeck, J. H. and D. A. Bryant (1991). "Photosystem I." *Current Topics in Bioenergetics* **16**: 83-177.

Grotjohann, I. and P. Fromme (2005). "Structure of cyanobacterial photosystem I." *Photosynth. Res.* **85**: 51-72.

Guergova-Kuras, M., B. Boudreaux, A. Joliot, P. Joliot and K. Redding (2001). "Evidence for two active branches for electron transfer in photosystem I." *Proc. Natl. Acad. Sci. USA* **98**: 4437-4442.

Halverson, K. M. and B. A. Barry (2003). "Evidence for spontaneous structural changes in a dark-adapted state of photosystem II." *Biophys. J.* **85**: 2581-2588.

Hastings, G., V. M. Ramesh, R. Wang, V. Sivakumar and A. Webber (2001). "Primary donor photo-oxidation in photosystem I: a re-evaluation of (P_{700}^{+} - P_{700}) Fourier transform infrared difference spectra." *Biochemistry* **40**: 12943-12949.

Heller, B. A., D. Holten and C. Kirmaier (1995). "Control of electron-transfer between the L- and M-sides of photosynthetic reaction centers." *Science* **269**: 940-945.

Hippler, M., F. Drepper, J. Farah and J. D. Rochaix (1997). "Fast electron transfer from cytochrome c6 and plastocyanin to photosystem I of *Chlamydomonas reinhardtii* requires PsaF." *Biochemistry* **36**: 6343-6349.

Holzwarth, A. R., M. G. Muller, J. Niklas and W. Lubitz (2006). " Ultrafast transient absorption studies on photosystem I reaction centers from *Chlamydomonas reinhardtii*. 2: Mutations near the P_{700} reaction center chlorophylls provide new insight into the nature of the primary electron donor." *Biophys. J.* **90**: 552-565.

Huang, D. D. and W. Y. Wang (1986). "Chlorophyll biosynthesis in *Chlamydomonas* starts with the formation of glutamyl-tRNA." *J. Biol. Chem.* **261**: 13451-13455.

Joliot, P. and A. Joliot (1999). "In vivo analysis of the electron transfer within Photosystem I: are the two phylloquinones involved?" *Biochemistry* **38**: 11130-11136.

Jordan, P., P. Fromme, H. T. Witt, O. Klukas, W. Saenger and N. Krauss (2001). "Three-dimensional structure of cyanobacterial photoystem I at 2.5A resolution." *Nature* **411**: 909-917.

Kaess, H., P. Fromme, H. T. Witt and W. Lubitz (2001). "Orientation and electronic structure of the primary donor radical cation P_{700}^{+} in photosystem I: a single crystal EPR and ENDOR study." *J. Phys. Chem. B* **105**: 1225-1239.

Kim, S. and B. A. Barry (2000). "Identification of carbonyl modes of P_{700} and P_{700}^{+} by in situ chlorophyll labeling in photosystem I." *J. Am. Chem. Soc.* **122**: 4980-4981.

Kim, S., C. A. Sacksteder, K. A. Bixby and B. A. Barry (2001). "A reaction-induced FT-IR study of cyanobacterial photosystem I." *Biochemistry* **40**: 15384-15395.

Kirmaier, C., D. Weems and D. Holten (1999). "M-side electron transfer in reaction center mutants with a lysine near the nonphotoactive bacteriochlorophyll." *Biochemistry* **38**: 11516-11530.

Kitson, F. G., B. S. Larsen and C. N. McEwen (1996). Amino Acids. *Gas Chromatography and Mass Spectrometry, A Practical Guide*. San Diego, Academic Press**:** 87-94.

Li, Y., M. G. Lucas, T. Konovalova, B. Abbott, F. MacMillan, A. Petronko, V. Sivakumar, R. Wang, G. Hastings, F. Gu, J. van Tol, L. C. Brunal, R. Timkovich, F. Rappaport and K. Redding (2004). "Mutation of the putative hydrogen-bond donor to P_{700} of photosystem I." *Biochemistry* **43**: 12634-12647.

Merchant, S. and L. Bogorad (1986). "Regulation by copper of the expression of plastocyanin and cytochrome c-552 in *Chlamydomonas reinhardtii*." *Mol. Cell. Biol.* **6**: 462-469.

Nabedryk, E., M. Leonhard, W. Maentele and J. Breton (1990). "Fourier transform infrared difference spectroscopy shows no evidence for an enolization of chlorophyll *a* upon cation formation either in vitro or during P_{700} photooxidation." *Biochemistry* **29**: 3242-3247.

Noren, G. H., R. J. Boerner and B. A. Barry (1991). "EPR characterization of an oxygen-evolving photosystem II preparation from the transformable cyanobacteria *Synechocystis* 6803." *Biochemistry* **30**: 3943-3950.

Pantelidou, M., P. R. Chitnis and J. Breton (2004). "FTIR spectroscopy of *Synechocystis* 6803 mutants effected on the hydrogen bonds to the carbonyl groups of the PsaA chlorophyll of P_{700} supports an extensive delocalization of the charge in P_{700}^{+}." *Biochemistry* **43**: 8380-8390.

Parson, W. W. and A. Warshel (2004). "Dependence of photosynthetic electron-transfer kinetics on temperature and energy in a density-matrix model." *J. Phys. Chem. B* **108**: 10474-10483.

Patzlaff, J. S. and B. A. Barry (1996). "Pigment quantitation and analysis by HPLC reverse phase chromatography: a characterization of antenna size in oxygen-evolving photosystem II preparations from cyanobacteria and plants." *Biochemistry* **35**: 7802-7811.

Porra, R. J., O. Klein and P. E. Wright (1983). "The proof by ^{13}C-NMR spectroscopy of the predominance of the C5 pathway over the Shemin pathway in chlorophyll biosynthesis in higher plants and of the formation of the methyl ester group of chlorophyll from glycine." *Eur. J. Biochem.* **130**: 509-516.

Porra, R. J. and H. Scheer (2001). "^{18}O and mass spectrometry in chlorophyll research: derivation and loss of oxygen atoms at the periphery of the chlorophyll macrocycle during biosynthesis, degradation and adaptation." *Photosynth. Res.* **66**: 159-175.

Rieble, S. and S. I. Beale (1988). "Transformation of glutamate to delta-aminolevulinic acid by soluble extracts of *Synechocystis* sp. PCC 6803 and other oxygenic prokaryotes." *J. Biol. Chem.* **263**: 8864-8871.

Rippka, R., J. Deruelles, J. B. Waterbury, M. Herdman and R. Y. Stanier (1979). "Generic assignments, strain histories and properties of pure cultures of cyanobacteria." *Journal of General Microbiology* **111**: 1-61.

Sachs, R. K., K. M. Halverson and B. A. Barry (2003). "Specific isotopic labeling and photooxidation-linked structural changes in the manganese-stabilizing subunit of photosystem II." *J. Biol. Chem.* **278**: 44222-44229.

Sacksteder, C. A., S. L. Bender and B. A. Barry (2005). "Role for bound water and CH-pi aromatic interactions in photosynthetic electron transfer." *J. Am. Chem. Soc.* **127**: 7879-7890.

Schneegurt, M. A. and S. I. Beale (1992). "Origin of the chlorophyll b formyl oxygen in *Chlorella vulgaris*." *Biochemistry* **31**: 11677-11683.

Schön, A., G. Krupp, S. Gough, S. Berry-Lowe, C. G. Kannangara and D. Söll (1986). "The RNA required in the first step of chlorophyll biosynthesis is a chloroplast glutamate tRNA." *Nature* **322**: 281-284.

Sigfridsson, K., S. Young and O. Hansson (1997). "Electron transfer between spinach plastocyanin mutants and photosystem 1." *Eur. J. Biochem.* **245**: 805-812.

Sommer, F., F. Drepper, W. Haehnel and M. Hippler (2004). "The hydrophobic recognition site formed by residues PsaA-Trp651 and PsaB-Trp627 of photosystem I in *Chlamydomonas reinhardtii* confers distinct selectivity for binding of plastocyanin and cytochrome c6." *J. Biol. Chem.* **279**: 20009-20017.

Sommer, F., F. Drepper and M. Hippler (2002). "The luminal helix l of PsaB is essential for recognition of plastocyanin or cytochrome c6 and fast electron transfer to photosystem I in *Chlamydomonas reinhardtii*." *J. Biol. Chem.* **277**: 6573-6581.

Sun, J., M. Hervas, J. A. Navarro, M. A. De la Rosa and P. R. Chitnis (1999). "Oxidizing side of the cyanobacterial photosystem I: mutational analysis of the luminal H loop of the PsaB subunit." *Photosynth. Res.* **62**: 241-250.

van der Est, A. (2001). "Light-induced spin polarization in type I photosynthetic reaction centres." *Biochim. Biophys. Acta* **1507**: 212-225.

Walker, C. J., K. E. Mansfield, K. M. Smith and P. A. Castelfranco (1989). "Incorporation of atmospheric oxygen into the carbonyl functionality of the protochlorophyllide isocyclic ring." *Biochem. J.* **257**: 599-602.

Wang, H., S. Lin, J. P. Allen, J. C. Williams, S. Blankert, C. Laser and N. W. Woodbury (2007). "Protein dynamics control the kinetics of initial electron transfer in photosynthesis." *Science* **316**: 747-750.

Warshel, A., Z. T. Chu and W. W. Parson (1989). "Dispersed polaron simulations of electron transfer in photosynthetic reaction centers." *Science* **246**: 112-116.

Webber, A. N. and W. Lubitz (2001). "P_{700}: the primary electron donor of photosystem I." *Biochim. Biophys. Acta* **1507**: 61-79.

Witt, H., C. Teuloff, J. Niklas, E. Bordignon, D. Carbonera, S. Kohler, A. Labahn and W. Lubitz (2002). "Hydrogen bonding of P_{700}: site-directed mutagenesis of threonine A739 of photosystem I in *Chlamydomonas reinhardtii*." *Biochemistry* **41**: 8557-8569.

Wong, Y. S., P. A. Castelfranco, D. A. Goff and K. M. Smith (1985). "Intermediates in the formation of the chlorophyll isocyclic ring." *Plant Physiol.* **79**: 725-729.

Xu, W., P. Chitnis, A. Valieva, A. van der Est, Y. N. Pushkar, M. Krzystyniak, C. Teutloff, S. G. Zech, R. Bittl, D. Stehlik, B. Zybailov, G. Shen and J. H. Golbeck (2003a). "Electron transfer in cyanobacterial photosystem I: I. Physiological and spectroscopic characterization of site-directed mutants in a putative electron transfer pathway from A_0 through A_1 to F_x." *J. Biol. Chem.* **278**: 27864-27875.

Xu, W., P. R. Chitnis, A. Valieva, A. van der Est, K. Brettel, M. Guergova-Kuras, Y. N. Pushkar, S. G. Zech, D. Stehlik, G. Shen, B. Zybailov and J. H. Golbeck (2003b). "Electron transfer in cyanobacterial photosystem I: II. Determination of forward electron transfer rates of site-directed mutants in a putative electron transfer pathway from A_0 through A_1 to F_x." *J. Biol. Chem.* **278**: 27876-27887.

Table 1. Amount of ^{13}C chl labeling from ^{13}C-labeled glutamate

1 m/z	2 Isotope distribution for natural abundance chl*†	3 Isotope distribution for ^{13}C-labeled chl	4 ^{13}C-labeled chl minus natural abundance chl (column 3-minus-2)	5 Predicted $^{+1}{}^{13}C$ isotopomer distribution‡	6 Measured $^{+2}$-^{13}C isotopomer contribution (column 4-minus-5)	7 Predicted $^{+2}{}^{13}C$ isotopomer distribution‡
871.6 (molecular ion)	100	100	0	0	0	0
872.6 ($^{+}$1-^{13}C isotopomer)	63.7 ± 7.7	106.3 ± 2.1	42.6 ± 8.0	42.6 ± 8.0	0	0
873.6 ($^{+}$2-^{13}C isotopomer)	23.6 ± 0.7	77.3 ± 3.5	53.7 ± 3.5	27.1 ± 6.1	26.6 ± 7.0	26.6 ± 7.0
874.6 ($^{+}$3-^{13}C isotopomer)	5.7 ± 0.4	40.6 ± 1.0	34.9 ± 1.1	10.0 ± 1.9	24.9 ± 2.2	16.9 ± 4.9
875.6 ($^{+}$4-^{13}C isotopomer)	2.9 ± 0.5	18.5 ± 1.0	15.6 ± 1.1	2.4 ± 0.5	13.2 ± 1.2	6.3 ± 1.7
876.6 ($^{+}$5-^{13}C isotopomer)	1.1 ± 0.8	6.6 ± 0.3	5.5 ± 0.9	1.2 ± 0.2	4.3 ± 0.9	1.5 ± 0.4
877.6 ($^{+}$6-^{13}C isotopomer)	1.1 ± 0.5	2.2 ± 0.4	1.1 ± 0.6	0.5 ± 0.4	± 0 .7	± 0.2

1 m/z	8 Measured $^{+}$3-^{13}C isotopomer contribution (column 6-minus-7)	9 Predicted $^{+}$3-^{13}C-isotopomer contribution‡	10 Measured $^{+}$4-^{13}C isotopomoer contribution (column 8-minus-9)	11 Predicted $^{+}$4-^{13}C-isotopomer contribution‡	12 Total ^{13}C-labeling for each isotopomer	13 Probability of ^{13}C incorporation into the keto position§
871.6 (molecular ion)	0	0	0	0	0	0
872.6 ($^{+}$1-^{13}C isotopomer)	0	0	0	0	42.6 ± 8.0	5.3
873.6 ($^{+}$2-^{13}C isotopomer)	0	0	0	0	26.6 ± 7.0	6.6
874.6 ($^{+}$3-^{13}C isotopomer)	8.0 ± 5.4	8.0 ± 5.4	0	0	8.0 ± 5.4	3.0
875.6 ($^{+}$4-^{13}C isotopomer)	6.9 ± 2.1	5.1 ± 3.5	1.8 ± 4.3	1.8 ± 4.3	1.8 ± 4.3	0.9
876.6 ($^{+}$5-^{13}C isotopomer)	2.8 ± 1.0	1.9 ± 1.3	0.9 ± 1.6	1.2 ± 2.3	ND¶	0
877.6 ($^{+}$6-^{13}C isotopomer)						0

*Values reported as percentages (%); †Predicted isotope distribution from the Isotopident tool (http://education.expasy.org/student_projects/isotopident/). 871.6 *m/z*, 100%; 872.6 *m/z*, 64.4%; 873.6 *m/z*, 21.4%; 874.6% *m/z*, 4.9%; 875.6 *m/z*, 0.9%; 87.6 *m/z*, 0.1%; ‡Based on measured isotope distribution in column 2; §Based on the statistical probability of labeling at 8 possible carbon positions; ¶ND, not detected, $\leq$1%.

Table 2. Isotopic labeling of PSI amino acids as determined with GC/MS

Amino Acid	[^{13}C] Glu[*]
Glutamic Acid[†]	16.0 ± 0.1
Proline	14.0 ± 0.5
Serine	ND[§]
Aspartic Acid[‡]	ND
Alanine	ND
Glycine	ND
Valine	ND
Leucine	ND
Isoleucine	ND
Threonine	ND
Phenylalanine	ND
Lysine	ND

[*]Values reported as percentages (%); [†]Glutamic acid and deamidated glutamine; [‡]Aspartic acid and deamidated asparagine; [§]ND, not detected, $\leq$ 1%.

Table 3. Chlorophyll keto assignments for P_A and P_B in Photosystem I, based on ^{13}C and ^{18}O keto labeling

Natural Abundance*	^{18}O keto Labeled*	^{13}C keto Labeled*	Assignment
1718	1681	1679	P_B^+
1698	1666	1663	P_B
1687	1643	1644	P_A^+
1653	1608	1608	P_A^+
1638	1602	1593	P_A

*Frequencies in wavenumbers (cm^{-1})

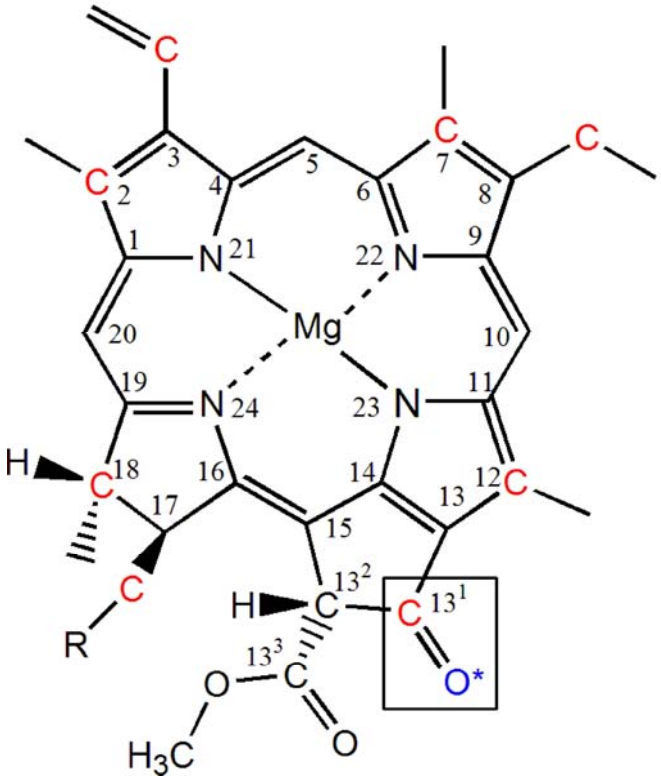

Figure 1. (A) Structure of chlorophyll *a* displaying the 8 carbons (red) that will be isotopically labeled from glutamic-^{13}C-3 acid. The keto group of chl is boxed. The keto oxygen (blue) will be isotopically labeled from $^{18}O_2$.

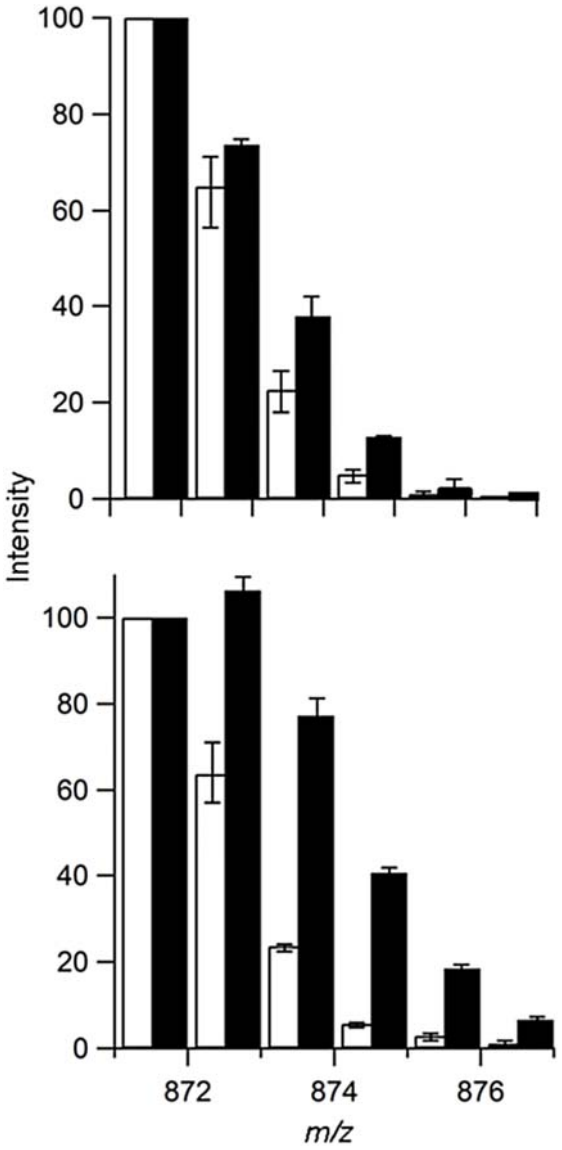

Figure 2. MALDI mass spectrometry showing incorporation of ^{18}O and ^{13}C into cyanobacterial chl. In **(**A), the cyanobacteria were cultured in the presence of $^{16}O_2$ (white) or $^{18}O_2$ (black). In (B), the cyanobacteria were cultured in the presence of natural abundance glutamic acid (white) or L-glutamic-3-^{13}C-acid (black). The normalized 871.5 *m/z* peak corresponds to the [M+H] ion of pheophytin, which was generated by acid treatment of the chl sample immediately before the measurement. See Supplemental Materials and Methods for additional information.

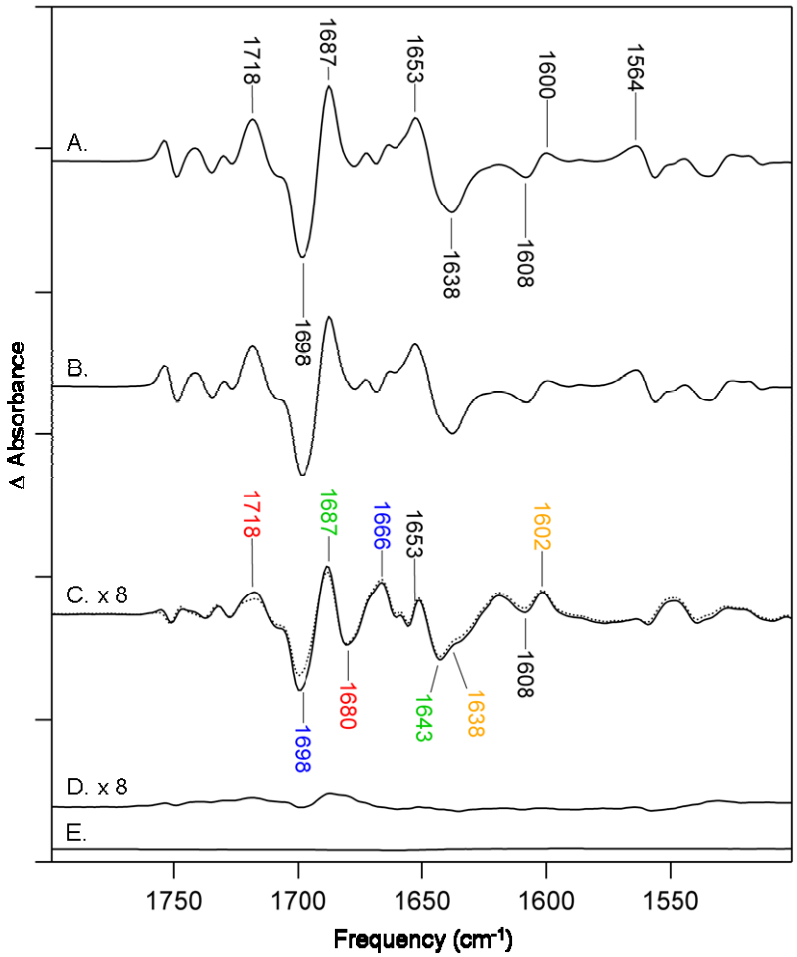

Figure 3. Light-induced FT-IR difference spectra, associated with the oxidation of P_{700} in PSI. In (A), the samples were derived from cyanobacteria cultured in the presence of $^{16}O_2$. In (B), the samples were derived from cyanobacteria cultured in the presence of $^{18}O_2$. In (C, solid line), the isotope-edited spectrum, ^{16}O-minus-^{18}O, was generated by interactive subtraction of (B) minus (A) and multiplication by a factor of 8. A subtraction factor of 0.9663 was used to minimize ester contributions to the isotope-edited spectrum. In (C, dotted line), the isotope-edited spectrum was generated by a direct one-to-one subtraction and multiplication by a factor of 8. (D) shows a control double difference spectrum, in which no vibrational bands are expected. This control was generated by taking one-half of the data set in (A), subtracting it from the other half of the data set in

Figure. 3 continued

(A), and dividing by the square root of two. (D) was also multiplied by a factor of 8 for comparison to (C). (E) is a dark-minus-dark control spectrum. 69 spectra were averaged in A-C and E. Each tick mark on the y axis represents $5x10^{-3}$ absorbance units. The color-coding scheme for band labels is described in the paper. See Material and Materials for additional information.

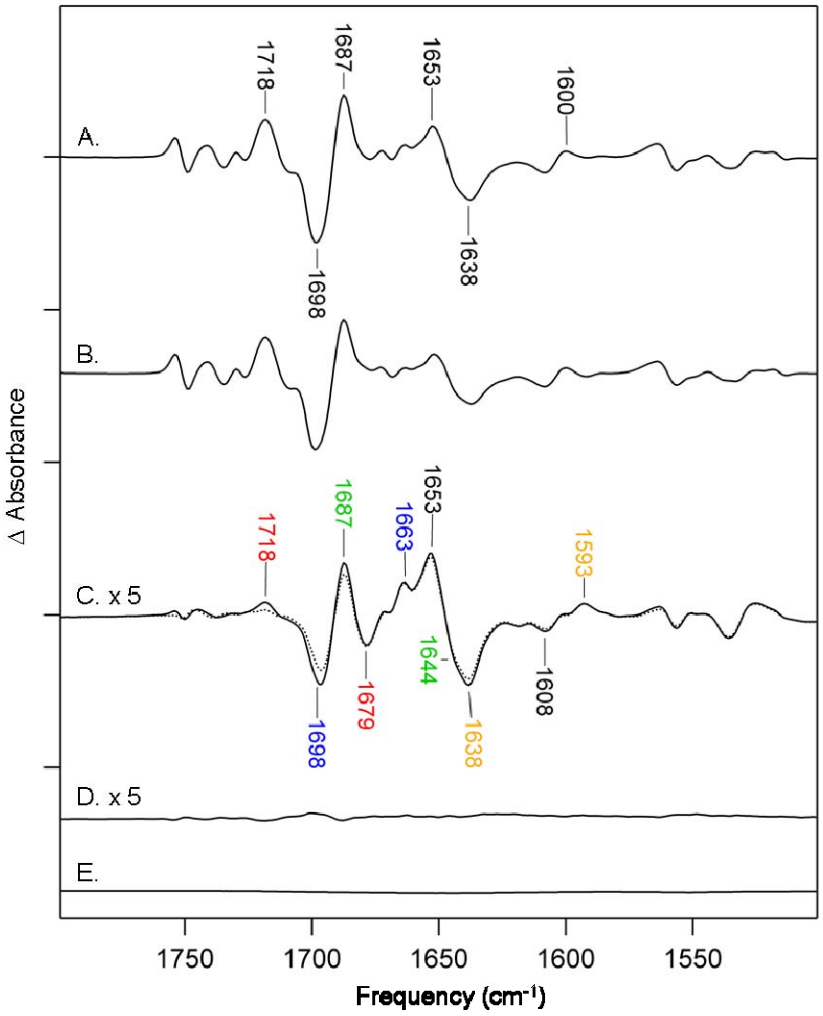

Figure 4. Light-induced FT-IR spectra, associated with the oxidation of P_{700} in PSI. In (A), the samples were derived from cyanobacteria cultured in the presence of natural abundance glutamate. In (B), the samples were derived from cyanobacteria cultured in the presence of L-glutamic-3-^{13}C-acid. In (C, solid line), the isotope-edited spectrum, ^{12}C-minus-^{13}C, was generated by interactive subtraction of (B) minus (A) and multiplication by a factor of 5. A subtraction factor of 0.9584 was used to minimize ester contributions to the isotope-edited spectrum. In (C, dotted line), the isotope-edited spectrum was generated by a direct one-to-one subtraction and multiplication by a factor of 5. (D) shows a control double difference spectrum, in which no vibrational bands are

Figure 4. continued

expected. This control was generated by taking one-half of the data set in (A), subtracting it from the other half of the data set in (A), and dividing by the square root of two. (D) was also multiplied by a factor of 5 for comparison to (C). (E) is a dark-minus-dark control spectrum. 64 spectra were averaged in A-C and E. Each tick mark on the y axis represents $5x10^{-3}$ absorbance units. The color-coding scheme for band labels is described in the paper. Material and Material and Methods for additional information.

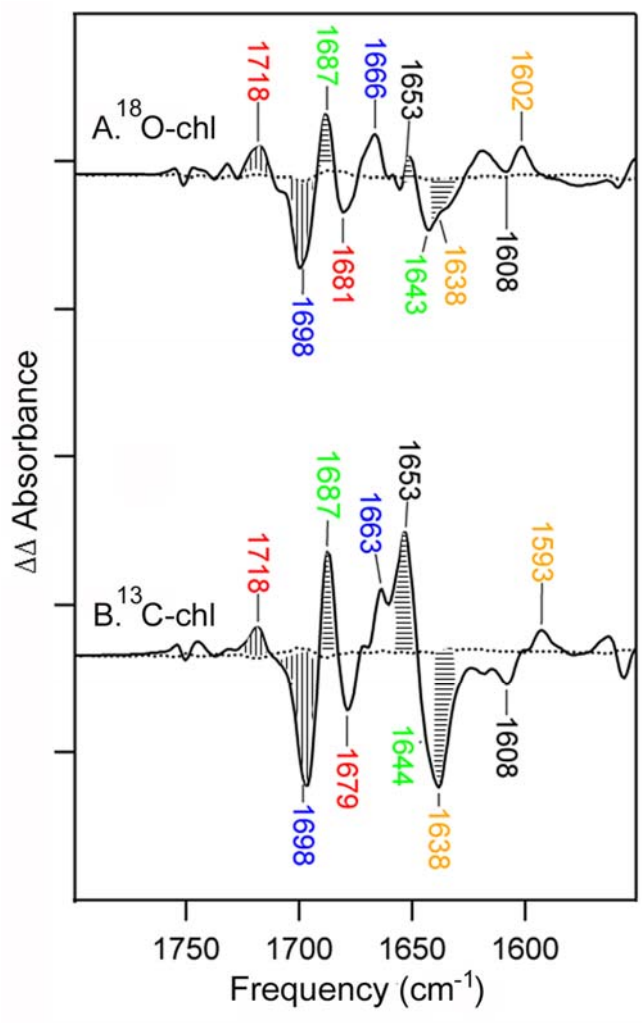

Figure 5. Isotope-edited FT-IR spectra showing the effects of ^{18}O and ^{13}C chl labeling on P_{700}^{+}/P_{700} keto vibrational bands. (A) is the ^{16}O-minus-^{18}O spectrum, and (B) is the ^{12}C-minus-^{13}C spectrum. In (A) and (B), control difference spectra, in which no vibrational bands are expected, are also presented as the dotted lines. Natural abundance bands assigned to P_B and P_B^{+} are shaded with vertical lines. Natural abundance bands assigned to P_A and P_A^{+} are shaded with horizontal lines. The natural abundance band (filled) and its corresponding isotope-shifted component (unfilled) are labeled with the same color label. In (A), 69 spectra were averaged and in (B), 64 spectra were averaged.

Figure 5. continued

In (A) and (B), the sample size was 64 μg chl. Each tick mark represents $5x10^{-4}$ AU. See Materials and Methods for additional information.

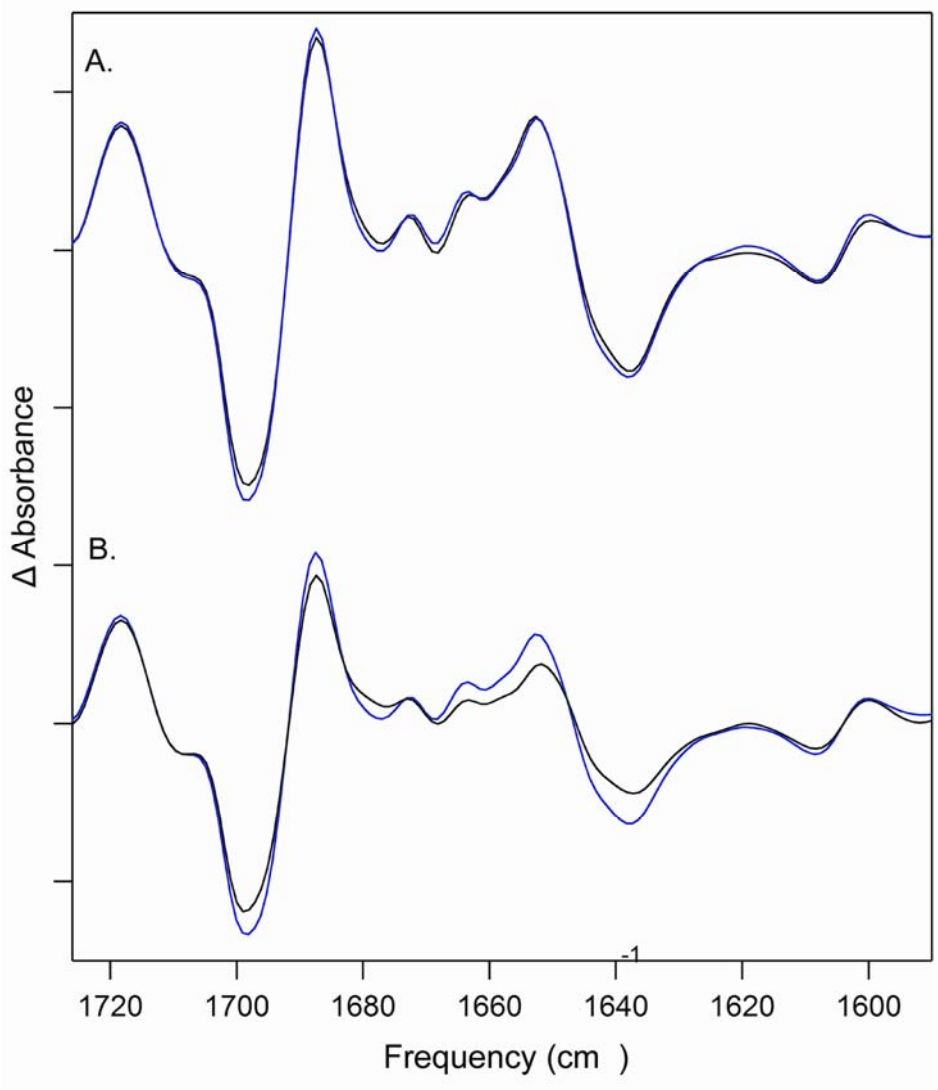

Figure 6. Comparison of the 1730-1590 cm^{-1} region in light-induced FT-IR spectra, associated with the oxidation of P_{700}. (A) is an overlay of Figure 3A (natural abundance, blue) and Fig. 3B (^{18}O-labeled, black). (B) is an overlay of Fig ure4A (natural abundance, blue) and Fig. 4B (^{13}C-labeled, black). Each tick mark on the y axis represents $2x10^{-3}$ absorbance units. See Material and Material and Methods for additional information.

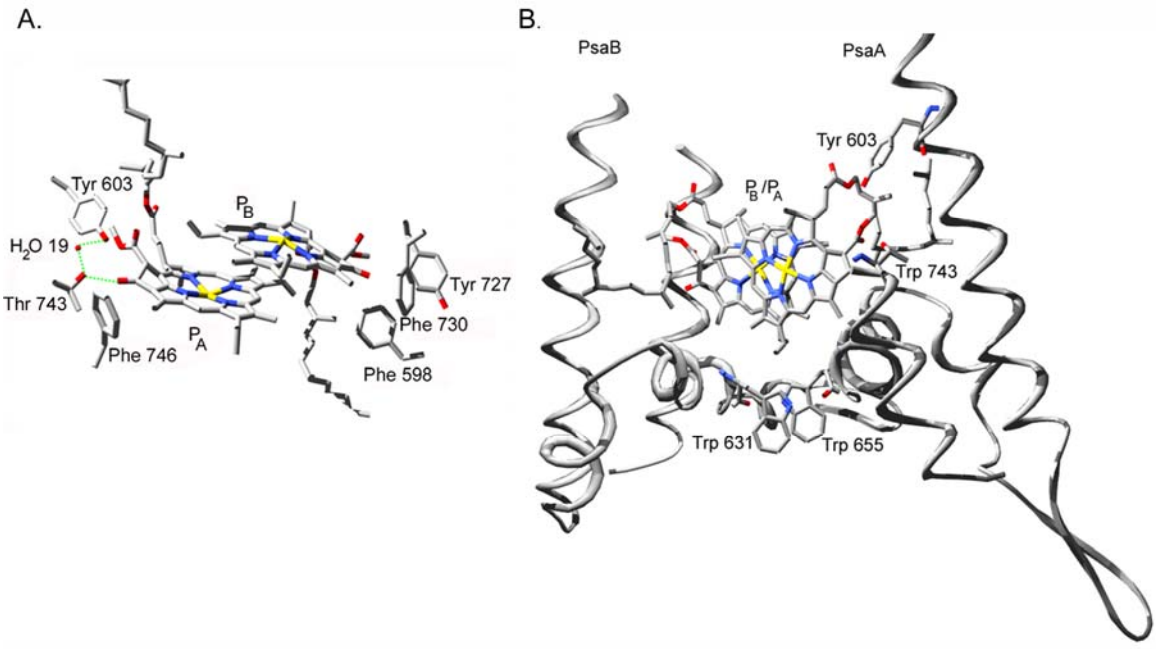

Figure 7. (A) The protein environment of P_A and P_B in P_{700}. The hydrogen bonding network of P_A with Thr 743, H_2O and Tyr 603 is represented by dashes. (B) The luminal helices of PsaB and PsaA near P_{700}. The figure is reproduced from the 2.5 Å resolution crystal structure of PSI from *S. elongatus* (PDB file accession number 1JB0 (Jordan et al. 2001)) using Swiss-Pdb viewer (v3.7; www.expasy.ch/spdbc) with numbering according to *S. elongatus*, and rendered using POV-Ray (v3.5; www.povray.org).

CHAPTER 5

PROBING ELECTRON TRANSFER IN PSI

5.1 Abstract

In oxygenic photosynthesis, photosystem I (PSI) catalyzes the light-driven oxidation of plastocyanin or cytochrome c and the reduction of ferredoxin. Studies have underscored the importance of protein interactions in efficient electron transfer from plastocyanin to PSI; however specific characterization of these interactions has not been forthcoming. In this work we have used deuterium exchange methods and isotope labeling of tryptophan to investigate light-induced protein dynamics associated with stable charge separation in PSI. Reaction-induced FT-IR spectroscopy and isotope-edited spectra reveal protein relaxation events that may be linked to structural conformational changes. The deuterium exchange isotope-edited spectra reveal light-induced perturbations to amide I (C=O) of the protein backbone, and perturbations of aspartate and glutamate residues. Isotope-based assignments for tryptophan may provide new information concerning this amino acid's involvement with electron transfer reactions in PSI. The protein dynamics described in this work may be associated with the oxidation of soluble electron carriers or other electron transfer reactions in PSI. These studies provide unique information concerning electron transfer in oxygenic photosynthesis.

5.2 Introduction

Photosystem I is a protein complex responsible for the light-induced oxidation of plastocyanin and the reduction of ferredoxin (Golbeck 1994). It is one of two protein complexes involved in light-induced charge separation across the thylakoid membrane in plants, green algae, and cyanobacteria. Three polypeptides are responsible for binding the electron cofactors in PSI. Subunits PsaA and PsaB form a heterodimeric core and are responsible for binding chl, phylloquinone and an iron-sulfur cluster. The PsaC subunit of PSI, an extrinsic subunit located on the stromal side of the thylakoid membrane, is responsible for binding two iron-sulfur clusters (Jordan et al. 2001).

The primary donor in PSI is believed to be a chlorophyll monomer, which reduces A_0, a second chlorophyll monomer. (Holzwarth et al. 2006) The electron from A_0^- is transferred to A_1, a phylloquinone, and then to the iron-sulfur cluster F_X. These electron cofactors are bound by the PsaA and PsaB subunits. F_A, a second iron-sulfur cluster oxidizes F_X and is itself oxidized by the terminal electron acceptor F_B. F_A and F_B are bound to the PsaC subunit. (Jordan et al. 2001) The primary donor is reduced by P_{700}, a chlorophyll heterodimer comprised of chl a and chl a'. P_{700} is the terminal electron donor of PSI and is reduced by plastocyanin or cytochrome c, depending on copper availability (Wood 1978; Merchant et al. 1986; Ho et al. 1988).

Plastocyanin, a 10kDa soluble copper protein, is responsible for the reduction of the photoxidized dimer, P_{700}, in PSI and is reduced by the cytochrome b_6f complex. The crystal structures of oxidized and reduced forms of plastocyanin reveal two conserved regions that are believed to be involved in recognition and binding to PSI. In

cyanobacteria, a single oriented collisional mechanism has been reported for the reduction of PSI by plastocyanin. This process involves electrostatic interactions without formation of a kinetically detectable electron-transfer complex (Hervas et al. 1994; Hervas et al. 1995; Hervas et al. 1996). In iron-deficient conditions, cytochrome c will act as the reducing agent for PSI (Wood 1978). Studies have shown that cytochrome c and PSI may form a transient complex before electron transfer and do not follow the same kinetics as plastocyanin (Hervas et al. 1995). In these studies, second order kinetics were observed for reduction of P_{700}^{+} by cytochrome c compared to pseudo-first order kinetics for plastocyanin reduction of P_{700}^{+}.

The docking site for the soluble electron carriers are made up of two helices from the PsaA and PsaB subunits, designated in the crystal structure of *S. elongates* as transmembrane helices I and J (Fromme et al. 2001; Jordan et al. 2001). Sequence alignments of PsaB subunits from various organisms have shown several amino acids residues in the loop region of helix J to be conserved. Mutation studies have suggested a role in the extra-membrane loop in the interaction with soluble electron donor proteins (Sun et al. 1999a; Sun et al. 1999b). Furthermore mutation studies of conserved tryptophan residues located in the luminal loop regions of PsaA and PsaB have shown these residues to be important in efficient reduction of P_{700}^{+} from plastocyanin or cytochrome c (Sun et al. 1999b; Sommer et al. 2002; Sommer et al. 2004). In contrast to cyanobacteria, eukaryotic organisms require the subunit PsaF for efficient electron transfer from plastocyanin to P_{700}^{+}. In eukaryotes, it is believed that this subunit is responsible for coordinating and binding plastocyanin (Bottin et al. 1985; Haehnel et al. 1994).

Vibrational spectroscopy has underscored the importance of protein dynamics associated with light-induced electron transfer in PSI (Kim et al. 2000; Kim et al. 2001; Bender et al. 2008a). These experiments have demonstrated specific protein relaxation events near P_{700} that may be linked to interactions with soluble electron carriers. Furthermore, isotope labeling of tyrosine residues in PSI also showed perturbations associated with CH-π interactions. These perturbations may be associated with protein dynamics around P_{700} (Sacksteder et al. 2005). To investigate protein dynamics that may be associated with electron transfer in PSI, deuterium was used as a molecular probe of the system.

In this chapter, difference FT-IR spectroscopy was performed on ^2H_2O buffer exchanged PSI samples. PSI samples containing all the polypeptides or PSI samples missing the PsaC, PsaD, and PsaE subunits were compared. Isotope-edited spectra reveal protein perturbations consistent with light-induced structural changes of the PsaA and/or PsaB subunits. These findings identify specific conformation changes that may be important in interactions with soluble electron carriers and in efficient reduction of P_{700}^+. To further characterize the structural dynamics during electron transfer in PSI, tryptophan residues were isotopically labeled. The results reported here may be consistent with perturbations of tryptophan residues, which may be associated with structural dynamics controlling the oxidation of plastocyanin/cytochrome c_6.

5.3 Materials and Methods

5.3.1 PSI purification for ^1H_2O and ^2H_2O buffer exchanged samples Wild-type *Synechocystis* PCC 6803 liquid cultures (15L) were grown and supplemented with 5mM

glucose. Trimeric PSI samples were purified as previously described (Noren et al. 1991; Kim et al. 2001). Briefly, thylakoid membranes were solubilized with 1% dodecyl-ß-D-maltiside, centrifuged for one hour at 100,000 x g, and loaded onto a Q-sepharose column. A linear gradient was applied, and PSI trimer fractions with an absorbance ≥679 absorbance units (AU) were pooled and were exchanged into $^{1}H_2O$ or $^{2}H_2O$ buffers containing 5 mM HEPES-NaOH pH 7.5, 0.04% dodecyl-ß-D-maltiside (LM) by dialysis. The p^{2}H of the $^{2}H_20$ buffer is reported as the uncorrected meter reading (Kim et al. 2001), because the small solvent isotope effects on weak acid pK_a values are essentially cancelled by the $^{2}H_2O$ change in response of the pH electrode (Schowen et al. 1982). Three rounds of dialysis were performed over three days. The total volume of buffer exchange was 1.5 L, which correspond to 500 ml exchanged three times. Trimeric PSI was concentrated using an Amicon (Bedford, MA) Ultra 100,000 MWCO centrifugal filter device to a final concentration of 2 mg chl/ml.

5.3.2 PsaC, PsaD and PsaE removal. The stromal subunits PsaC, PsaD, and PsaE along with the terminal electron acceptors F_A and F_B were removed as previously described (Parrett, K. G. et al. 1989; Parrett, K. G.; et al. 1990). Briefly PSI samples were incubated in 6.8 M Urea, 10 mM Tris and 5 mM glycine-pH 10 for 70 minutes. Afterwards, an equal volume of tris buffer was added to stop the reaction. Samples were dialyzed into $^{1}H_2O$ or $^{2}H_2O$ buffers as described above. Afterwards, samples were concentrated to 2 mg/ml.

5.3.3 Growth conditions and PSI purification for $^{2}H_5$-tryptophan. Feedback inhibition of the chorismate biosynthetic pathway was performed by adding 0.25 mM tyrosine, 0.25 mM tryptophan (control) or $^{2}H_5$-tryptophan (98% purity, Isotec,

Maimisburg, OH), and 0.50 mM phenylalanine to the BG-11 media (Srinivasan et al. 1959; Smith 1962; Barry et al. 1987; Poulson et al. 1991). *Synechocystis* cells were grown in 1L BG-11 buffered with 1mM TES NaOH- pH 8.0. Cultures were grown for 11 days and harvested with an OD reading of 1.3-1.5. PSI was purified as previously described.(Bender et al. 2008a)

5.3.4 FTIR Spectroscopy. FT-IR spectra were collected at -10 °C as described previously (Sacksteder et al. 2005; Bender et al. 2008b). Samples contained 3 mM potassium ferricyanide and 3 mM potassium ferrocyanide and were concentrated at room temperature under a steady flow of nitrogen gas. Concentration times were 20-30 minutes. Spectral conditions were as follows: resolution, 4 cm^{-1}; zero filling, 1; data acquisition time, 4.0 min. Difference spectra (light-minus-dark) were generated by taking the ratio of single beam spectra collected before and during illumination and converting to absorbance. FT-IR spectra were obtained in the dark or under continuous illumination with red- and heat-filtered light, as previously described (Kim et al. 2001; Sacksteder et al. 2005; Bender et al. 2008b). A 60 min dark relaxation time was used between successive illuminations. Sixty difference spectra were averaged for $^{1}H_2O$ and $^{2}H_2O$ PSI intact samples; forty-five difference spectra averaged for $^{1}H_2O$ and $^{2}H_2O$ PsaC, PsaD and PsaE removed PSI samples. Fifty difference spectra were averaged for $^{1}H_5$-trp PSI samples, and forty-nine difference spectra were averaged for $^{2}H_5$-trp PSI samples. Spectra were normalized for small differences in sample concentration and path length. The amplitude of the amide I band in the infrared absorption spectra was used for normalization of the $^{1}H_2O$ and $^{2}H_2O$ buffer exchanged PSI samples. The amide II band in the infrared absorption spectra was used for normalization of the $^{1}H_5$-trp and $^{2}H_5$-trp

PSI samples. The infrared absorption spectra were created by normalizing dark scans to backgrounds not containing protein.

Isotope-edited spectra were generated by subtracting the isotope difference spectra from the control difference spectra. A direct 1 to 1 subtraction was used for all isotope-edited spectra reported here. Control double difference spectra were created by subtracting ½ of the control data from the second half of the control data set and multiplying by the square root of 2. Dark spectra were obtained by subtracting subsequent dark spectra from one another.

5.4 Results

PSI samples were dialyzed for three days into $^{2}H_2O$ containing 5mM HEPES pH 7.5 buffer. In contrast to our earlier solvent exchange protocol, which gave 20% labeling (Kim et al. 2001), here a dialysis method was used to increase the amount of solvent isotope exchange (Rath et al. 1998; Kim et al. 2001; Jenson et al. 2007). The amount of exchange was measured to be 42 $\pm$ 5% for samples containing all extrinsic subunits, and 55± 16% for the PsaC, PsaD and PsaE removed samples. The exchange was assessed by FT-IR spectroscopy (Rath et al. 1998; Kim et al. 2001).

In Figure 1, difference FT-IR spectra, associated with $P_{700}^{+}F_B^{-}$-minus-$P_{700}F_B$, in $^{1}H_2O$-exchanged samples (Figure 1A) and $^{2}H_2O$-exchanged samples (Figure 1B) are presented. Figure 1C is the $^{2}H_2O$ isotope-edited spectrum generated by subtracting the difference spectrum in Figure 1B from the difference spectrum in Figure 1A. The isotope-edited spectrum in Figure 1C will contain frequencies associated with electron transfer reactions and isotope-exchange. For a frequency to be observed in the isotope-

edited spectrum, the frequency must be sensitive to both of these conditions. Bands corresponding to the protein in the dark will appear negative, with the isotope shifted bands appearing positive. Those frequencies corresponding to the protein under illumination will appear as positive bands, with isotope shifts appearing as negative bands. Differences arise in the amplitudes of bands in the isotope-edited spectra presented here, compared to previous ^2H_2O exchange experiments (Kim et al. 2001). This may be due to differences in the hydration of the samples and differences in the amount of exchange.

To better assess the protein dynamics observed for the ^2H_2O isotope-edited spectrum in Figure 1C, the stromal subunits PsaC, PsaD and PsaE were removed. Figure 2 shows the resulting gel from PSI samples that were subjected to urea treatment (lane 1) and from intact PSI samples (lane 2). Three bands are missing in lane 1 compared to lane 2, these bands have previously been assigned to the subunits PsaC, PsaD, and PsaE (Kruip et al. 1997). Removal of the PsaC subunit will also result in the loss of the two terminal electron acceptors, F_A and F_B. The resulting PSI samples will contain F_X as the terminal electron acceptor, and the photoaccumulated species will be P_{700}^+ and F_X^-. The samples were ^2H_2O buffer-exchanged as outlined in the Materials and Methods section. The exchange was measured by FT-IR spectroscopy and was found to be 55 ± 16% (Rath et al. 1998; Kim et al. 2001).

In Figure 3, the light-minus dark FT-IR spectra, associated with $P_{700}^+F_X^-$-minus-$P_{700}F_X$ are presented. The spectrum in Figure 3A corresponds to ^1H_2O-exchanged PSI, and the spectrum in Figure 3B is from ^2H_2O-exchanged PSI. The ^2H_2O-exchanged isotope-edited spectrum is shown in Figure 3C. The ^2H_2O-exchanged isotope-edited

spectrum was generated by subtracting the spectrum in Figure 3B from the spectrum in Figure 3A. The spectrum in Figure 3C shows significant spectral features compared to the noise, as assessed by a dark-minus-dark (Figure 3E), or a control double difference spectrum (Figure 3D) in which no vibrational bands are expected. Similar spectral features are observed in the stromal subunit removed isotope-edited spectrum (Figure 3C) and the intact isotope-edited spectrum (Figure 1C).

A comparison of the isotope-edited spectra of the intact samples (Figure 4A) and samples with the stromal subunits removed (Figure 4B) is shown in Figure 4. Figure 4A contains the isotope-edited spectrum of PSI samples containing all stromal subunits and F_B as the terminal electron acceptors. Frequencies above 1700 cm^{-1} are most likely due to COOH stretching vibrations of aspartic acid or glutamic acid (Chirgadze et al. 1975; Barth 2000; Wolpert et al. 2006). Evidence for these assignments comes from the derivative shaped band observed at (+) 1275 and (-) 1267 cm^{-1} in the ^2H_2O isotope-edited spectrum in Figure 4A. This frequency can be associated with COH bending of aspartic acid and glutamic acid This stretching mode is expected to shift to lower frequencies in ^2H_2O buffer, and can be assigned to the derivate-shaped band at (-) 1048 and (+) 1038 cm^{-1}.

Isotope-shifted bands corresponding to amide I C=O stretching are observed in (+) 1663 and (-) 1658 cm-1 in Figure 4A. Other frequencies observed in the 1700-1600 cm^{-1} region of the spectrum may be associated with glutamine or asparagine and basic amino acids such as lysine and arginine. Frequencies in Figure 4A observed at (+) 1696 cm^{-1}, (-) 1670 cm^{-1}, (+) 1678 cm^{-1}, and (+) 1641 cm^{-1} may be assigned to these amino acids. The complex spectral banding pattern in this region may be the result of multiple

amino acid side chain contributions. Therefore, it is not possible to assign frequencies to specific amino acids in this region of the isotope-edited spectrum.

Unique bands observed in the isotope edited spectra of Figure 4A are derivative shaped bands at (-) 1541 cm^{-1} and (+) 1550 cm^{-1}; (+)1588 cm^{-1} and (-)1597 cm^{-1}. These bands are of interest, because few amino acid side chain groups contribute to this region of the spectrum and are expected to be sensitive to deuterium exchange. The lower frequency pair, (-) 1541 cm^{-1} and (+) 1550 cm^{-1}, may be from deprotonated aspartate or glutamate in the dark state of PSI. Model compound studies have shown an increase in frequency in ^2H_2O of the asymmetric COO^- stretching of both amino acids (Chirgadze et al. 1975; Tamm et al. 1997; Barth 2000; Wolpert et al. 2006). These bands shift to higher frequencies ((+) 1588 cm^{-1} and (-) 1597 cm^{-1}) under illumination. This shift to higher frequency suggests a conformational change associated with charge separation. The symmetric stretching of the COO- group of aspartate and glutamate is also sensitive to deuterium exchange. However model compounds report a frequency shift of 2-3 cm^{-1}; this small isotope-shift may be below the spectral resolution of the spectrum presented here.

Figure 4B contains the isotope-edited spectrum associated with PSI samples with the stromal subunits removed and containing F_X as the terminal electron acceptor. The terminal electron acceptor has changed from F_B in Figure 4A to F_X in Figure 4B. Frequencies observed in both isotope-edited spectra in Figure 4 are most likely due to the donor side of PSI, which has not changed in Figure 4B compared to Figure 4A. Therefore, similar bands observed in both isotope-edited spectra in Figure 4 can be assigned to perturbations of the PsaA and PsaB subunits. Frequencies at (+) 1725 cm^{-1},

and (+) 1726 cm^{-1} are observed in the isotope-edited spectra depicted in Figure 4A and Figure 4B respectively. These bands are most likely due to the COOH antisymmetric stretching of aspartic acid and/or glutamic acid residues located in the PsaA and/or PsaB subunits. From model compounds, these frequencies are expected to shift to lower frequency in both isotope-edited spectra. The isotope-shifted bands may contribute to the complex spectral features observed from 1720-1680 cm^{-1}.

Similar frequencies are also observed in the 1700-1600 cm^{-1} region of both isotope-edited spectra in Figure 4. Frequencies at (+) 1696/4 cm^{-1}, (-) 1670 cm^{-1}, (+) 1678 cm^{-1}, and (+) 1641 cm^{-1} may be assigned to the side chains of glutamine, asparagine, arginine and/or lysine located in the PsaA and/or PsaB subunits. Isotope shifted bands corresponding to amide I C=O stretching, are observed at (+) 1663 and (-) 1658 cm^{-1} in both isotope-edited spectra. These results suggests protein relaxation of the PsaA and/or PsaB subunits associated with electron transfer. Frequencies at (-) 1541 and (+) 1550/1 cm^{-1} observed in both isotope-edited spectra are assigned to aspartate and glutamate COO^- antisymmetric stretching. These bands are believed to shift to (+) 1588 and (-) 1597 cm^{-1} during light-induced electron transfer in PSI.

To further probe specific protein relaxation during stable charge separation tryptophan was used as a molecular probe of the system. The tryptophan dimer located on the luminal side of PSI has been reported to be essential for efficient electron transfer from plastocyanin to P_{700} (Sun et al. 1999b; Sommer et al. 2002; Sommer et al. 2004). Light induced difference spectra were generated from samples containing $^2H_5$-trp labeled PSI to investigate tryptophan perturbations during electron transfer. Figure 5 shows the difference spectra from PSI samples containing $^1H_5$-Trp (Figure 5A) or PSI samples

containing $^{2}H_5$-Trp (Figure 5B). An isotope-edited spectrum was created by subtracting the spectrum in Figure 5B from the spectrum in Figure 5A. The resulting isotope-edited spectrum is depicted in Figure 5C. Only vibrational frequencies that are perturbed during electron transfer and sensitive to $^{2}H_5$-Trp incorporation are expected to contribute to the spectrum in Figure 5C. Vibrational frequencies observed in Figure 5C are above the noise as shown in Figure 5D and 5E. To assign the isotope shifted bands of tryptophan in PSI, absorbance spectra of $^{1}H_5$-Trp and $^{2}H_5$-Trp were collected (data not shown).

Vibrational bands associated with isotope incorporation and perturbations of tryptophan are expected between 1660-1200 cm^{-1} based on model compounds and UVRR studies (Maruyama et al. 1995; Hu et al. 1997; Barth 2000; Wolpert et al. 2006). A derivative shaped band at (-) 1659/ (+) 1654 cm^{-1} can be assigned to amide I stretching or to scrambling of the label into other amino acids. From the model UVRR compound studies, vibrational modes associated with the indole ring are expected to contribute to the spectrum from ~1560-1200 cm^{-1} (Hu et al. 1997). Figure 5C contains multiple vibrational frequencies in this region; however model compound studies suggest larger spectral features in the 1480-1300 cm^{-1} region of the spectrum in association with tryptophan vibrations. The spectral features observed in the $^{2}H_5$-Trp isotope-edited spectrum may be from isotope scrambling or assigned to vibrational frequencies of the tryptophan dimer. The π-stacking interaction of the conserved tryptophan dimer located near P_{700} may affect the vibrational spectrum; π-π interactions may shift vibrations to unique frequencies. To resolve these discrepancies, hydrolyzed PSI samples were subjected GC/MS analysis to quantify the amount of isotope enrichment into amino acids other than tryptophan. From this analysis, less the 1% label scrambling was found in the

thirteen amino acids monitered using this procedure (data not shown). UVRR absorbance spectra from $^{1}H_5$-Trp PSI and $^{2}H_5$-Trp PSI samples showed multiple tryptophan vibrational frequencies shifted in the labeled PSI samples (data not shown). These results indicate that the vibrational frequencies observed in Figure 5C are from tryptophan.

5.5 Discussion

Previous studies have illustrated the importance of protein relaxation due to electron transfer in photosynthesis (Kim et al 2000; Kim et al/ 2001; Sacksteder et al. 2005; Bender et al. 2008a; Bender et al. 2008b). In the bacterial reaction center, it has been demonstrated that protein relaxation events occur on the same time scale as electron transfer (Wang et al. 2007). In PSI, studies have demonstrated heterogeneity of the vibrational frequencies of the terminal electron donor P_{700}. These studies have suggested light-induced structural changes during charge separation (Kim et al. 2000; Kim et al. 2001; Bender et al. 2008a). Furthermore, hydration studies on PSI have shown a profound effect of hydration levels on the rate of P_{700}^{+} reduction and its interaction with the protein environment (Sacksteder et al. 2005). These protein dynamics may influence the oxidation of soluble electron carriers.

To probe the protein dynamics that may be associated with these interactions, we have employed a dialysis method for deuterium solvent exchange (Jenson et al. 2007). A three-day dialysis, which included exchange of the buffer solution daily, was employed (see Materials and Methods). The hydration levels of the FTIR samples were kept constant, with a ratio of the OH stretching at 3300 cm^{-1} to amide 1 between 1.1-1.5.

The isotope-edited spectra presented here are of intact PSI (Figure 4A), and PSI samples with the stromal subunits removed (Figure 4B). All the samples have undergone the three-day dialysis into either $^{1}H_2O$ HEPES pH 7.5 buffer and 0.04% dodecyl-ß-D-maltiside or $^{2}H_2O$ HEPES pH 7.5 buffer and 0.04% dodecyl-ß-D-maltiside. In Figure 4A, the photoaccumulated species are P_{700}^{+} and F_B^{-}. Vibrational frequencies are expected from amino acids perturbed by these photoaccumulated species and sensitive to deuterium exchange. The photoaccumulated species associated with Figure 4B is P_{700}^{+} and F_X^{-}. Amino acids perturbed by these photoaccumulated species and are sensitive to deuterium exchange are expected to contribute to the spectrum in Figure 4B. Similar bands observed in the 1800-1200 cm^{-1} region of both spectra are expected to be from puerturbations associated with the oxidation of P_{700}^{+}. These perturbations may be associated with the PsaA/PsaB heterodimer that binds P_{700}, A_0, A_1 and F_X. Bands assignable to aspartate and glutamate anitsymmetric COO^{-} stretching are observed in both spectra. The carboxylate vibrational bands shift to higher frequencies during charge separation, indicating structural changes around these residues. Bands assignable to amide I C=O stretching vibrations are also observed in both spectra. The amide I stretching may be associated with a light-induced structural change. These structural changes are most likely associated with the PsaA and/or PsaB subunits since they are observed in both spectra.

Previous mutation studies of in the H loop of PsaB have suggested basic amino acid residues located in this region are important for electrostatic interactions with plastocyanin (Navarro et al. 2000; Durán et al. 2006). Furthermore, mutations to conserved residues including tryptophan 622 (*Synechocystis* numbering) in the luminal J

loop of the PsaB subunit, demonstrated the role of the loop in the interaction with soluble electron carriers. This study underlined the importance of the luminal J loop, which includes tryptophan and aspartic acid residues, in the interaction of PSI with plastocyanin and cytochrome c_6 (Sun et al. 1999b). The perturbations observed in the tryptophan isotope-edited spectrum (Figure 5C) may be from a protein conformational change in this conserved luminal loop region.

Figure 6A shows the tryptophan residues located in the PsaA, PsaB, PsaC, PsaD, and PsaE subunits. Three tryptophan residues are found in PsaD and PsaE and may also be perturbed during charge separation in PSI. Figure 6B shows the protein structure of the PsaA and PsaB subunits with the acidic amino acids highlighted (Jordan et al. 2001). The two large loops of PsaA and PsaB are believed to be important with the interaction of the soluble electron donor plastocyanin (Sun et al. 1999a; Sun et al. 1999b; Fromme et al. 2003). Both loops contain glutamate and aspartate, and may be perturbed during P_{700} oxidation.

Two conserved tryptophan residues (Trp 655 and Trp 631) on the luminal side of PSI have been shown to be important in electron transfer from plastocyanin to P_{700}^{+} (Sommer et al. 2004). These tryptophan residues are within π-stacking distance, and may contribute to the $^{2}H_5$-Trp isotope-edited spectrum in Figure 5C. Near these conserved tryptophan molecules are two aspartate residues (Asp 652 and Asp 628). Figure 7 shows these residues as well as P_{700}. The deuterium studies presented here indicate acidic amino acids perturbed during electron transfer in PSI. Furthermore these studies indicate a protein conformational change in PsaA and/or PsaB which may be a result of the luminal loop regions. Both of the aspartate residues shown in Figure 7 may be perturbed

during P_{700}^{+} formation, and may be important in electron transfer from plastocyanin to P_{700}^{+}. Further studies are needed to indicate the precise role these aspartate residues and tryptophan residues may play in light-induced electron transfer in PSI.

5.6 Acknowledgements

This work was supported by NIH GM 43273 (B.A.B). The authors would like to thank Professor Roseann Sachs for performing the PSI acid-hydrolysis.

5.7 References

Barry, B. A. and G. T. Babcock (1987). "Tyrosine radicals are involved in the photosynthetic oxygen evolving system." *Proc. Natl. Acad. Sci. USA* **84**: 7099-7103.

Barth, A. (2000). "The infrared absorption of amino acid side chains." *Prog. Biophys. Mol. Biol.* **74**: 141-173.

Bender, S. L. and B. A. Barry (2008a). "Light-induced protein dynamics in Photosystem I." *Biophys. J.* **93**: 3927-3934.

Bender, S. L., J. Keough, S. E. Boesch, R. A. Wheeler and B. A. Barry (2008b). "The vibrational spectrum of the secondary electron acceptor, A_1, in photosystem I." *J. Phys. Chem. B* **112**: 3844-3852.

Bottin, H. and P. Mathis (1985). "Interaction of plastocyanin with the photosystem I reaction center: a kinetic study by flash absorption spectroscopy " *Biochemistry* **24**: 6453-6460.

Chirgadze, U. N., O. V. Fedorov and N. P. Trushina (1975). "Estimation of amino acid residue side-chain absorption in the infrared spectra of protein solutions in heavy water." *Biopolymers* **14**: 679-694.

Durán, R. V., M. Hervas, B. De la Cerda, M. A. De la Rosa and J. A. Navarro (2006). "A laser flash-induced kinetic analysis of in vivo Photosystem I reduction by site directed mutants of plastocyanin and cytochrome c_6 in *Synechocystis* sp. PCC 6803." *Biochemistry* **45**: 1054-1060.

Fromme, P., P. Jordan and N. Krauss (2001). "Structure of photosystem I." *Biochim. Biophys. Acta* **1507**: 5-31.

Fromme, P., A. Melkozernv, P. Jordan and N. Krauss (2003). "Structure and function in Photosystem I: interaction with its soluble electron carriers and external antenna systems." *FEBS Letters* **555**: 40-44.

Golbeck, J. H. (1994). *In The Molecular Biology of Cyanobacteria*. Dordrecht, Kluwer Academic Publishers.

Haehnel, W., T. Jansen, K. Guase, R. B. Kloegen, B. Stahl, D. Michl, B. Huvermann, M. Karas and R. G. Hermann (1994). "Electron transfer to plastocyanin to Photosystem I." *The EMBO Journal* **13**: 1028-1038.

Hervas, M., J. A. Navarro, A. Diaz, H. Bottin and M. A. De la Rosa (1995). "Laser-flash kinetic analysis of the fast electron transfer from plastocyanin and cytochrome c6

to Photosystem I. Experimental evidence on the evolution of the reaction mechanism." *Biochemistry* **34**: 11321-11326.

Hervas, M., J. A. Navarro, A. Diaz and M. A. De la Rosa (1996). "A comparative thermodynamic analysis by laser-flash absorption spectroscopy of Photosystem I reduction by plastocyanin and cytochrome c_6 in *Anabaena* PCC 7119, *Synechocystis* PCC 6803, and spinach." *Biochemistry* **35**: 2693-2698.

Hervas, M., J. M. Ortega, J. A. Navarro, A. Diaz, M. A. De la Rosa and H. Bottin (1994). "Laser flash kinetic analysis of *Synechocystis* PCC 6803 cytochrome c_6 and plastocyanin oxidation by Photosystem I." *Biochim. Biophys. Acta* **1184**: 235-241.

Ho, K. K. and D. Krogmann, W, (1988). "Electron donor to P_{700} in cyanobacteria and algae. An instance for unusual genetic variabilitiy." *Biochim. Biophys. Acta* **766**: 310-316.

Holzwarth, A. R., M. G. Muller, J. Niklas and W. Lubitz (2006). " Ultrafast transient absorption studies on photosystem I reaction centers from *Chlamydomonas reinhardtii*. 2: Mutations near the P_{700} reaction center chlorophylls provide new insight into the nature of the primary electron donor." *Biophys. J.* **90**: 552-565.

Hu, X. and T. G. Spiro (1997). "Tyrosine and tryptophan structure markers in hemogloben utlraviolet resonance raman spectra: mode assignments via subunit-specific isotope labeling of the recombinant protein." *Biochemistry* **36**: 15701-15712.

Jenson, D. L., A. Evans and B. A. Barry (2007). "Proton-coupled electron transfer and tyrosine D of photosystem II." *J. Phys. Chem. B* **111**: 12599-12604.

Jordan, P., P. Fromme, H. T. Witt, O. Klukas, W. Saenger and N. Krauss (2001). "Three-dimensional structure of cyanobacterial photoystem I at 2.5A resolution." *Nature* **411**: 909-917.

Kim, S. and B. A. Barry (2000). "Identification of carbonyl modes of P_{700} and P_{700}^{+} by in situ chlorophyll labeling in photosystem I." *J. Am. Chem. Soc.* **122**: 4980-4981.

Kim, S., C. A. Sacksteder, K. A. Bixby and B. A. Barry (2001). "A reaction-induced FT-IR study of cyanobacterial photosystem I." *Biochemistry* **40**: 15384-15395.

Kruip, J., P. Chitnis, B. Lagoutte, M. Rogner and E. J. Boekema (1997). "Structural organization of the major subunits in cyanobacterial Photosystem I." *J. Biol. Chem.* **272**: 17061-17069.

Maruyama, T. and H. Takeuchi (1995). "Effects of hydrogen bonding and side-chain conformation on the raman bands of tryptophan-2,4,5,6,7-d_5." *J. Raman Spectrosc.* **26**: 319-324.

Merchant, S. and L. Bogorad (1986). "Regulation by copper of the expression of plastocyanin and cytochrome c-552 in *Chlamydomonas reinhardtii*." *Mol. Cell. Biol.* **6**: 462-469.

Navarro, J. A., M. Hervas, J. Sun, B. De la Cerda, P. R. Chitnis and M. A. De la Rosa (2000). "Negatively charged residues in the H loop of PsaB subunit in Photosystem I from *Synechocystis* sp PCC 6803 appear to be responsible for electrostatic repulsions with plastocyanin." *Photosynth. Res.* **65**: 63-68.

Noren, G. H., R. J. Boerner and B. A. Barry (1991). "EPR characterization of an oxygen-evolving photosystem II preparation from the transformable cyanobacteria *Synechocystis* 6803." *Biochemistry* **30**: 3943-3950.

Parrett, K. G., T. Mehari and J. H. Golbeck (1990). "Resolution and reconstitution of the cyanobacterial Photosystem I complexes." *Biochim. Biophys. Acta* **1015**: 341-352.

Parrett, K. G., T. Mehari, P. G. Warren and J. H. Golbeck (1989). "Purification and properties of the intact P_{700} and F_X containing Photosystem I core protein." *Biochim. Biophys. Acta* **973**: 324-332.

Poulson, C. and R. Verpoorte (1991). "Roles of chorismate mutase, isochorismate synthase and anthranilate synthase in plants." *Phytochemistry* **30**: 377-386.

Rath, P., W. J. DeGrip and K. J. Rothschild (1998). "Photoactivation of rhodopsin causes an increased hydrogen-deuterium exchange of buried peptide groups." *Biophys. J.* **74**: 192-198.

Sacksteder, C. A., S. L. Bender and B. A. Barry (2005). "Role for bound water and CH-pi aromatic interactions in photosynthetic electron transfer." *J. Am. Chem. Soc.* **127**: 7879-7890.

Schowen, K. B. and R. L. Schowen (1982). "Solvent isotope effects of enzyme systems." *Methods Enzymol.* **87**: 551-606.

Smith, L. C. (1962). "Control of 3-deoxy-D-arabino-heptulosonic acid 7-phosphate synthesis by phenylalanine and tyrosine." *J. Biol. Chem.* **237**: 3566-3570.

Sommer, F., F. Drepper, W. Haehnel and M. Hippler (2004). "The hydrophobic recognition site formed by residues PsaA-Trp651 and PsaB-Trp627 of photosystem I in *Chlamydomonas reinhardtii* confers distinct selectivity for binding of plastocyanin and cytochrome c6." *J. Biol. Chem.* **279**: 20009-20017.

Sommer, F., F. Drepper and M. Hippler (2002). "The luminal helix l of PsaB is essential for recognition of plastocyanin or cytochrome c6 and fast electron transfer to photosystem I in *Chlamydomonas reinhardtii*." *J. Biol. Chem.* **277**: 6573-6581.

Srinivasan, P. R. and D. B. Sprinson (1959). "2-keto-3-deoxy-D-arabo-heptonic acid 7-phosphate synthetase." *J. Biol. Chem.* **234**: 716-722.

Sun, J., M. Hervas, J. A. Navarro, M. A. De la Rosa and P. R. Chitnis (1999a). "Oxidizing side of the cyanobacterial photosystem I: mutational analysis of the luminal H loop of the PsaB subunit." *Photosynth. Res.* **62**: 241-250.

Sun, J., W. Xu, M. Hervas, J. A. Navarro, M. A. De la Rosa and P. R. Chitnis (1999b). "Oxidizing side of the cyanobacterial Photosystem I. Evidence for interaction between the electron donor proteins and a luminal surfance helix of the PsaB subunit." *J. Biol. Chem.* **274**: 19048-19054.

Tamm, L. K. and S. A. Tatulian (1997). "Infrared spectroscopy of proteins and peptides in lipid bilayers." *Quarterly Reviews of Biophysics* **30**: 365-429.

Wang, H., S. Lin, J. P. Allen, J. C. Williams, S. Blankert, C. Laser and N. W. Woodbury (2007). "Protein dynamics control the kinetics of initial electron transfer in photosynthesis." *Science* **316**: 747-750.

Wolpert, M. and P. Hellwig (2006). "Infrared Spectra and Molar Absorption Coefficients of the 20 Alpha Amino Acids in Aqueous Solution in the Spectral Range of 1800-500 cm-1." *Spectrochim. Acta, Part A* **64**: 987-1001.

Wood, P. M. (1978). "Interchangeable copper and iron proteins in algal photosynthesis. Studies on plastocyanin and cytochrome c-552 in *Chlamydomonas*." *Eur. J. Biochem.* **87**: 9-19.

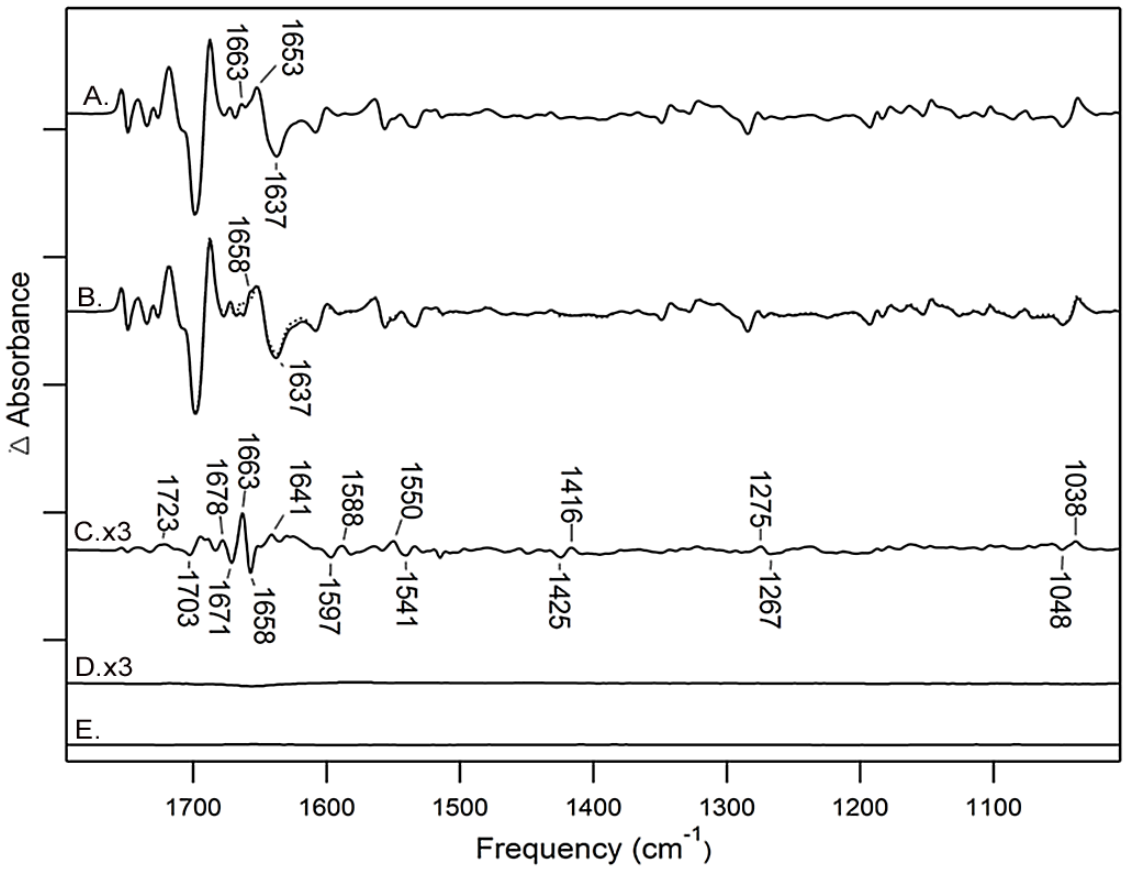

Figure 1. Light-induced FT-IR difference spectra of intact PSI. (A) The $P_{700}^{+}F_B^{-}$-minus-$P_{700}F_B$ spectrum from PSI dialyzed with ^1H_2O HEPES-NaOH pH 7.5 buffer. (B) $P_{700}^{+}F_B^{-}$-minus-$P_{700}F_B$ spectrum from PSI dialyzed with ^2H_2O HEPES-NaOH pH 7.5 buffer. The spectrum in (A) is overlaid as a dotted line. (C) The isotope-edited spectrum generated by a direct one to one subtraction of the spectrum in (B) from the spectrum in (A). (D) Control double difference spectrum generated by subtracting ½ the data set in (A) from the second half of the data set. (E) Dark minus dark spectrum of PSI dialyzed with ^1H_2O HEPES-NaOH pH 7.5 buffer. Spectra in (A) (B) and (E) are an average of 64 spectra. Each mark on the y-axis represents $2x10^{-3}$ Absorbance units (AU). See Materials and Methods for additional information.

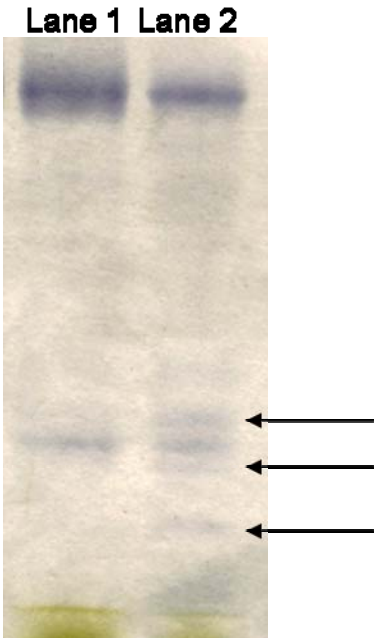

Figure 2. SDS-Urea page gel of PSI samples. Lane 1 is of PSI samples that have been treated with 6.8M urea to remove the PsaC, PsaD, and PsaE subunits. Lane 2 contains PSI samples containing all extrinsic subunits (PsaC, PsaD, and PsaE) as shown by the arrows.

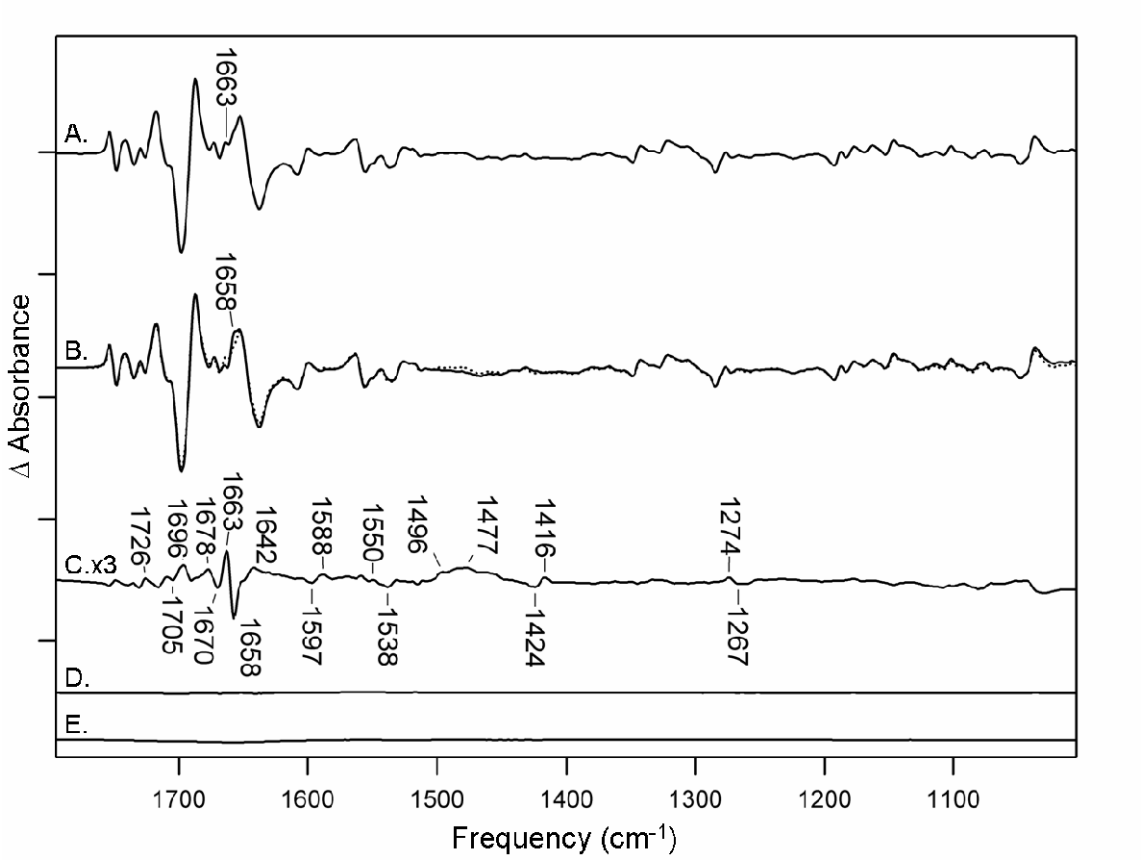

Figure 3. Light-induced FT-IR difference spectra of PSI samples treated with 6.8M urea to remove the PsaC, PsaD and PsaE subunits. (A) The $P_{700}^{+}F_X^{-}$-minus-$P_{700}F_X$ spectrum of dialyzed with ^1H_2O HEPES-NaOH pH 7.5 buffer. (B) The $P_{700}^{+}F_X^{-}$-minus-$P_{700}F_X$ spectrum of dialyzed with ^2H_2O HEPES-NaOH pH 7.5 buffer. The spectrum in (A) is overlaid as a dotted line. (C) The isotope-edited spectrum generated by a direct one to one subtraction of the spectrum in (B) from the spectrum in (A). (D) Control double difference spectrum generated by subtracting ½ the data set in (A) from the second half of the data set. (E) The Dark minus dark spectrum of PSI dialyzed with ^1H_2O HEPES-NaOH pH 7.5 buffer. Spectra in (A) (B) and (E) are an average of 50 spectra. Each mark on the y-axis represents $2x10^{-3}$ (AU). See Materials and Methods for more information.

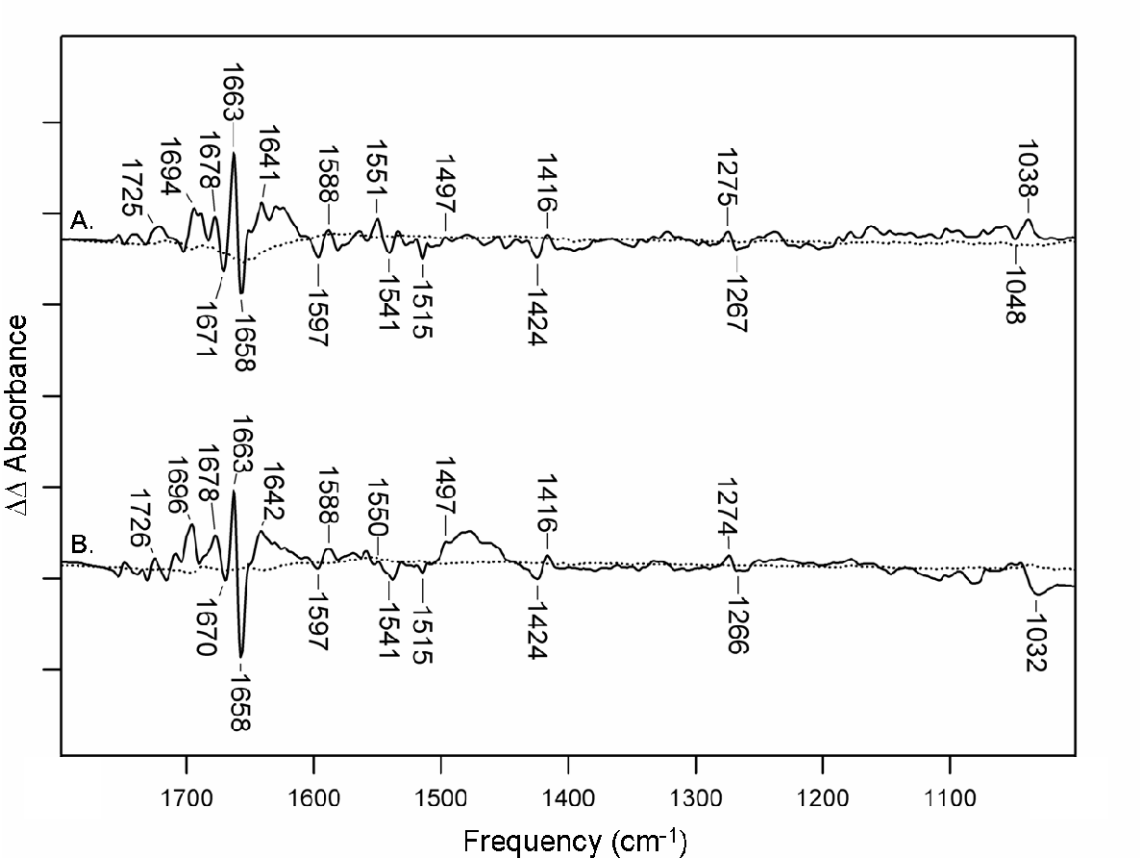

Figure 4. The isotope-edited spectra of deuterium exchanged PSI. (A) $P_{700}^{+}F_{B}^{-}$-minus-$P_{700}F_{B}$ isotope edited spectrum. (B) $P_{700}^{+}F_{X}^{-}$-minus-$P_{700}F_{X}$ isotope edited spectrum. The dotted spectra overlayed in (A) and (B) are the control double difference spectra in which no vibrational bands are expected. Each mark on the y-axis represents $2x10^{-4}$ (AU). See Materials and Methods for additional information.

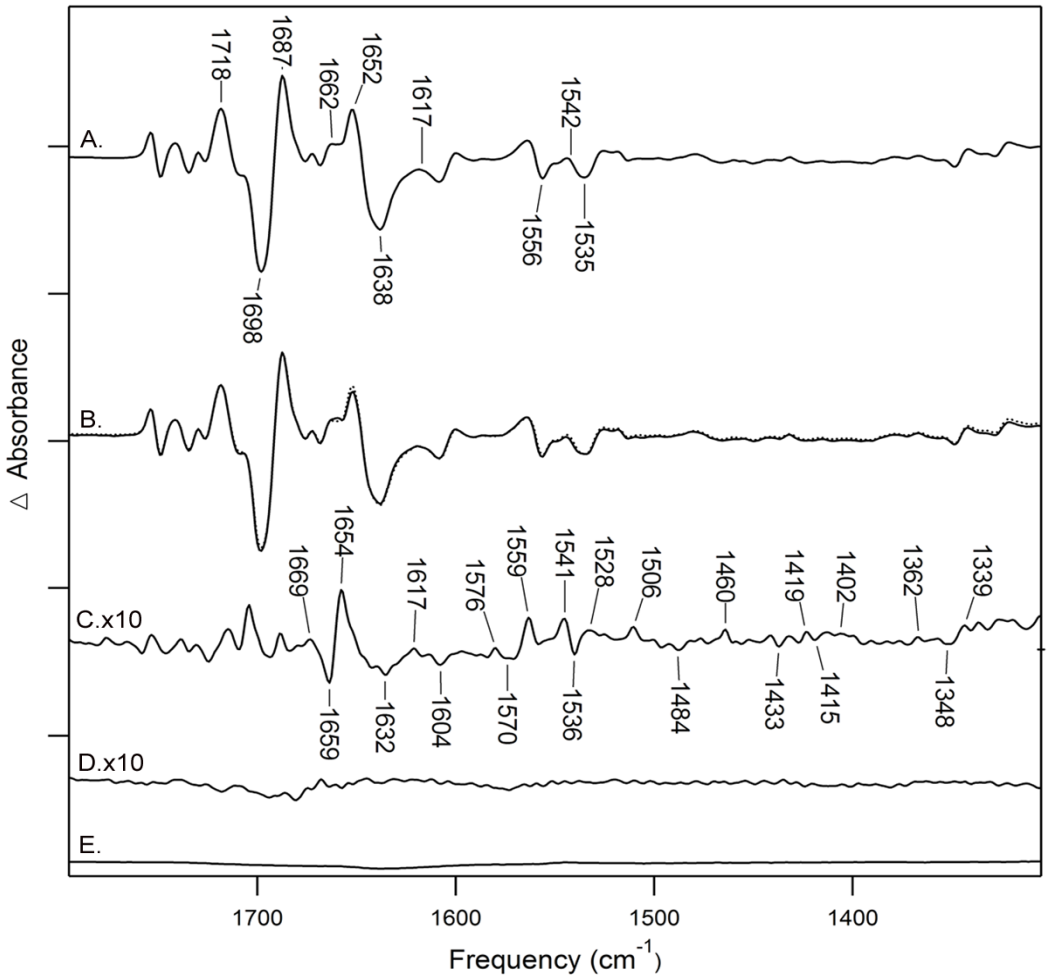

Figure 5. Light-induced FT-IR difference spectra of intact PSI. (A) The $P_{700}^{+}F_B^{-}$-minus-$P_{700}F_B$ spectrum of PSI isolated from *Synechocystis* cultures grown with 0.25 mM $^1H_5$-tryptophan. (B) The $P_{700}^{+}F_B^{-}$-minus-$P_{700}F_B$ spectrum from PSI isolated from *Synechocystis* cultures grown with 0.25 mM $^2H_5$-tryptophan. (C) The isotope-edited spectrum generated by a direct one to one subtraction of the spectrum in (B) from the spectrum in (A). (D) Control double difference spectrum generated by subtracting ½ the data set in (A) from the second half of the data set. (E) The dark minus dark spectrum of PSI isolated from *Synechocystis* cultures grown with 0.25 mM $^1H_5$-tryptophan.. Spectra in (A) (B) and (E) are an average of 50 spectra. Each mark on the y-axis represents $2x10^{-3}$ (AU). See Materials and Methods for more information.

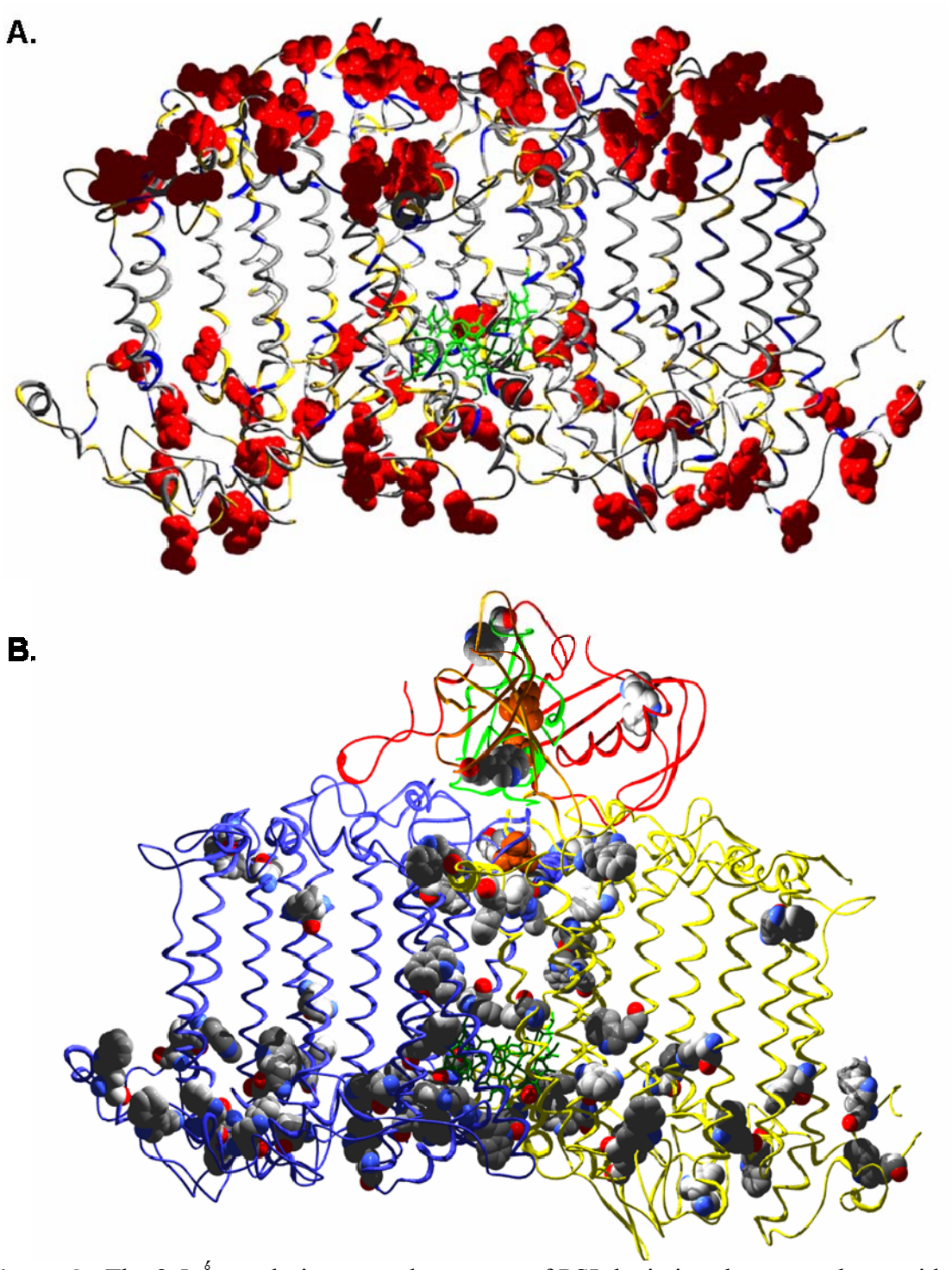

Figure 6. The 2.5 Å resolution crystal structure of PSI depicting the tryptophan residues in the PsaA, PsaB, and PsaC subunits of PSI (A) and acidic amino acids found in the PsaA and PsaB subunits of PSI (B). The figure is reproduced from the 2.5 Å resolution crystal structure of PSI from *S. elongatus* (PDB file accession number 1JB0 (Jordan et al.

2001)) using Swiss-Pdb viewer (v3.7; www.expasy.ch/spdbc), and rendered using POV-Ray (v3.5; www.povray.org).

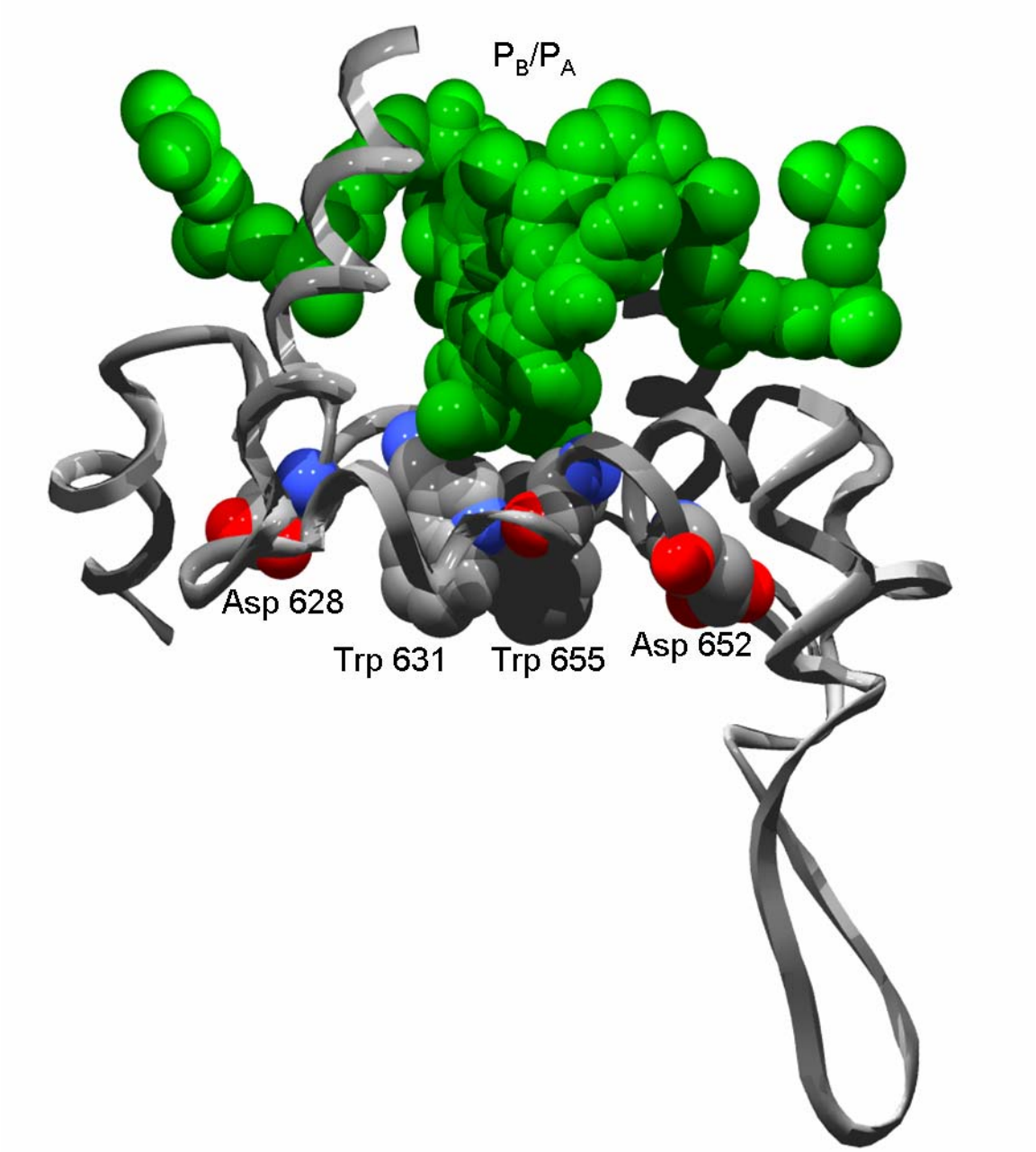

Figure 7. The protein environment around P_{700}. The two conserved tryptophan residues and aspartate residues located in the luminal loop region that may be perturbed during electron transfer in PSI are shown. The luminal loop regions of PsaA and PsaB are also shown as ribbons. The figure is reproduced from the 2.5 Å resolution crystal structure of PSI from *S. elongatus* (PDB file accession number 1JB0 (Jordan et al. 2001)) using Swiss-Pdb

Figure 7 continued

viewer (v3.7; www.expasy.ch/spdbc), and rendered using POV-Ray (v3.5; www.povray.org).

CHAPTER 6

CONCLUSION

Photosystem I (PSI) is a protein complex involved in light-induced electron transfer across the thylakoid membrane. Electron transfer in PSI involves a series of oxidation reduction reactions of cofactors bound to the subunits PsaA, PsaB and PsaC (Jordan et al. 2001) Protein dynamics have shown to play a major role in photosynthetic electron transfer reactions (Warshel et al. 1989; Gehlen et al. 1994; Halverson et al. 2003; Parson et al. 2004; Barry et al. 2006; De Riso et al. 2006; Wang et al. 2007). The studies presented here have underscored the role of protein dynamics and cofactor interactions in the control of electron transfer in PSI. The protein relaxations observed in these studies have the potential to control the bidirectionality inherent to PSI, and may control the interactions with soluble electron donors and acceptors.

Characterization of the secondary electron acceptor A_1 has shown the influence of noncovalent interactions on the vibrational spectrum. Hydrogen-bonding, π-stacking and electrostatic interactions observed in previous studies have the potential to modulate the redox properties of the secondary electron acceptor (Pushkar, Y. et al. 2004; Pushkar, Y. N. et al. 2005; Feldman et al. 2007; Bender et al. 2008). The work presented here has shown the effect of these interactions on the vibrational spectrum of A_1 in comparison to DFT calculations of the quinone molecule.

Novel experiments incorporating various isotopes into the keto group of chl have given greater insight into the oxidation of P_{700}^{+}. These studies suggested a light-induced conformational change in PSI, which may regulate the oxidation of soluble electron donors or other electron transfer reactions. Deuterium exchange studies revealed a light-induced conformational change in PSI, which may be related to the previous protein relaxations identified by isotope labeling of P_{700}. Furthermore, these studies have characterized aspartate or glutamate perturbations associated with the PsaA subunit and/or the PsaB subunit. These novel perturbations indicate structural changes associated with the loop regions of these two subunits. To further investigate protein dynamics associated with stable charge separation, tryptophan residues were isotopically labeled in PSI.

The isotope-edited spectrum of $^{2}H_{5}$-Trp PSI reveal vibrational frequencies that can be associated with amide I perturbations as well as the indole ring of tryptophan. These results indicate unique vibrational frequencies of tryptophan that may be indicative of the conserved tryptophan dimer found on the luminal side of PSI (Sun et al. 1999; Jordan et al. 2001; Fromme et al. 2003; Sommer et al. 2004). These results combined with the deuterium-exchange results emphasize the importance of protein relaxation events that accompany electron transfer reaction in PSI.

The studies presented here underscore the importance of protein dynamics and cofactors interactions in oxygenic photosynthesis. The results signify specific protein relaxation events that accompany stable charge separation in PSI. Further studies are needed to specify the role of these protein dynamics; however, the studies presented here

are indicative of protein conformational changes that may control the oxidation of soluble electron carriers or other electron transfer reactions in PSI.

6.1 References

Barry, B. A., I. Cooper, A. De Riso, S. H. Brewer, D. M. Vu and R. B. Dyer (2006). "Time-resolved vibrational spectroscopy detects protein-based intermediates in the photosynthetic oxygen-evolving cycle." *Proc. Natl. Acad. Sci. USA* 103: 7288-7291.

Bender, S. L., J. Keough, S. E. Boesch, R. A. Wheeler and B. A. Barry (2008). "The vibrational spectrum of the secondary electron acceptor, A_1, in photosystem I." *J. Phys. Chem. B* 112: 3844-3852.

De Riso, A., D. L. Jenson and B. A. Barry (2006). "Calcium exchange and structural changes during the photosynthetic oxygen evolving cycle." *Biophys. J.* 91: 1999-2008.

Feldman, K. S., D. K. Hester 2nd and J. H. Golbeck (2007). "A relationship between amide hydrogen bond strength and quinone reduction potential: Implications for photosystem I and bacterial reaction center quinone function." *Bioorg. Med. Chem. Lett.* 17: 4891-4894.

Fromme, P., A. Melkozernv, P. Jordan and N. Krauss (2003). "Structure and function in Photosystem I: interaction with its soluble electron carriers and external antenna systems." *FEBS Letters* 555: 40-44.

Gehlen, J. N., M. Marchi and D. Chandler (1994). "Dynamics affecting the primary charge transfer in photosynthesis." *Science* 263: 499-502.

Halverson, K. M. and B. A. Barry (2003). "Evidence for spontaneous structural changes in a dark-adapted state of photosystem II." *Biophys. J.* 85: 2581-2588.

Jordan, P., P. Fromme, H. T. Witt, O. Klukas, W. Saenger and N. Krauss (2001). "Three-dimensional structure of cyanobacterial photoystem I at 2.5A resolution." *Nature* 411: 909-917.

Parson, W. W. and A. Warshel (2004). "Dependence of photosynthetic electron-transfer kinetics on temperature and energy in a density-matrix model." *J. Phys. Chem. B* 108: 10474-10483.

Pushkar, Y., D. Stehlik, M. Van Gastel and W. Lubitz (2004). "An EPR/ENDOR study of the asymmetric hydrogen bond between the quinone electron acceptor and the protein backbone in Photosystem I." *Journal of Molecular Structure* 700: 233-241.

Pushkar, Y. N., O. Ayzatulin and D. Stehlik (2005). "Transient and pulsed EPR study of ^{17}O-substituted methyl-naphthoquinone as radical anion in the A_1 binding site of photosystem I and in frozen solution." *Appl. Magn. Reson.* 28: 195-211.

Sommer, F., F. Drepper, W. Haehnel and M. Hippler (2004). "The hydrophobic recognition site formed by residues PsaA-Trp651 and PsaB-Trp627 of photosystem I in *Chlamydomonas reinhardtii* confers distinct selectivity for binding of plastocyanin and cytochrome c6." ***J. Biol. Chem.*** 279: 20009-20017.

Sun, J., W. Xu, M. Hervas, J. A. Navarro, M. A. De la Rosa and P. R. Chitnis (1999). "Oxidizing side of the cyanobacterial Photosystem I. Evidence for interaction between the electron donor proteins and a luminal surfance helix of the PsaB subunit." ***J. Biol. Chem.*** 274: 19048-19054.

Wang, H., S. Lin, J. P. Allen, J. C. Williams, S. Blankert, C. Laser and N. W. Woodbury (2007). "Protein dynamics control the kinetics of initial electron transfer in photosynthesis." *Science* 316: 747-750.

Warshel, A., Z. T. Chu and W. W. Parson (1989). "Dispersed polaron simulations of electron transfer in photosynthetic reaction centers." *Science* 246: 112-116.